TEXTILE RESEARCH JOURNAL

VOLUME XXI November, 1951 *NUMBER 11*

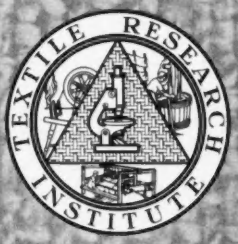

PUBLICATION OF

TEXTILE RESEARCH INSTITUTE

Editorial Office: 10 East 40th Street, New York 16, N. Y.

Rayon Reports

Prepared Monthly by American Viscose Corporation, New York, N. Y. NOVEMBER, 1951

Industry-Wide Interest Reported for Avcoset*

NEW STABILIZING PROCESS ACHIEVES SHRINKAGE CONTROL FOR RAYON

The recent Avisco announcement of the achievement of permanent shrinkage control for rayon has produced an extremely favorable reaction in the field. The news that Avcoset eliminates progressive shrinkage through 50 washings has caused particularly enthusiastic comment—as has the lack of chlorine retention and subsequent immunity to bleaching agents.

Results of Wash Test—Comparing* AVCOSET *with a Commercial Process

Two 100% Viscose Rayon shirting fabrics

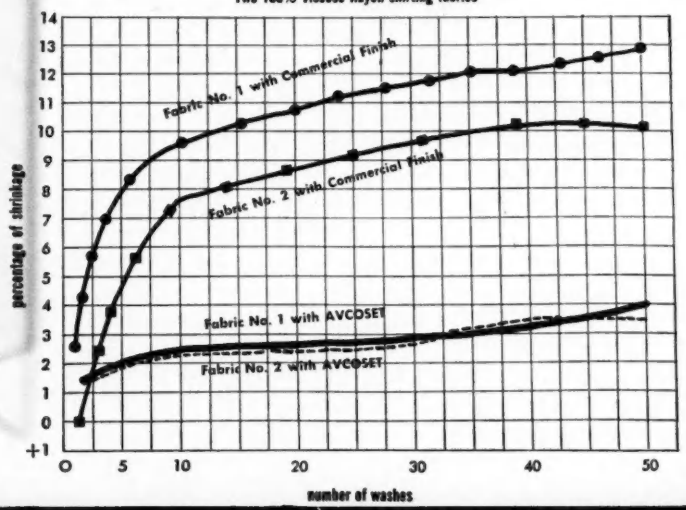

It is emphasized that Avcoset is a cellulose finish for a cellulose fiber. Intended primarily for shirting weight fabrics, the new process affects only viscose. However, it can be successfully applied to fabrics combining rayon with percentages of nylon, acetate or other fibers.

The new process is the result of more than two years' laboratory evaluation by Avisco's Textile Research Department. It has already been utilized on a commercial scale—and is ready for adoption by all those in the industry alert to improving rayon textiles. Inquiries about the Avcoset process are welcomed. Address: American Viscose Corporation, Converting Relations Department, 350 Fifth Avenue, New York 1, N. Y.

*Reg. Trade Mark

RAYON 20 YEARS AGO

NEW YORK, N.Y., November, 1931—More than 68,000 yards of rayon fabric were used in decorating the newly-opened Waldorf-Astoria.

CALCUTTA, INDIA, November, 1931—Rayon imports into India have greatly increased in the past few months.

NEW YORK, N.Y., November, 1931—The National Retail Dry Goods Association has passed a resolution protesting the weighting of rayon fabrics.

MAKE USE OF *Avisco*® 4-PLY SERVICE

To encourage continued improvement in rayon fabrics, American Viscose Corporation conducts research and offers technical service in these fields:

1 FIBER RESEARCH
2 FABRIC DESIGN
3 FABRIC PRODUCTION
4 FABRIC FINISHING

AMERICAN VISCOSE CORPORATION

America's largest producer of rayon

Sales Offices: 350 Fifth Avenue, New York 1, N. Y.; Charlotte, N. C.; Cleveland, Ohio; Philadelphia, Pa.; Providence, R. I.

TEXTILE RESEARCH JOURNAL

VOL. XXI. No. 11 • November, 1951

In This Issue

Cotton Fineness and Immaturity as Measured by the Arealometer
K. L. Hertel and C. J. Craven 765

Flow Through Fabric-like Structures
S. E. Penner and A. F. Robertson 775

Molecular Theory of Damping in Fibers
Taikyue Ree, Mei Chio Chen, and Henry Eyring

Part I: Vibrational Study of Saran Fibers 789

Part II: The Effect of Temperature and Heat Treatment on the Energy Loss in Saran 799

Quantitative X-Ray Studies of Order in Amorphous and Crystalline Polymers Scattering from Various Polymers and a Study of the Glass Transition in Polystyrene and Polymethyl Methacrylate
Samuel Krimm and Arthur V. Tobolsky 805

The Felting of Wool as Related to the Elastic and Swelling Behavior of the Fiber
Herman Bogaty, Arnold M. Sookne, and Milton Harris 822

The Felting of Shrink-Resistant Wool as Related to Some Properties of the Single Fiber
Arnold M. Sookne, Herman Bogaty, and Milton Harris 827

Chemical Substitution in Fibrous Cotton and Resistance of Substituted Cotton to Microbiological Deterioration
Charles F. Goldthwait, Edmund M. Buras, Jr., and Albert S. Cooper 831

Thermal Degradation in Tire Cords
Part II: Effects on Modulus, Toughness, and Degree of Resilience
Verne W. Tripp, Trinidad Mares, and Carl M. Conrad 840

Editor: Julian S. Jacobs *Production Editor:* Lois E. Emma

Associate Editors

H. J. Ball — Gustavus J. Esselen — H. Mark
Earl E. Berkley — Milton Harris — E. R. Schwarz
Henry Eyring — K. L. Hertel — Kyle Ward, Jr.

TEXTILE RESEARCH JOURNAL, published monthly at Prince and Lemon Streets, Lancaster, Pa., is devoted to the interest of research in textile and allied industries. It is the official publication of Textile Research Institute.

Manuscripts and communications should be sent to the editorial office, 10 East 40th Street, New York 16, N. Y.

Subscription rates (including, monthly, bound copy of the Abstracts from the *Journal of the Textile Institute*): General—$15.00 per year; additional for postage, 50 cents to Canada, $1.00 to all other countries. Special—$10.00 per year for United States and Canadian students, teachers, educational institutions, public libraries, governmental libraries and departments, plus 50 cents for postage to Canada. Single copies, $1.50 each.

Entered as second-class matter, April 27, 1945, at the postoffice at Lancaster, Pa., under the Act of August 24, 1912. Accepted for mailing at special rate of postage provided for in paragraph (d-2), Section 34.40, P. L. & R. of 1948, authorized May 9, 1950.

Contents copyrighted 1951 by Textile Research Institute.

Advertising rates supplied on request.

From Filament to Fashion

SCOTT TESTERS*

give sure control of purchasing, manufacture, dyeing and finishing. World-standard machines for tensile, burst, stretch from 0 to 2000 lbs. tensile. Their "picturized" chart results are an invaluable record.

IP–2 Patented constant-rate-of-load Incline-plane Tester for tensile testing of yarn in single end in specimens as short as 1".

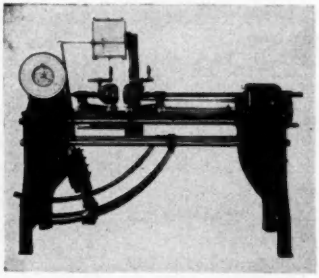

Model Q. Capacity 2,000 lbs. For tensile testing of duck, webbing, cords, twine, etc. Fulfills A.S.T.M. and Government specifications.

Model J. Standard Tensile Tester for both skein and fabric. Also for burst test. Fulfills A.S.T.M. and Government specifications.

Scott Testers provide you with "picturized" charts which are easy to read and convenient to file as a guide to further production, as well as proof of quality.

*Registered Trademark

REQUEST CATALOG 50

SCOTT TESTERS, INC., 145 BLACKSTONE ST., PROVIDENCE 5, R. I.

Scott Testers — Standard of the World

TEXTILE RESEARCH JOURNAL

VOL. XXI, No. 11 November, 1951

Cotton Fineness and Immaturity as Measured by the Arealometer*

K. L. Hertel and C. J. Craven

Agricultural Experiment Station, The University of Tennessee, Knoxville, Tennessee

Introduction

The quality and usefulness of a quantity of lint cotton are affected, among other things, by the average physical dimensions of the individual fibers. Staple length, or some kind of average length arrived at in one of various possible ways, has long been used to evaluate cotton. Average dimensions of cross sections, however, have not been so easy to determine. Several properties of cotton which are closely associated with cross-section dimensions have been measured, such as linear density, perimeter, cross-sectional area, wall thickness, specific area, and percent maturity. Some of the methods used in these measurements are: arraying and weighing, examining sections under a microscope, measuring resistance to flowing air, swelling in caustic soda solution, differential dyeing, and examining with polarized light.

Each of the above properties has been useful to a limited extent, but none of them, when taken separately, describes completely the cross sections of fibers. This follows from the fact that a cross section is a two-dimensional property, and requires the measurement of two independent parameters in order to be completely described. An examination of the above properties shows that each of them, except for percent maturity, is a geometric property. If maturity also is defined in geometric terms, a knowledge of any two of these properties implies the other four, which may easily be obtained by calculation.

The present paper deals with the development of an air-flow instrument, the arealometer, which is responsive to two of these properties: specific area, A, defined as the ratio of the external surface of the fibers to the volume of fibrous material; and immaturity ratio, I, defined as the ratio of the area of a circle having the same perimeter as an average fiber to the actual cross-sectional area of the fiber. A primary cause of resistance to the flow of air is the amount of external fiber surface exposed to the air flow, and this resistance is used as a measure of specific area. The resistance, however, is modified by the distribution and orientation of these surfaces; hence, on suitably compressing the sample, that change in resistance which is essentially due to reorientation of flattened fibers becomes a measure of the immaturity ratio.

Theory

When a gas (*e.g.*, air) is caused to flow through a porous medium, such as a plug of cotton fibers confined in a cylinder, the rate of flow is governed by certain properties of both the fluid and the medium. Expressions describing the flow of a gas through cylindrical capillaries under special conditions have been given by Knudsen [5] and Poiseuille

* This paper was delivered in part before the Agronomy Section of Southern Agricultural Workers, Memphis, Tenn., Feb. 5, 1951, and the Cotton Clinic of the National Cotton Council, Pinehurst, N. C., Feb. 8, 1951.

A paper on this subject based on preliminary observations was prepared for publication in *Proceedings of Congress of Sciences Applied to the Textile Industry*, University of Ghent, Belgium, September, 1951. The present paper is based on new and more extensive data.

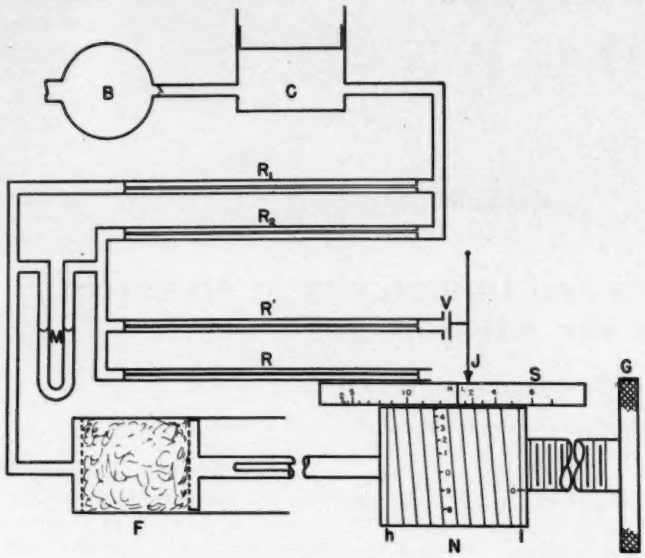

FIG. 1. *Diagram of the arealometer.*

[4]. Poiseuille's expression describes "viscous flow," and applies when the mean free path of the gas molecules is small compared to capillary diameter. This condition causes the gas molecules to collide with each other more frequently than with the wall, making gas viscosity an important factor. Knudsen's expression describes "diffusive flow," and applies when intermolecular collisions are much less frequent than wall collisions. It was found in this work that at atmospheric pressure the Knudsen-type contribution to the total flow through a plug of cotton fibers has a negligible effect on the determination of specific area.

Poiseuille's expression may be modified to describe flow through a porous plug by assuming that the "effective mean pore radius" of the plug is proportional to the ratio of the volume of the voids in the plug to their surface. This ratio has the dimension of length, and in a capillary is equal to half the radius. The resulting expression is equivalent to a relationship arrived at by Kozeny [3] and by Fair and Hatch [1], and may be written as

$$Q = \frac{Ka\Delta P\epsilon^3}{\mu A^2 L(1-\epsilon)^2}, \qquad (1)$$

where Q = volume flow rate of gas; a = cross-sectional area of porous plug; L = length of plug; ΔP = pressure difference between ends of plug; ϵ = void fraction, or porosity (ratio of void volume to total volume of plug); μ = viscosity of gas; A = specific area of solid material in the plug; K = a constant whose value depends upon the shape of the voids and particles and on their orientation with respect to macroscopic flow direction.

The proportionality constant, K, has been separated by Hertel and Sullivan into two parameters, an orientation factor, ζ, and a shape factor, k_o, so that $K = \zeta/k_o$. The effect of particle orientation on resistance to air flow through porous media has been studied by Muskat and Botset [7], Fowler and Hertel [2], and Sullivan [8]. Theoretically, $\zeta = 0.5$ for the case of flow perpendicular to a bed of cylinders [6]. If this condition is met in a plug of cotton fibers, there remains the shape factor, k_o, to be determined empirically. It has been found by experiment that k_o may not be considered to be constant over a wide range of void fractions, but in the range covered by the arealometer ($\epsilon = 0.63$ to $\epsilon = 0.85$) the factor may be assumed to be practically constant.

Equation (1) may be rewritten in the form

$$R = \frac{\Delta P}{Q} = \frac{k_o}{\zeta}\frac{\mu m^2 \rho A^2 L^2}{(\rho a L - m)^2}, \qquad (2)$$

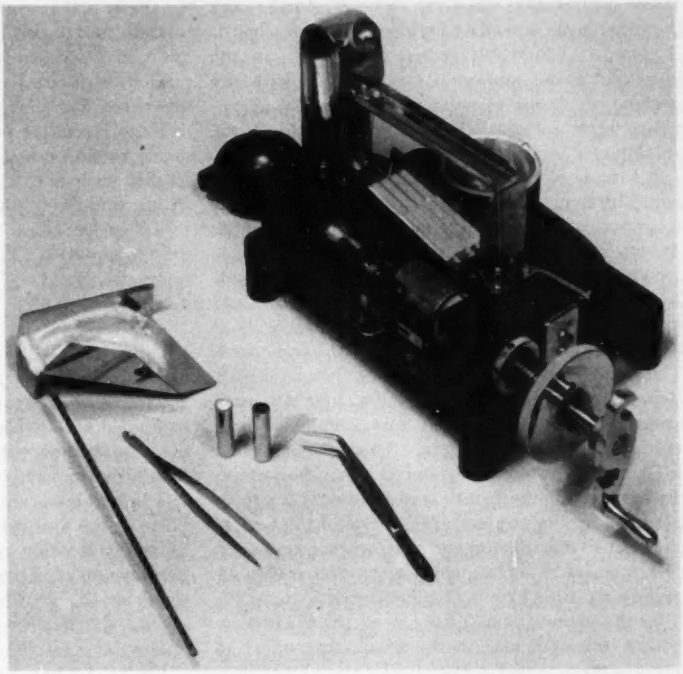

FIG. 2. *Photograph of the arealometer.*

where m = mass of fibers in the plug, ρ = density of fibers, $R = \Delta P/Q$ = resistance offered by the plug to gas flow. This equation relates three variable quantities: resistance, length of plug, and specific area. The remainder of the equation may be held fixed by inserting a fixed solid volume of fibrous material in a cylinder of fixed cross section while achieving the proper orientation of the fibers. Hence, an experimental determination of specific area, A, may be made if one measures R and L, or measures either of these quantities while holding the other one fixed.

Method and Instrument

The method adopted for the arealometer is to fix the resistance to air flow, R, and find by experiment the length, L, to which a plug of fiber must be compressed in order that it shall have this resistance. In electrical measurements, the Wheatstone bridge has provided a very reliable and accurate method for comparing resistances. The arealometer is similar to a Wheatstone bridge in which three of the resistances consist of copper capillaries and the fourth is the compressible porous plug of fiber being tested. Figure 1 shows a diagram of the instrument. An aspirator bulb, B, forces air into a cylinder, C, containing a loose-fitting, weighted piston. This cylinder supplies air to the bridge at a steady pressure of about 1 in. of water. It is clear from the diagram that the circuit consists of two parallel branches, with each branch containing two resistances in series. All of the air entering R_1 passes on through the fibers in F to the atmosphere, while that entering R_2 reaches the atmosphere through R or R and R′, depending upon the position of valve V. Since R_1 is essentially equal to R_2, the inclined manometer, M, will indicate zero pressure difference when the fiber sample in F has a resistance equal to that of R (or R and R′ combined). The necessary degree of compression is achieved by driving a piston into the sample chamber by means of a screw which carries a calibrated drum. The end of the piston is perforated, as is also the bottom of the chamber. Two spiral scales engraved on the drum give direct readings of specific area in square millimeters per cubic millimeter. One scale is read

at low compression when the valve, V, is open, and the other scale is read at high compression when V is closed. A movable screen (not shown in the diagram) whose motion is synchronized with the opening or closing of valve V uncovers the appropriate scale. Figure 2 is a photograph of the arealometer.

A sample of fibrous material to be tested is prepared by first weighing out an amount whose mass in grams is numerically equal to one-tenth of its density in grams per cubic centimeter. This yields a volume of fibrous material of 0.1 cc. The sample is then pulled apart and fluffed up with tweezers until it resembles a short length of very loose sliver in which the fibers tend to be somewhat parallelized. The fluffed and elongated sample is then fed into a sloping tray with converging sides, and is wound around the end of a small wire spindle as it is twirled between the fingers. The resulting plug, while being rotated, is introduced into a short cylindrical tube, and the spindle is withdrawn. A sample prepared in this way and transferred to the sample chamber of the arealometer will, when compressed to a fraction of its original length, offer resistance to flowing air which will differ by less than 2% from the value it would have if all the fibers were exactly perpendicular to the flow. Any effort to increase the degree of perpendicularity to flow seems to be undesirable because, in addition to extending the time required for sample preparation, this appears to interfere with the homogeneous distribution of the fibers throughout the volume of the plug.

Calibration of Arealometer

In order to bring this method of testing to a state where it can actually indicate numerical values of specific area, a calibration must be made. The purpose of this calibration is twofold. First, it tests the applicability of the flow equation throughout the chosen range of porosity; second, it indicates a best value for the shape factor, k_o. Several years ago an extended calibration was undertaken using an assortment of cotton varieties. The perimeter and cross-sectional area of many thousands of fiber sections were measured, and an average value of specific area was computed for each variety. When the same procedure was used on some man-made fibers having uniform profile, it became apparent that calibration points associated with cottons were not consistent with those derived from these synthetic fibers. This inconsistency proved to be due to the fact that cotton fibers are thickest near the middle and taper at the ends. Since the usual method of preparing sections for microscopic examination tends to select sections from near the middle of cotton fibers, the results of such measurements are too large. A new calibration was then made using round or nearly round filaments of uniform profile, such as nylon, vinyon, rayon, and Fortisan. A few samples of fine wool were used also.

To make more convenient use of calibration points, equation (2) was rearranged in the form

$$(AL)^{2/3} = \left(\frac{\zeta}{k_o}\frac{1}{\mu m^2 \rho}\right)^{1/3} R^{1/3}\rho a L - \left(\frac{\zeta}{k_o}\frac{1}{\mu m^2 \rho}\right)^{1/3} R^{1/3} m. \quad (3)$$

Values of A measured with the microscope were combined with values of L from the arealometer to plot a graph showing $(AL)^{2/3}$ as a function of L. It is clear from the equation that this should result in a line whose straightness is a test of the applicability of the flow relation within the range covered by the calibration samples, and whose slope for a given value of R indicates the best value for the shape factor, k_o. This procedure was followed using several different values of arealometer standard resistance, R.

Figure 3 shows two rows of points plotted in the above manner for R = 4,000 c.g.s. units and R = 14,335 c.g.s. units (the values adopted for the

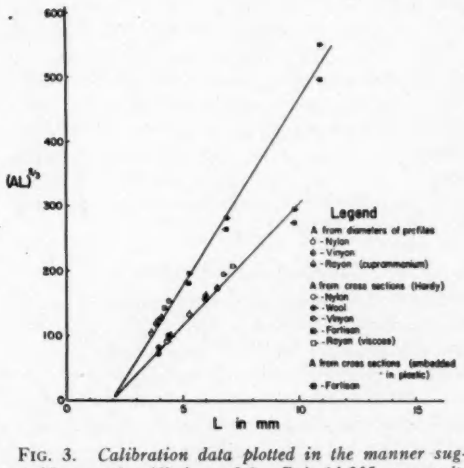

FIG. 3. *Calibration data plotted in the manner suggested by equation (3);* $k_0 = 2.9$. *R is 14,335 c.g.s. units for the upper line and 4,000 c.g.s. units for the lower line.*

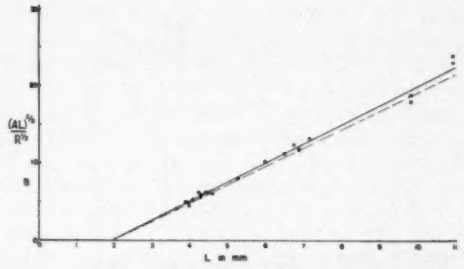

FIG. 4. *Corrected calibration data plotted to indicate a common line for all values of* R. k_0 *is 2.55 for the solid line and 2.9 for the broken line.*

arealometer). Two points are given for each Fortisan value, one obtained from sections embedded in plastic and examined with a metallograph and the other obtained from sections prepared by the usual (Hardy) method. It was at first believed that the plastic-embedded values were more accurate, and the lines drawn in Figure 3 take these points into account. These lines indicate a best value for k_o of about 2.9. Later work on Fortisan based on linear-density determinations indicates that the filaments were slightly swollen by the plastic in which they were embedded, and that the Hardy-section values are more nearly correct. Subsequent to this discovery, linear-density determinations were made on all of the materials used in the calibration. These results, when combined with specific-gravity determinations, allowed all values of A to be corrected for errors in apparent microscope magnification.

Figure 4 makes use of the fact that all calibration points may be reduced to a common line by dividing both sides of equation (3) by $R^{1/3}$. All points in this figure have been corrected as indicated above. The solid line gives 2.55 for k_o. The broken line shows the position the line would have if k_o were 2.9. It is clear that although it is not yet possible to set a very precise value on k_o, the correlation between specific area, A, and arealometer length, L, is fortunately rather insensitive to this value.

Immaturity Ratio

The necessity for keeping the void fraction, ϵ, within a prescribed range puts limits on the range of values of specific area, A, which can be balanced against a given standard resistance, R. To overcome this limitation, a multi-range instrument was developed on which the operator could select a suitable standard R against which to balance the resistance of the fiber sample. Since these ranges could overlap to some extent, there were regions in which a specific-area determination could be made at two different porosities. If the material being tested was round or nearly round, the two values of A obtained were generally in close agreement (both scales having been calibrated with round filaments). Most samples of cotton, however, would yield two different values of A when tested on two ranges, the larger value always being obtained under higher compression. These results indicate an abnormally fast rate of growth of resistance under increasing compression in the case of many cottons.

The unexpected difference between two values of A measured on the same cotton seemed to be greatest for those cottons suspected of being immature. It seemed reasonable to suppose that the flattened or ribbon-like fibers in a plug of cotton would, as the plug is compressed and contacts between fibers are increased, tend to rotate so as to present their broad sides to the direction of the compressing force. This would be roughly analogous to a handful of leaves dropped upon the floor; in mid-air the leaves might be randomly oriented, but when they settle down on the floor they present their broad sides to the pull of gravity.

The tendency of elongated fiber sections to rotate under compression introduces a kind of preferential orientation altering the value of ζ in the flow equation. Since this orientation would tend to lengthen the tortuous path followed by a gas particle in traversing the porous plug, its effect would be to increase the resistance of the plug to flowing air. The extra resistance would then be interpreted as an apparent increase in specific area. If a satisfactory correlation could be established between the spurious increase in A and some property of cotton associated with average shape of fiber cross sections, it was hoped that the arealometer could be adapted to measure the maturity of a cotton sample as well as its fineness.

Before examining the definition of immaturity finally adopted for this work and its connection with arealometer readings, it may be helpful to think about an array of idealized fiber sections and some of the geometric relations which exist among them (Figure 5). Consider an assortment of cylindrical cell walls, circular in cross section and having a variety of diameters. Let cellulose be uniformly

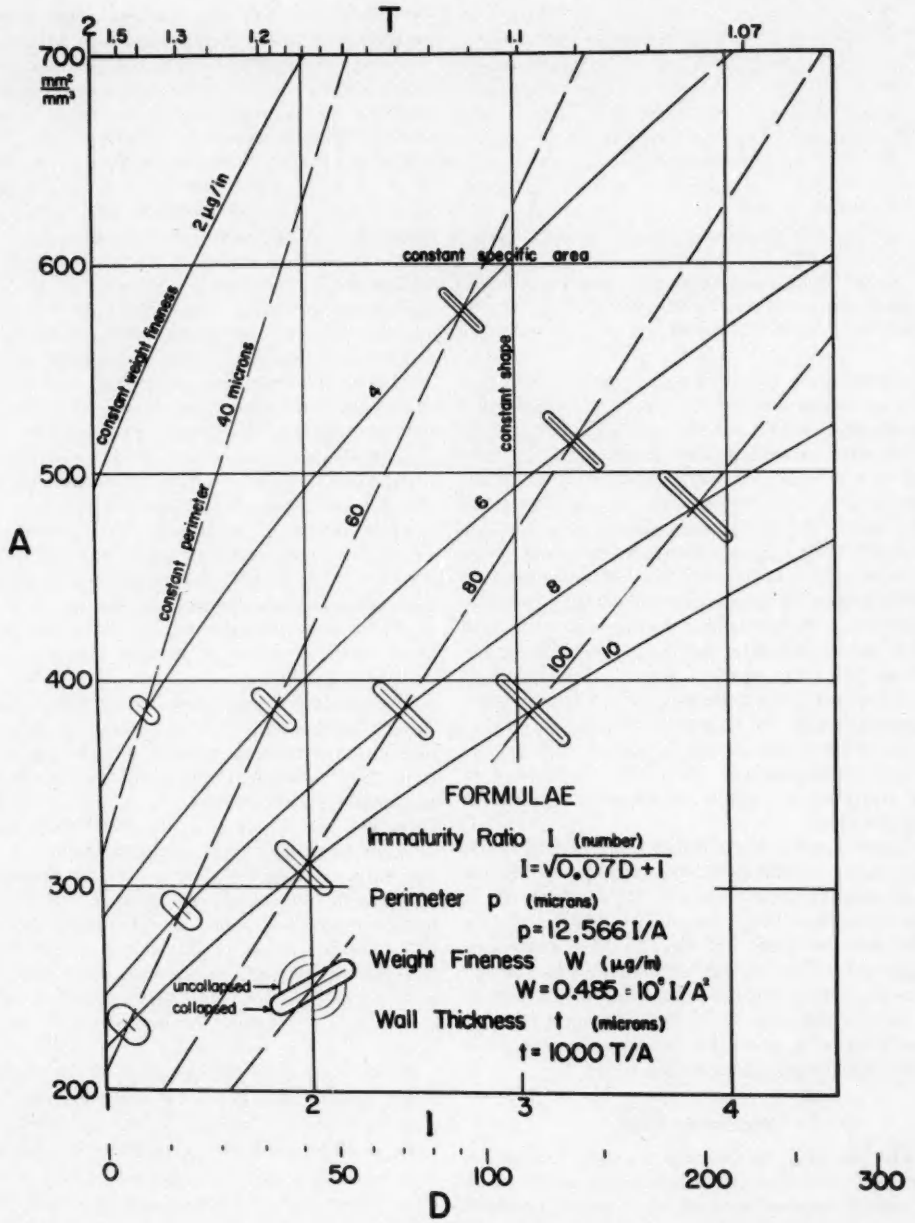

FIG. 5. *Fineness vs. immaturity array, illustrating certain geometric relations among idealized fiber sections.*

deposited on the inner surface of each cell wall, the thickness of the deposit varying from fiber to fiber. A right section through a fiber would then exhibit an annulus of cellulose, one of which is represented near the bottom of Figure 5. Suppose that when the boll opens and drying occurs, each fiber collapses in such a way that the outer perimeter of each annulus becomes two parallel straight-line segments joined at their ends by two semicircles, while the inner perimeter becomes a straight line. The lengths of the perimeters and the area of the annulus will remain unchanged during the collapse. A number of such sections are sketched in Figure 5.

These idealized collapsed sections are convenient in that they lend themselves nicely to calculations of their geometric properties. One property connected with the shape of each section is called the "immaturity ratio," and is defined as the ratio of the total area of a section (including the lumen) before collapse to its area after collapse. The specific area of each section is given by the ratio of its perimeter to its area.

Assume that the following properties have been obtained for each collapsed cross section: immaturity ratio, I; specific area, A; perimeter, p; weight fineness, W (in terms of area and density of cellulose); and wall thickness, t. If a coordinate frame is constructed whose horizontal axis represents values of I and whose vertical axis represents values of A, and if each idealized fiber section is plotted on this graph in its proper position, a number of interesting patterns become apparent in the resulting array. All fibers falling on the same horizontal line will, of course, have the same specific area. All fibers lying on the same vertical line will have the same shape, any one being a magnified or diminished image of any other lying above it or below it, respectively. All fibers having equal perimeters will be found on one of a family of lines radiating from the origin ($I = 0$, $A = 0$). Thus, when a developing fiber is in the process of depositing cellulose onto its primary wall, its future position on the graph may be thought of as progressing from upper right to lower left down one of these straight lines. All fibers having the same weight per unit length (assuming a common density for all cellulose) will lie along one of a family of parabolas having its vertex at the origin. Representative members of both of these families are drawn in Figure 5. Formulas relating p, W, and t with A and I are shown. The scale T at the top of Figure 5 is used to calculate wall thickness, t.

These relationships exist among idealized fiber sections formed in the manner described above, but two practical questions must be considered: how well do the relationships hold for actual fibers, and what is the connection between the property I and the value of D, the increase in apparent specific area produced by compression in the arealometer. It seems reasonable to suppose that D will be influenced by two things, the average degree of flattening of the fibers and the amount the fibers have rotated. The angular rotation itself, however, might also be expected to be proportional to the degree of flattening, or effective lever arm. Therefore, since I is a measure of the degree of flattening, D might be considered to be linearly related to I^2, as a first approximation. We may then write the expression

$$I^2 = CD + B,$$

or, since D must be zero when I is one (for round fibers),

$$I = \sqrt{CD + 1}. \qquad (4)$$

Therefore, if the proper value can be assigned to the constant C, the immaturity ratio, I, of a sample of cotton may be obtained directly from D, the apparent increase in specific area. This value of I, when combined with the arealometer measurement of A, determines the other cross-sectional properties discussed above. They may be estimated by interpolation on a graph like Figure 5, or they may be calculated using the equations listed below.

These equations are easily obtained as follows: let p = perimeter of a fiber; a_c = its area before collapse = $p^2/4\pi$; and a = its area after collapse = p/A. Then $I = a_c/a = Ap/4\pi$, or $p = 4\pi I/A$.

If A is in mm.^{2}/mm.^{3} (the unit in which the arealometer is calibrated), the above expressions will give p in mm. and a in mm.^{2}. p in microns would be given by

$$p = 12{,}566\, I/A. \qquad (5)$$

Weight per inch is equal to the volume of a 1-in. length times the density. Expressed in milligrams per inch, $W = 25.4a \times 1.52 = 38.6\, p/A$; or, expressed in micrograms per inch,

$$W = 0.485 \times 10^6\, I/A^2. \qquad (6)$$

Wall thickness in microns is given by

$$t = 1000\, T/A, \qquad (7)$$

where

$$T = 2/(1 + \sqrt{1 - 1/I}).$$

Experimental Results

In order to assign a numerical value to the constant C in equation (4), values of I must be obtained independent of D on a number of cotton samples. The equations listed above suggest that this might be done by combining arealometer values of A with independently measured values of perimeter, wall thickness, or weight per inch. Since voluminous microscopic section data were available for a number of cotton varieties from the first calibration attempt, described earlier in this paper, average values of perimeter were compared with corresponding values of D. The microscopic data were strongly suspected of bias, however, for the reasons given earlier. Although the perimeter values were apparently too large in absolute value, as suspected, their relative values were good enough to indicate general relationships and to support conclusions based on data otherwise considered meager.

No attempt was made to locate and use fiber wall-thickness data because of the probability of bias in microscopic sections. The weight-per-inch measurements by the array method, on the other hand, should be freer of such bias, although the accuracy claimed for this method leaves something to be desired. Thirty-five cottons from the 1947 Spinning Study were obtained from the Southern Regional Research Laboratory upon which weight-per-inch determinations were made by the Production and Marketing Administration. Six cottons which were tested extensively by a number of laboratories in a Round-Robin "Fineness" Test were also measured by the Production and Marketing Administration. The specific area, A, and the difference, D, were obtained by the arealometer on these cottons. Since $I^2 = 4.25 \times 10^{-12} W^2 A^4$, I was calculated from the weight fineness, W, in micrograms per inch, and the specific area, A, in square millimeters per cubic millimeter, and I^2 was plotted against D in Figure 6. The open circles represent the 1947 Spinning Study cottons, and the solid circles represent five of the "Round-Robin" cottons (the sixth cotton was beyond the arealometer range). It should be noted that W is raised to the second power and A is raised to the fourth power to give the appropriate I^2. Such treatment of data emphasizes the scatter, and hence serves to make the test more stringent. The position of the line was determined visually, and was made to pass through the point (1, 0), as required by equation (4). A value of 0.07 for C seems to be a good approximation to fit these data. This allows equation (4) to be rewritten

$$I = \sqrt{0.07D + 1}, \tag{8}$$

which is the source of the lower horizontal scale on Figure 5. It is tacitly admitted that this value is not determined with satisfactory precision, but can serve as a tentative value since the equation itself is only a first approximation. There is some indication that the value arrived at for C by this method depends to some extent upon the technique used to measure W and upon the state of crimp of the fibers. Further work on this problem is planned by this laboratory.

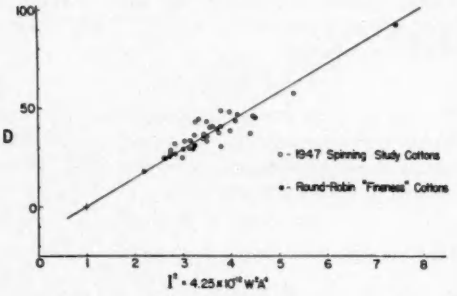

FIG. 6. *Calibration data used to evaluate the constant* C *in equation (4).*

The constancy of average fiber perimeter among all the bolls on the same cotton plant suggests a qualitative check of one of the geometric relations exhibited by Figure 5—*i.e.*, that a plot of A *vs.* I should result in a row of points lying on one of a family of straight lines radiating from the origin. All bolls from three or four plants grown together were analyzed, and the results are shown in Figure 7. Four plants of Trice and three plants of Stoneville 2B each had 46 bolls. The measured difference, D, of each boll converted to immaturity ratio, I, is plotted against the corresponding measured specific area, A, on the left, followed by similar plots of I with the derived perimeter, weight fineness, and wall thickness. The A-I plot shows the approach to linearity, while the horizontal tendency of the p-I plot shows the relative constancy of the perimeter. The W-I and the t-I plots show the variation of weight fineness and wall thickness with maturity among bolls on plants of the same variety grown together. Although the test is not quantitatively critical, it is consistent with what would be expected.

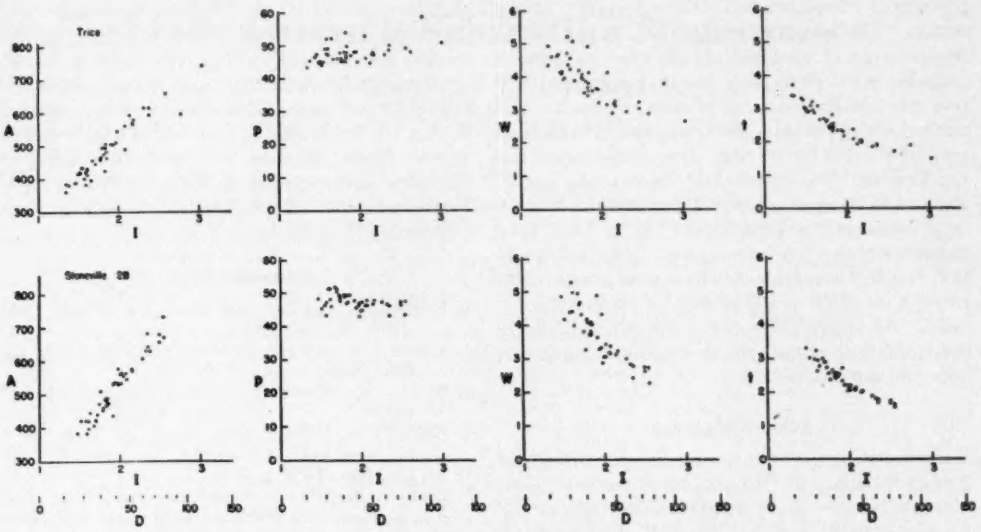

FIG. 7. *Relations among idealized fibers illustrated in Figure 5 applied to data obtained on all bolls from a few plants of two varieties of cotton.*

The comparison of the percent maturity, determined by the caustic soda method, with the immaturity ratio is shown in Figure 8. The open circles represent the 1948 Spinning Study cottons (NaOH data by P.M.A.), and the solid circles represent some special samples being investigated by the Southern Regional Research Laboratory (NaOH data by S.R.R.L.). The crosses represent twelve cottons which had been analyzed at the Vezelinstituut, T.N.O., Holland, and at the Textile Laboratory, University of Ghent, Belgium, by several maturity methods, including the NaOH test. The regression line (not including the crosses) is

$$M\ (\%\ \text{maturity}) = 150.5 - 38.1\,I. \qquad (9)$$

The coefficient of correlation is -0.93. It is not surprising that an extension of the line would give 100% maturity before the immaturity ratio became unity. A fiber may be considered mature by the NaOH test even though the section is elongated to the extent of having an immaturity ratio of 2 or possibly 3.

Conclusions

The preliminary tests reported here indicate that the increase in apparent specific area as observed on the arealometer at low porosity over that at high

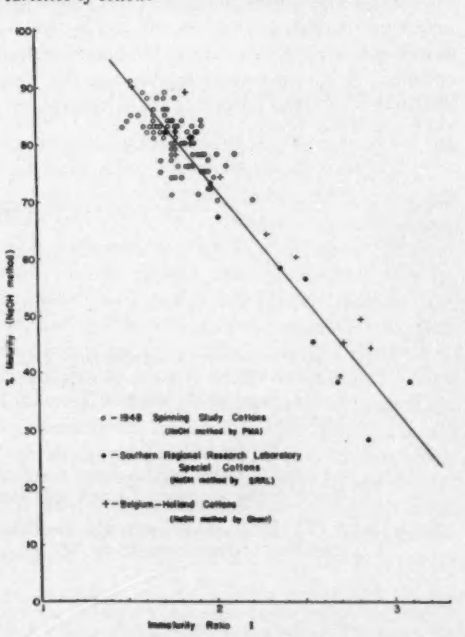
% Maturity (NaOH method)
Immaturity Ratio I
• – 1948 Spinning Study Cottons
(NaOH method by PMA)
• – Southern Regional Research Laboratory
Special Cottons
(NaOH method by SRRL)
+ – Belgium–Holland Cottons
(NaOH method by Ghent)

FIG. 8. *Comparison of percent maturity, determined by the NaOH method, with immaturity ratio, I.*

porosity is correlated with the immaturity of the cotton. The suggested explanation, based on the reorientation of idealized oblong fiber sections, is probably not strictly true but it is approximately true over the limited range of cottons tested. The method does provide a quick measure of both fineness and immaturity from two readings on the arealometer. The standard deviation of the specific area is 4 to 10 mm.^{2}/mm.^{3} in 250 to 600 mm.^{2}/mm.^{3}, or a coefficient of variation of 2% or less. The difference of the two readings has a standard deviation of 3 to 6 mm.^{2}/mm.^{3}, which results in a coefficient of variation of 5% to 10% in the immaturity ratio. An individual operator can make duplicate determinations of both fineness and immaturity on about 50 samples per day.

Acknowledgment

The authors wish to thank the Southern Regional Research Laboratory for samples of the 1947 Spinning Study cottons and weight-fineness data on the "Round-Robin" cottons. They also wish to thank the Production and Marketing Administration for the inclusion of weight-fineness data on 1947 Spinning Study cottons and the "Round-Robin" cottons, as well as the maturity data on 1948 Spinning Study cottons. Acknowledgment is also due the Vezelinstituut of Holland and the Textile Laboratory at the University of Ghent, Belgium, for samples and maturity data on special cottons. Finally, the authors are indebted to Miss Reba Lawson for the arealometer determinations and all calculations included in this paper. This research was supported in part by 9b3 Research and Marketing Administration funds allocated by the Cotton Genetics Technical Committee of the Regional Project S−1, National Cooperative Research in Plant Science for Improvement of Cotton.

Literature Cited

1. Fair, G. M., and Hatch, L. P., *J. Am. Water Works Assoc.* **25**, 1551 (1933).
2. Fowler, J. L., and Hertel, K. L., *J. Applied Phys.* **11**, 496 (1940).
3. Kozeny, J., *Wasserkraft u. Wasserwirtschaft* **22**, 67 (1927).
4. Loeb, L. B., "The Kinetic Theory of Gases," 2nd ed., New York and London, McGraw-Hill Book Co., Inc., 1934, p. 283.
5. Loeb, L. B., "The Kinetic Theory of Gases," 2nd ed., New York and London, McGraw-Hill Book Co., Inc., 1934, p. 293.
6. Kraemer, E. O. (editor), in collaboration with Bartell, F. E., and Kistler, S. S., "Advances in Colloid Science," Vol. I, New York, Interscience Publishers, Inc., 1942, p. 47.
7. Muskat, M., and Botset, H. G., *Physics* **1**, 27 (1931).
8. Sullivan, R. R., *J. Applied Phys.* **12**, 503 (1941).

(Manuscript received August 13, 1951.)

Correction

In the article "Contradictory Data on Spiral Structures in the Secondary Cell Wall of Fibers of Flax, Hemp, and Ramie," by P. A. Roelofsen, which appeared in the June, 1951, issue of TEXTILE RESEARCH JOURNAL, note the following corrections:

(1) In the third paragraph of the Introduction, p. 412, the sentence "In hemp an outer Z-spiral and an inner S-spiral was found" should read "In hemp an outer Z-spiral and an inner Z-spiral was found."

(2) In the table on p. 413 the data of Reimers ([10] and [11]) for the spiral structure of hemp should be "Z" for both the outer and the inner layers.

Flow Through Fabric-like Structures*

S. E. Penner† and A. F. Robertson‡

Institute of Textile Technology, Charlottesville, Virginia

Abstract

A method is presented for the visual investigation of flow through fabrics. The fabric pores are considered as orifices, and the effect of weave structure on the fluid flow is investigated in the range of Reynold's numbers 10 to 400.

For this investigation, a liquid is forced past models representing the four possible combinations of yarns in a woven fabric interstice, and the fluid motion is visualized by using air bubbles, which are detected by means of a suitable light source, as the distinguishing medium. Since both the fluid and the construction material for the models and viewing chamber are translucent and possess the same refractive indices, it is possible to obtain uninterrupted, undistorted visualization of the fluid flow through and past the fabric-like structures. Visual and photographic investigations of the flow are made in various significant planes normal to the fabric-like structures, or parallel to the direction of flow. The resulting photographs are analyzed and interpreted to provide information concerning the effect of fabric construction and variation of Reynold's number on the area available for the passage of fluids through each pore type, or the so-called "effective pore area."

It is shown that the four pore types do not behave like geometrically similar orifices, so that for a given diameter/pitch ratio the effective pore area is not the same in all cases. This area decreases with increasing Reynold's number. Except at very low Reynold's numbers, the effective pore area proves to be less than the actual minimum pore area, but greater than the projected area, with the exception of the plain-weave pore type. Assuming a minimum cross-sectional pore area, as determined by graphical analysis, it is shown that the effective pore area/minimum pore area ratio is almost a constant for all four pore types of the models tested at a Reynold's number of 400.

Introduction

The subject of fluid ** flow through fabrics has been extensively investigated. It is of practical importance in the utilization of fabrics for parachutes, clothing, filtration media, collapsible shelters, and dust-collecting bags. It is also associated with many problems involving the drying of fabrics. No attempt has been made, however, to actually visualize the flow of fluids through fabrics, although studies of this nature have been applied in other fields. The data obtained by such a study could contribute to a better understanding of the flow process and prove useful in developing the most efficient design of the fabric. The porosity †† of a fabric is dependent upon many factors, weave structure being one of basic importance. The effect of weave structure readily lends itself to visual investigation. The purpose of the experiments described herein was to help explain the influence of fabric weave on porosity.

The previous investigations of fluid flow through fabrics and fabric-like structures assumed diverse forms, with various objectives in view. One approach was to consider the resistance or drag coefficients of screens, perforated plates, grids of metal tape, and textile fabrics; this was done both theoretically and experimentally by several different investigators [8, 11, 22, 31, 32, 33]. In the usual consideration of textile fabrics, on the other hand, the emphasis has been on permeability or porosity rather than resistance. Some investigations were designed to correlate the porosity of fabrics with their thermal insulating properties [23, 27], windproofness and waterproofness [23], and drying characteristics [6]. Most of the early work, however,

* This paper is based on work done by S. E. Penner in partial fulfillment of the requirements for the M.S. degree at the Institute of Textile Technology, Charlottesville, Va.

† Present address: Department of Chemical Engineering, Columbia University, New York, N. Y.

‡ Present address: Building Technology Division, National Bureau of Standards, Washington, D. C.

** "Fluid" in this paper refers to liquids and gases.

†† The term "porosity" is used in this paper, as in a previous one [26], to mean a measure of the ability of a fabric to allow mass flow of air through it. "Porosity" is used in this way to distinguish the resulting type of flow from that occurring in very closely woven fabrics, where the flow becomes a linear function of pressure drop. The term "permeability" is more descriptive of the type of flow occurring in the latter case.

involved developing an instrument and establishing the principles and conditions for measuring the air permeability and porosity of fabrics; this work was reviewed in a series of articles by Sieminski and Hotte [29, 30]. More recently, Rainard [25] proposed a new technique for measuring permeability.

Of particular interest is the work that has been done to explain the effect of fabric construction variables on permeability [5]. Although Wakeham and Spicer [35] showed a good correlation to exist between permeability and the interfiber and intrafiber voids of a tightly woven fabric, it is usually conceded that the porosity of an open-weave fabric is mainly dependent upon the interyarn pores. Many workers recognized that for fabrics of a given fiber, yarn diameter, and texture, the porosity to air and other fluids is further dependent upon the type of weave. Thus, Draper [7] concluded, on a logical basis, that a fabric of plain weave would be more resistant to the passage of air than a twill, the latter, in turn, being less porous than a satin. Draper's deductions were semiquantitatively confirmed by other workers [2, 26, 28]. A similar relationship between weave and moisture transference was noticed by Gregory [13]. Hance [14] found that the filtration-resistance of plain-weave, oxford-weave, 2/1 regular twill, 2/1 herringbone twill, and 5-harness sateen fabrics decreased in that order.

In a different approach to the study of fluid flow through fabrics, the interyarn pores (which are dependent upon the picks and ends per inch, yarn diameter, and type of weave) were considered to behave like orifices. Gregory, one of the first to draw the analogy, assumed the pores to act as orifices in explaining the effect of pore size and distribution on the moisture-transference properties of fabrics. Blue [4] and Robertson [26] also attempted to show the relationship between fabric pores and circular orifices or nozzles by calculating discharge coefficients for a series of plain-weave screens and fabrics, plotting them against Reynold's numbers, and comparing the resultant curves to curves obtained similarly for circular orifices or nozzles. In both of these papers, the discharge coefficients, C, and Reynold's numbers, Re, were calculated from the same formulas as used for the circular orifices:

$$C = \frac{Q}{A_2 \sqrt{\dfrac{2gh}{1 - \left[\dfrac{A_2}{A_1}\right]^2}}};$$

and

$$\mathrm{Re} = \frac{V d_e \rho}{\mu}.$$

The ratio A_2/A_1 was determined from the projected area of the openings, A_2, and the total area of the sample A_1, while the volumetric flow, Q, was observed experimentally. In calculating Reynold's number, the geometric dissimilarity of the bodies was bridged by using the value of four times the hydraulic radius of the fabric pore for the equivalent diameter, d_e.* The hydraulic radius may be defined in this case as the projected area of the pore divided by the length of the projected perimeter.

While the results of these investigations did demonstrate the possibility of treating fabric pores as orifices or nozzles, and the dependence of the discharge coefficient (and, consequently, porosity) on the Reynold's number, they did not account for the difference in behavior of the plain and twill weaves. It was indicated, however, that the relationship of discharge coefficient to Reynold's number would probably depend upon the type of fibers comprising the yarn—*i.e.*, cotton, wool, rayon, etc.

It seems fairly well established, then, that the flow through fabrics may be quantitatively treated by the use of basic dimensionless units in a manner similar to that used for nozzles and orifices. The application of this principle has been limited because the orifice-like behavior of a fabric interstice, or pore, is not only dependent upon the diameter/pitch † ratio, but is significantly dependent upon the weave. This means that unless the geometrical dissimilarity between the possible types of pores is bridged by a suitable parameter, it will be possible to obtain only generalized theoretical relationships between the discharge coefficient and Reynold's number for a given type of weave. In practice, it would be useful to compare the porosity of fabrics which not only differ in basic weave type, but also consist of combinations of weaves. Consequently, in order to enlarge the scope of this fundamental approach to the flow of fluids through fabrics, it is necessary to characterize fabric pores in such a way that the expression for the open area is not dependent upon the type of weave.

* This procedure is given in "Chemical Engineers' Handbook" (edited by Perry, J. H.), New York, McGraw-Hill Book Company, 1941, p. 799.

† The ratio of yarn diameter to the distance between centers of adjacent yarns (pitch) is called the diameter/pitch, or d/p ratio.

TABLE I. DESCRIPTION OF PORE TYPES AND MODELS TESTED

Pore type	Description	Typical relative M.P.A.*	Model No.	Model d/p
A	None of the yarns in the unit cell alternate from the top to the bottom surface of the cloth or vice versa	1.000	1	0.364
B	Either two warp yarns or two filling yarns alternate	0.934	2	0.348
C	One warp and one filling yarn alternate	0.934	3	0.364
D	All four yarns alternate from top to bottom surface	0.698	4	0.326

* Relative minimum pore area based on pore type A.

A method for expressing the fabric open area in a manner independent of weave was proposed by Backer [3], on the basis of the geometry of the interstices. If planes perpendicular to the fabric surfaces and bisecting any two adjacent warp and filling yarns be used to form a unit cell, four basic categories of pores can be established; these are given in Table I. By taking successive sections of each unit cell at various depths below the fabric face and graphically measuring the ratio of open area to obstructed area, it is possible to arrive at a value called the "minimum cross-sectional pore area" * for each typical type. This area is defined as the total area of a unit cell minus the maximum yarn area in the plane of the section. For constant diameter/pitch ratio, the four interstice types will not have the same minimum pore area, although the projected area in each case may be equal. For a typical fabric of constant diameter/pitch ratio (0.4), the relative minimum pore areas are indicated in Table I. Upon comparison of these data with the empirically known performance of various types of weaves, it is apparent that the pore types having the largest minimum pore areas actually do predominate in the fabrics with the greatest porosity. For example, satins and twills, consisting predominantly of pore types A, B, and C, are more porous than plain weaves, which consist entirely of pore type D. For this reason, Backer proposed the minimum pore area as better than the projected area for defining the area actually available for the passage of fluids. The use of a minimum pore area such as he suggests is not sufficient in itself; it must be used in a more general equation which will allow for viscous effects of the flowing fluid.

In the final analysis, the rate of fluid flowing through a fabric pore (and, consequently, the porosity) is essentially dependent upon the minimum cross-sectional area of the stream tube, or jet, and the velocity of fluid flowing. Although the projected area has been used as an estimate of the jet area, and the minimum pore area has been proposed by Backer as a better estimate of this area, no conclusive evidence has been presented concerning the nature of the jet issuing from orifices of the type under consideration here. In view of the complex nature of these fabric pores and the geometrical dissimilarities among them, it is not possible to consider them as analogous to conventional orifices in a flat plate, or even to nozzles. It was felt, therefore, that a suitable visual investigation would, in some measure, provide evidence concerning the nature of the flow process through each of the possible types of pores.

Experimental Procedure

Theory of Fluid-Flow Visualization

There are certain fundamentals of fluid dynamics and commonly accepted definitions which provide the basis for the visual investigation of fluid flow. Before proceeding to the application of this technique, it is necessary first to consider briefly the important underlying theory.

Liquids and Gases as Continua.—The study of fluid flow is concerned with a determination of the behavior of the fluid as a whole, or such parts of it as contain a great many molecules. In other words, it is not the motion of the molecules themselves which is of interest, but rather their mean values in space and time. Liquids and gases may usually be considered to have molecular mean free paths of negligible dimensions, and can therefore be considered as continuous media. In this respect, it has been shown by Knudsen [17] that if the mean free path of gaseous molecules is less than one-tenth of the diameter of the opening, mass motion occurs, in contrast to molecular streaming. Since a typical fabric * to which the results of this investigation are to be extended has pores of the order of 1.5×10^{-2} cm. wide, and since the mean free path of the air molecules is only 6.40×10^{-6} cm. at atmospheric pressure, it seems reasonable to assume that the air flow through a fabric pore may be considered as continuous.

* To be called "minimum pore area," "cross-sectional" being understood.

* Cotton cloth, warp and filling of 80's yarn, texture of 100×100 threads per inch, and diameter/pitch ratio of 0.4.

Laws of Similarity.—Since in the proposed investigation the usual prevailing conditions were altered, in that a liquid was substituted for a gas (air) and a fabric-like structure was utilized instead of a fabric, the question arises as to the potential validity of the results. By observing the following laws of similarity, apparently divergent results obtained from similar fluid phenomena may be correlated:

(1) Geometric Similarity: The shape and ratio of the dimensions between the model and prototype must be the same.

(2) Kinematic Similarity: If two similar objects are placed in similar fluid flows, another type of similarity, kinematic similarity, exists if the motion of the fluid about the objects is the same.

(3) Dynamic Similarity: Combined geometric and kinematic similarity results in dynamic similarity. Only one ratio, the Reynold's number, is necessary to characterize dynamic similarity.

If, then, the Reynold's number is the same for each of two different flows around geometrically similar bodies, it is to be expected that the streamlines themselves would also be geometrically similar. In addition, this fixes no theoretical restrictions as to the fluid which may be used in the testing of a model; any fluid may be used, providing that the Reynold's number of the model can be made equal to that of the prototype, and provided that compressibility can be neglected.

In spite of the great differences in compressibility of gases and liquids, it seems possible for the purpose of this investigation to neglect this difference. This is justified by the very small pressure drops that are actually effective across the fabric as compared to the static pressure at which porosity tests are usually conducted. The ratio of these two pressures is about one to 800 for standard A.S.T.M. permeability tests.

On the basis of these principles, a visual investigation of liquid flow through fabric-like structures may be conducted, and an indication of the nature of air flow through open-weave fabrics obtained.

Principles and Construction of the Apparatus

There are numerous methods of visualizing fluid flow. The early work of this nature has been discussed and summarized by Goldstein [12] and Prandtl and Tietjens [24]. In addition, the technique of visualizing fluid flow has frequently been applied in more recent years [1, 9, 15, 16, 19, 20, 21, 34, 36, 37]. Many of the previously employed methods used air as the fluid, but this may not be as convenient to work with as a liquid. Sometimes the visual investigation was confined merely to the surface or boundary layer of the object, an approach which was of little interest in the present study. In the past, where liquids (usually water) were used, the investigations were often conducted in open channels, but this technique involves the objectionable presence of an air-water interface. More recently, pipes or tunnels have been used with a liquid as the fluid [10, 18]. None of these attempts permitted visualization of the flow through the object. A new technique, therefore, which permits visualization of the fluid flowing through and past the model was devised.

The underlying principle in the method used here is to force a liquid through and past transparent models representing fabric pores. In order to make the fluid flow visible, air bubbles are dispersed in the liquid so that upon suitable illumination they reflect the light in a manner similar to that used in the ultramicroscope. The behavior of these bubbles is indicative of the fluid motion in their vicinity, and can be conveniently visualized and photographed. A unique feature of the method is the use of a transparent model and viewing tunnel having the same refractive index as that of the fluid. This permits an uninterrupted view of the whole flow channel, and thus makes possible the study of flow conditions around the model in locations which would otherwise be hidden by a normally opaque model. The models and tunnel were made of a methacrylate plastic, and Immersion Oil * was used as the fluid.

A variety of materials were investigated for mixture with the oil to provide a means for making the flow visible. None of these solids or liquids proved to be as satisfactory as air. Although a substance with a density more nearly equal to that of the oil would have been preferable, it was felt that for the degree of accuracy required in this investigation the air bubbles would serve the purpose. The viscosity of the fluid, the velocity of the bubbles, and the short path under observation combine to effectually eliminate serious errors resulting from the influence of bouyancy.

* Immersion Oil, D line 25°C, 1.490 ± 0.001, sp.gr. = 0.935; manufactured by R. P. Cargille, New York, for inspection of glass and quartz. This particular oil proved to be very stable with respect to all materials used in construction of the apparatus. It did attack rubber, but not the synthetic substitutes which were used. Its volatility was so low as to be no cause for concern.

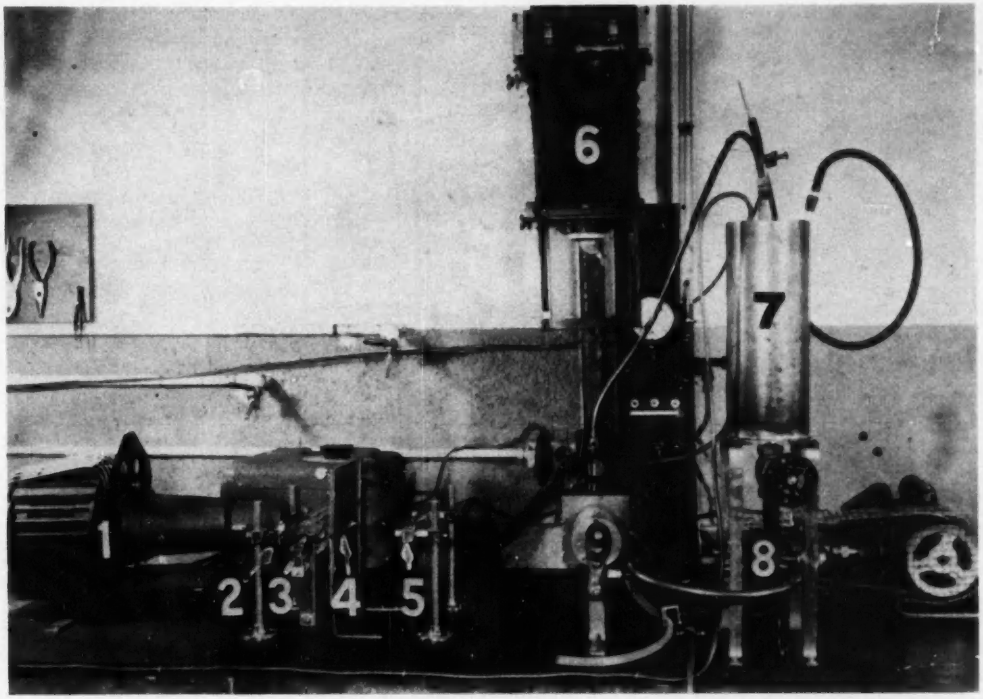

FIG. 1. *General view of the apparatus.* 1—*Projection lamp.* 2—*Cylinder lens.* 3—*Cylindrical light interrupter.* 4—*Slit.* 5—*Cylinder lens.* 6—*Camera.* 7—*Reservoir.* 8—*Pump.* 9—*Viewing chamber and tunnel.*

Figure 1 shows a general view of the apparatus. The viewing chamber consists of a 10-in. length of Lucite tubing, of approximately 2 in. inner diameter and $2\frac{1}{2}$ in. outer diameter, surrounded by a 4-in. square Lucite rectangular housing which is filled with Immersion Oil to eliminate astigmatic distortion that would ordinarily result from the curved surface of the tube. At the top of the rectangular housing is a small overflow reservoir to allow for thermal expansion of the oil. The housing is constructed of $\frac{1}{4}$-in. Lucite sheet, joined by immersing the connecting edges in glacial acetic acid for approximately 15 min., fitting into position, and allowing to set. The end plates were made of $\frac{1}{2}$-in. brass sheet, coated with Duco Cement, and fastened by machine screws at each end of the Lucite housing. The tube passes through the rectangular housing, the liquid-tight seal between the end plates on the housing and the tube being accomplished by means of "O" rings.* The whole assembly (Figure 2) is connected to the fluid circulating system by means of brass adapters at each end, with "O" ring seals between the adapters and the tube.

The Immersion Oil is recirculated from a reservoir of about 0.7 gal. capacity by a small centrifugal pump. The pump is driven by a $\frac{1}{3}$-h.p., 1,725-r.p.m. electric motor, with a "V" belt drive providing a pump speed of about 3,450 r.p.m. The flow is throttled by a gate valve at the outlet fitting of the pump. Half-inch copper tubing connects the throttling valve to the inlet of the viewing chamber. A perforated brass baffle plate and wide-mesh screen at the inlet of the viewing chamber and a fine-mesh screen just preceding the model serve to produce almost uniform velocity of the fluid approaching the model. The average

* For a discussion of the use of "O" rings, see "A Handbook on Synthetic Rubber Packings," 2nd edition, 1948, Philadelphia, E. F. Houghton & Co., 1948, p. 63.

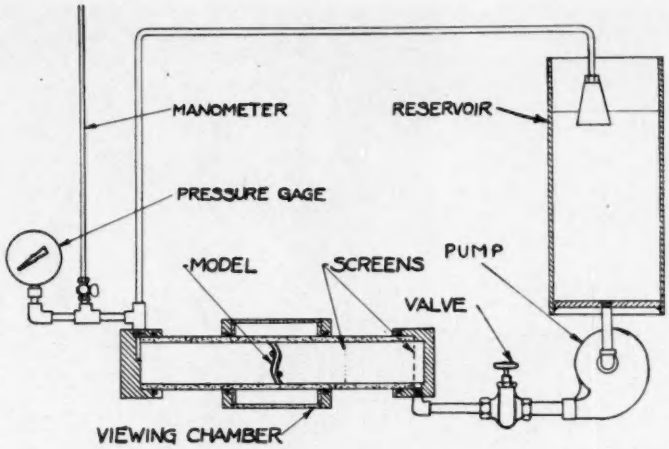

FIG. 2. *Viewing-chamber assembly.*

liquid velocities in the system are indicated by a 0–30 p.s.i. pressure gage and an open-end manometer, which measure pressure drop across the fluid return line. The manometer is used for accurate indication in the low-velocity range. To prevent excessive aeration, the return line, of three-eighths copper tubing, discharges through an expansion nozzle and screen arrangement located below the surface of the liquid in the reservoir. The reservoir has a water-cooling coil immersed in it for temperature control. A valve at the outlet of the reservoir and a drain line from the viewing chamber permit dismantling the apparatus for inserting the models.

The illuminating system, as shown in Figure 1, consists of a 500-watt projection lamp with a mirror reflector and collimating lens. As the light emerges from the lamp it is focused on an adjustable slit by means of a cylinder lens. The light from the slit is collected by another adjustable cylindrical lens, and is projected in a horizontal sheet (approximately $\frac{1}{16}$ in. thick), parallel to the direction of flow, across the 4-in. length of the viewing chamber. By vertical adjustment of this second lens, the light can be focused in any plane throughout the cross section of the viewing chamber. Between the light source and the slit is a cylindrical interrupter made of a Lucite tube ($2\frac{1}{2}$ in. outer diameter and 2 in. inner diameter) with sixteen longitudinal $\frac{1}{16}$-in. grooves which are painted black and equidistantly spaced along the surface. The interrupter is rotated around its cylindrical axis by a friction-disc type of variable speed drive, enabling adjustment of the interrupter speed. A mechanical counter is attached to the interrupter shaft which, with the aid of a stop watch, permits accurate determination of the interruptions per second. The purpose of the periodic interrupter is to break the photographed streamlines into discontinuous dashes. Since the interruptions per second can be determined, and the length of each dash measured, it is possible to calculate the velocity of the particles from the photographs, and thereby determine the velocity of the fluid in the vicinity of each particle track measured.

A 5 in. × 7 in. view camera, with an *f* 4.5 lens and a 4 in. × 5 in. reducing back, is mounted vertically above the viewing chamber. The lens axis is perpendicular to the light plane through the viewing chamber, so that the bubbles passing through the plane of illumination scatter a portion of the light into the camera. Some undesirable reflection results from glue joints in the model, from points of connection between the model and its supports, and, in some planes of visualization, from the supports themselves.

The models were mounted approximately in the center of the viewing chamber, normal to the direction of flow, by two supports emanating from downstream. Short lengths of $\frac{1}{8}$-in. plastic rod were threaded into the model at one end and fitted into the ends of $\frac{1}{8}$-in. brass rods at the other end. The plastic portion in the viewing chamber prevented, as far as possible, unwanted light scattering, while the remainder of the support was made of brass for rigidity. The supports were found to slightly affect the flow pattern in their immediate vicinity, so that

towards the end of the experimental work an attempt was made to secure the models in position by means of two very fine wires fastened upstream from the model. This proved to be a more satisfactory method.

Fabric Models

In the usual preparation of models for visual investigation of fluid-flow phenomena, it is customary to construct the models either full scale or on a smaller scale than the prototype. In view of the nature of this investigation, however, the models were made on a larger scale than actual fabrics. As long as the laws of similarity are considered and the walls of the viewing chamber do not affect the flow pattern, the large-scale models should cause streamlines that are geometrically similar to those that would result in the case of an actual fabric under the same conditions of flow.

Since the purpose of this work was confined to an investigation of the effect of pore construction, the four pore types proposed by Backer provided a scheme for variation of the models which was easily adapted to this method of studying fluid flow. The models shown in Figure 3 are all made of $\frac{1}{4}$-in. Plexiglas rods, and are described in Table I.

Calibration of Apparatus *

The velocities through the viewing tube were calibrated with reference to the pressure gage and open-end manometer by means of the discharge method. The manometer was used to measure velocities from 0 to 0.1 ft. per sec., while the pressure gage indicated the velocities from 0.1 ft. per sec. to the maximum attainable velocity. A temperature of 80°–90°F was maintained during the calibration and subsequent investigations. The viscosity and specific gravity of the Immersion Oil were also determined in this temperature range and were found to be approximately 8.8 centipoises and 0.935 g./c., respectively.

Using the velocity calibration, viscosity and density values of the Immersion Oil, and dimensions of the model and tube, the maximum attainable Reynold's number through the pore was found to be almost 400. The pressure readings corresponding to approximate Re = 10, 50, 70, 100, 300, and 400 were calculated for model No. 1. Since the other models had almost the same dimensions, and the same viscosity and density prevailed, these pressures were used also for models No. 2, No. 3, and No. 4 to give essentially the same Reynold's numbers. It should be mentioned that the projected area of the model was subtracted from the total cross-sectional area of the tube, and this projected open area was used to calculate the velocity through the model. The effective diameter was based on four times the projected hydraulic radius of the pore. These values of velocity and effective diameter were substituted in the Reynold's equation for calculation of the Reynold's number through the pore. As a result of this investigation, however, the use of projected areas for the above calculations might be questioned, as will be discussed later.

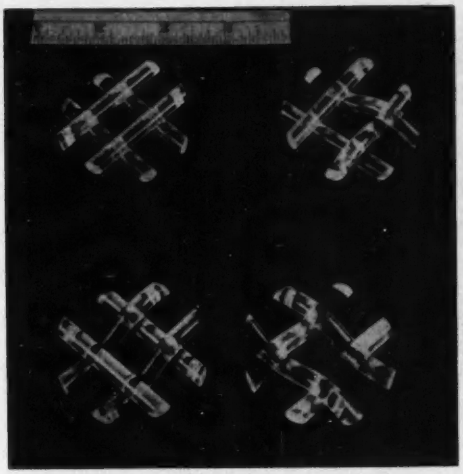

FIG. 3. *The models investigated.* Top left—*No. 1.* Bottom left—*No. 2.* Top right—*No. 3.* Bottom right—*No. 4.*

The uniformity of fluid velocity as it approached the models was determined in one plane at a Reynold's number of 400. One of the photographs was divided into cells, and the distances between consecutive interruptions of the light scattered by the air bubbles was measured. These values were recorded together with the average position at which the measurement was made. Upon consideration of the rate of periodic interruption and the distance between consecutive interruptions, it was possible to calculate the velocity of the fluid flowing. The average velocities in the area $\frac{1}{8}$–$\frac{3}{8}$ in. upstream from the model are graphically represented in Figure 4. This indicates that the screens are functioning approximately as

* Other data and sample calculations pertaining to the calibration are included in the Appendix of the original thesis.

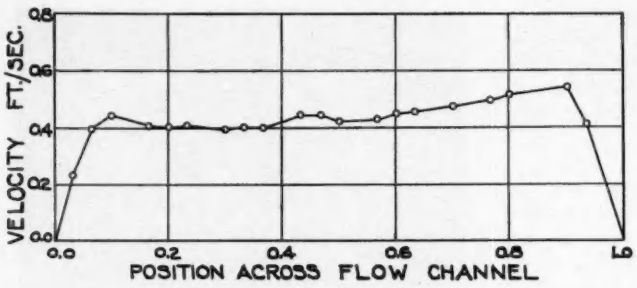

FIG. 4. *Velocity profile of fluid approaching the model.*

intended, by producing a nearly flat velocity profile of the fluid as it approaches the model, and also illustrates the technique of determining velocity profiles with this apparatus.

It was also important to know if the flow pattern changed with time or remained relatively constant. No indication of a fluctuating flow pattern was observed visually. A further check on the reproducibility was conducted by taking several pictures for a given set of operating conditions. Since each picture exhibited essentially the same streamline formation, the flow was assumed to be viscous, or nonturbulent.

A final consideration was to ascertain the effect of the walls of the viewing tube on the resultant streamlines. An inspection of the photographs indicated that at the higher velocities and in the regions where the fabric components intersected there was some distortion of the flow pattern due to the proximity of the walls to the model. For interpreting these pictures, therefore, it was decided to consider that the streamlines around the cylinders would be symmetrical if it were not for the walls of the viewing tube.

Procedure for Investigation

It was originally intended to investigate the models in the range of Reynold's numbers 10 to 1000. This range was chosen for two reasons: first, previous work on flow through fabrics [4, 26] and screens [9] had been conducted in this range; second, values within this range are used for testing fabrics on the Frazier permeability tester. Although the maximum attainable Reynold's number in the visualization apparatus was only 400, this limitation was accepted since to correct it would have necessitated time-consuming modifications of the apparatus or changing the size of the models.

The flow through and past the models was investigated over the available range of Reynold's numbers at the planes indicated in Figure 5. The temperature of the fluid was maintained between 80°–90°F by the cooling coil in the reservoir. The camera was held stationary, while the plane of illumination was moved vertically up or down and the model rotated as necessary. The number of different positions of each model that it was required to investigate depended upon the geometrical shape of the pore. The more symmetrical models required investigation at fewer positions. Each position was investigated at the six different pressures corresponding to the desired values of Reynold's numbers.

The light was projected in the desired plane by adjusting the second cylinder lens. The depth of the light plane could have been varied by changing the setting of the adjustable slit, but a constant depth of approximately $\frac{1}{16}$ in. was used. The interrupter speed was set to give a particle track on the film of $\frac{1}{8}$–$\frac{1}{4}$ in., regardless of the velocity.

The air bubbles used to distinguish the fluid elements were introduced by blowing through a pipet whose end was situated at the outlet of the reservoir. The usual procedure was to introduce an excessive amount of air, let the fluid circulate until some of the air had separated out, and, when the desired concentration remained, to take the picture. This procedure proved advantageous in that the concentration of reflecting particles could be easily varied independently of the shutter speed.

The pictures were taken at f 4.5, with shutter speeds of from 1 to $\frac{1}{25}$ sec., depending upon the velocity, concentration of air bubbles, and effect desired in the ultimate picture. The camera was set to give an image about three-quarters of full scale. Kodak, Super Panchro Press-Sports type, sheet film (ASA tungsten rating of 200) was used for most of the photographs. The film was developed for

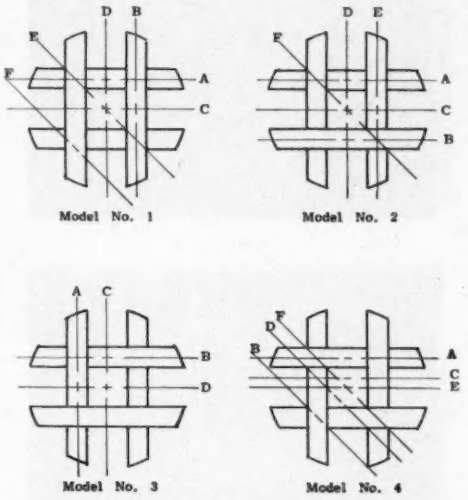

FIG. 5. *The planes through which the flow was photographed for each model. Flow is normal to and into the paper in the planes as indicated.*

10 min. in Kodak D-11 in order to get maximum contrast.

Experimental Results

Effective Pore Area of Fabric-like Structures

With the premise that an "effective pore area" is determined by the minimum cross-sectional area of the jet, or stream tube, through the pore, it would seem that the porosity of the structure is ultimately dependent upon this area and the average velocity of fluid flowing. The shape of the jet, in turn, is dependent upon the Reynold's number, the size and surface of the pore, and the manner in which its components are interlaced. In line with this reasoning, an experimental investigation was conducted in which the projected area and the surface of the pore walls were maintained constant, but the pore structure and Reynold's number were varied. More than 200 photographs were taken at various significant planes through the models and at different Reynold's numbers in order to obtain data concerning this effective pore area. Representative examples of these photographs are presented in Figures 6 and 7.

Influence of Reynold's Number.—The photographs in Figure 6 illustrate the development of the wake with increasing Reynold's number. The light plane was projected normal to the paper through plane D of model No. 1, and the Reynold's numbers varied approximately from 10 to 400, as indicated.

It is apparent that as the Reynold's number increases, there is a corresponding increase in the size of the wake. At the low Reynold's numbers (approximately 10) the flow around the cylinders is more nearly ideal, that is, very little separation or eddying taking place, and the minimum jet area approaches the minimum pore area, as proposed by Backer. As the Reynold's number increases, however, there is separation of the fluid from the walls of the pore and contraction of the jet. In this case, the area available for the further flow of fluids departs from the minimum pore area and is dependent upon the cross-sectional area of the jet at the plane of maximum contraction.

The possibility that the jet contraction may approach a constant as Reynold's number is increased has not been investigated because of the limited range of velocities possible with the apparatus. It must also be remembered that only one diameter/pitch ratio has been investigated, and conditions may change significantly for other ratios.

Influence of Pore Structure.—The size and characteristics of the wake, which are associated with jet contraction, not only vary with increasing Reynold's number, but also depend upon the construction of the pore. Figure 7 presents photographs of flow through corresponding planes of models No. 1 and No. 2. Inspection of these photographs, for example, shows that the flow is not so much affected by the individual pore components, whether they are straight or crimped, but rather by their arrangement. That is to say, the manner in which the components of the pore are interlaced (type A, B, C, and D, given in Table I) has a decided influence on the shape of the issuing jet.

In order to demonstrate the variation in jet pattern resulting for each of the pore types, an attempt was made to plot the jet cross-sectional area at the plane perpendicular to the direction of flow where it was a minimum. The location of this plane was estimated by study of the photographs of each of the four pore types at flow corresponding to a Reynold's number of 400. Measurements were then made of the width of the jet at this plane in each of the photographic sections which were recorded. Where the walls noticeably affected the streamlines, they were assumed to be symmetrical around the pore components, and the jet width was estimated accordingly. The measured and estimated jet widths obtained from

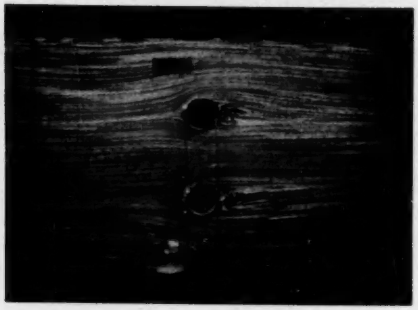

Re = 10

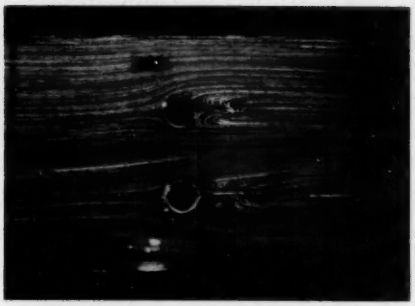

Re = 50

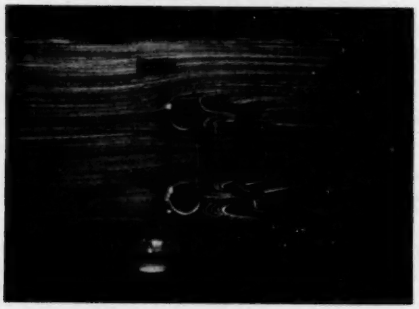

Re = 70

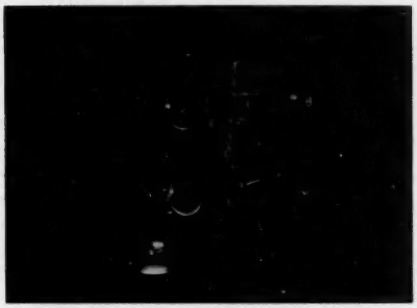

Re = 100

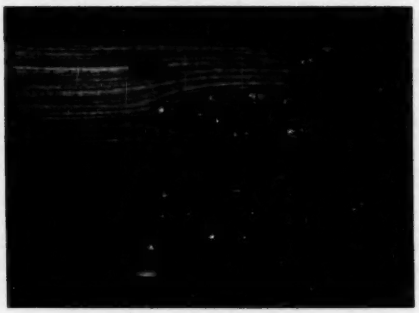

Re = 300

Re = 400

FIG. 6. *Flow in plane D past model No. 1, with increasing Reynold's number. Flow is from left to right.*

the photographs were then plotted on a projection drawing of the corresponding model. The points were joined by curves based on a study of the photographs and visual inspection during the course of investigating each model. Figure 8 shows the resulting minimum jet cross-sectional areas obtained by this method for each unit cell. These figures indicate that the performance of each pore type is dependent upon the construction of the pore, and not merely the projected area or diameter/pitch ratio.

The areas of the jets plotted in Figure 8 were subsequently measured with a planimeter. Projection prints of the models were made, and the projected area of both the pores and the unit cells were similarly measured. By graphical analysis of the pores, the relation between unit cell and minimum pore area was determined, permitting calculation of the minimum pore area. From these values the relations between the jet area, minimum pore area, and projected area were calculated; the data are given in Table II.

The plotted jet areas and subsequent ratios may, at best, be considered only as good approximations; but, bearing this in mind, they still permit certain conclusions. It is evident from the data that in the case of models No. 1, No. 2, and No. 3, the jet area,

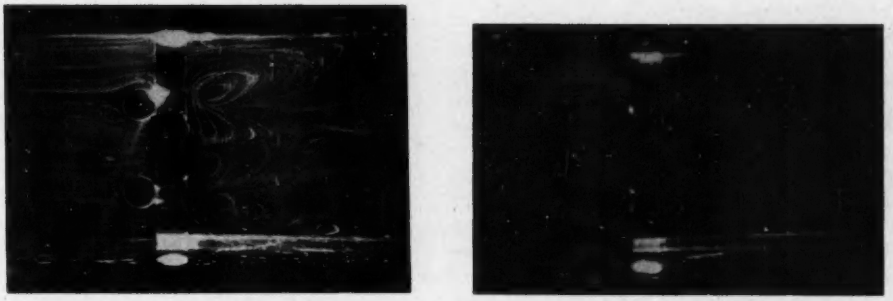

Plane A

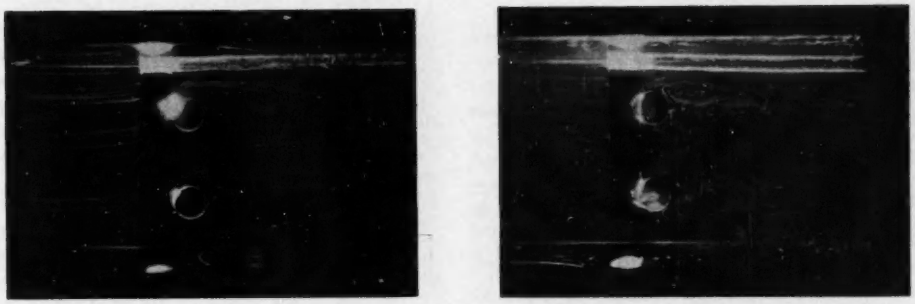

Plane B

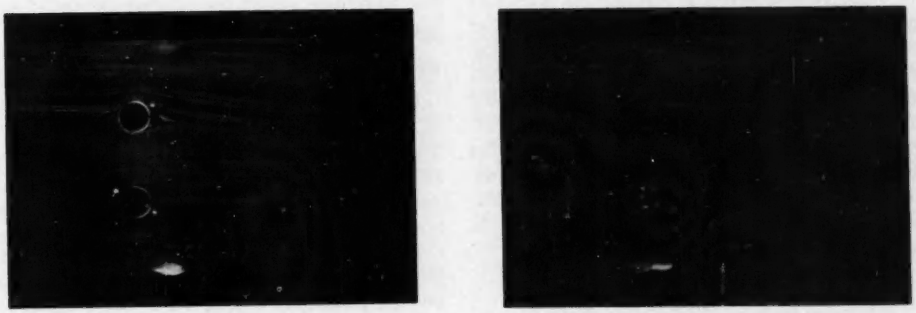

Plane C

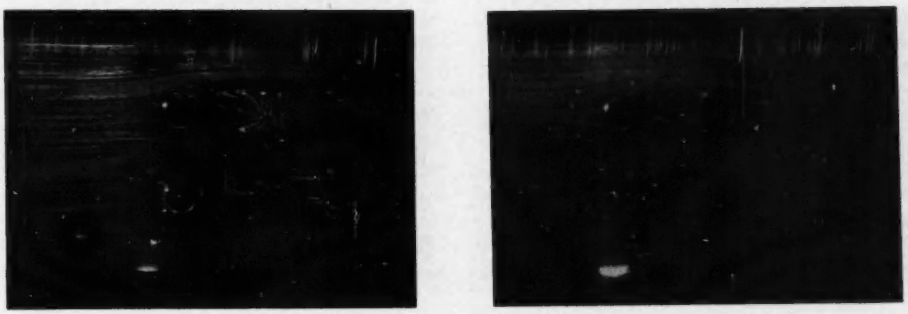

Plane D

FIG. 7. *Flow through corresponding planes of models No. 1* (left) *and No. 2* (right) *at* $Re = 400$. *Flow is from left to right.*

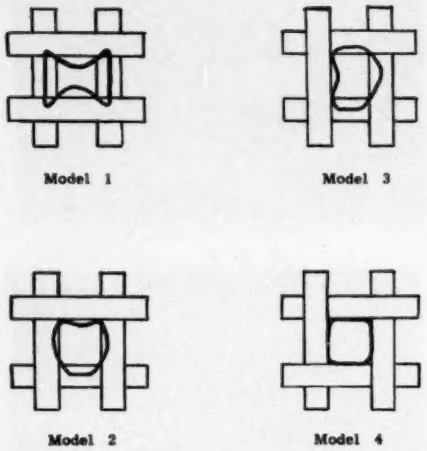

FIG. 8. *Minimum jet cross-sectional areas of the four models at Re = 400. Flow is normal to and out from the plane of the paper.*

or effective pore area, is approximately 30% greater than the projected area of the pore; model No. 4, with complete interlacing, produces a jet with area slightly less than the projected area. If, on the other hand, the proportionality of the jet area to the minimum pore area be considered, the results are rather interesting. The jet areas seem to be approximately 81% to 87% of the minimum pore area. Considering the accuracy of these measurements, the deviation of effective pore area from minimum pore area in the case of each model might also be regarded as a constant. This might be considered similar to the contraction coefficient for an orifice.

Interpretation of Results

One of the useful applications of fluid-flow visualization is that it often provides information concerning the model which may be utilized in predicting the behavior of the prototype. In the previous section an attempt was made to present the results derived from the experimental work. It is interesting to compare these results with those of other workers, and also to speculate on the applicability of these findings to other methods of fluid-flow study involving similar structures. Before extending the results of this study, however, certain limitations should be considered.

Limitation of Results

Although the models were made of nonporous, uniform cylindrical rods with a smooth surface, interlaced with balanced crimp, fastened at the intersections, and tested normal to the direction of flow at Re = 10 to 400, these rather ideal and limited conditions do not necessarily prevail in the testing or use of a real fabric. In fact, the porosity of the yarns and fibers, the value of the diameter/pitch ratio, the nature of the surface and uniformity of the yarns, the angle of the pore's plane relative to the direction of flow, the ability of the yarns to shift under stress, and the Reynold's number all have some influence on the porosity of the fabric. Thus, in attempting to draw conclusions or to compare the performance of the fabric-like structures to that of real fabrics, extreme caution must be observed.

Effect of Fabric Structure

During porosity measurements fabrics are usually supported perpendicular to the direction of flow. This condition, then, which is important in considering the effect of weave, has been maintained in the visual and the experimental investigations in question.

To consider one point consistently brought out in the literature, it was found, taking the two extremes, that the porosity of a satin-weave fabric was greater than that of a plain-weave fabric, other conditions being held approximately constant. In this respect, the results of the visual investigation conform to, if not explain, the trend exhibited by the real fabric.

TABLE II. JET AND PORE AREA RATIOS AT Re = 400

Model No.	Pore type	Projected area (P.A.) (in.²)	Minimum pore area (M.P.A.) (in.²)	Jet area (J.A.) (in.²)	J.A./P.A.	J.A./M.P.A.	Relative M.P.A.*
1	A	0.188	0.310	0.25	1.33	0.81	1
2	B	0.210	0.324	0.27	1.29	0.83	0.936
3	C	0.218	0.333	0.29	1.33	0.87	0.927
4	D	0.230	0.270	0.22	0.956	0.82	0.712

* Determined from M.P.A./P.A. ratio, and based on model No. 1.

The jet areas of models No. 1 and No. 3 (most common type in satin-weave fabrics) proved to be approximately 30% greater than that of model No. 4 (plain-weave pore type). Backer has also shown that the satin-type pores have about 30% greater minimum pore area than the plain-weave pores. Consequently, since the pore types other than plain weave have a greater percent open area, they offer considerably less resistance, or correspondingly greater porosity.

The visual study also indicated that the area of the jet was principally dependent upon the minimum pore area and the extent of wake formation, which, in turn, were influenced by the construction of the pore and the Reynold's number. It is apparent, therefore, that at the higher Reynold's numbers (when viscous effects may be neglected) one basic factor determining porosity is the area available for the passage of fluids, or "effective area." If the intrafiber and interfiber porosity may be neglected, a reasonable assumption at least in the case of open-weave fabrics, attention may be confined to the minimum cross-sectional area of the jet discharging from the pore, or "effective pore area." In that event, it would be convenient to treat pores as orifices, and thus permit scientific investigation of permeability on the established principles of fluid flow through orifices and/or nozzles. The question now is whether or not the different types of fabric pores may be treated as geometrically similar orifices, and thereby permit the prediction of relative porosity for all types of fabrics on the basis of a suitable parameter.

Fabric Pores as Orifices

Blue [4] compared discharge coefficients for a cotton fabric to those existing for sharp-edged orifices at equivalent Reynold's numbers. Robertson [26], on the other hand, selected to compare the performance of rayon fabrics with that of nozzles. In the latter paper it was shown that when the yarns forming a fabric pore are interlaced as for a plain weave, discharge-coefficient data based on projected area are very nearly the same for such widely different weaves as plain, basket, and mock leno. However, it was found impossible to correlate data for twill-weave fabrics with similar data for the others mentioned previously. Since in the work described here it is seen that the jet area/projected area ratio is not constant for all four pore types, to compare fabrics with different weaves on the basis of their projected areas would be to ignore the prerequisite of geometrical similarity. It seems, however, that the minimum pore-sectional area suggested by Backer would be a useful parameter for characterizing the pore orifices since on the basis of this investigation there is indication that the jet area/minimum pore area might be constant for a given Reynold's number, and since the known relative porosity of certain types of weaves are of the same order as the relative minimum pore areas which predominate in these weaves.

While the results of this study indicate that the jet area/minimum pore area ratio is nearly a constant for all pore types at $Re = 400$, if similar performance can be shown over a range of Reynold's numbers and a range of d/p ratios, then the average minimum pore area may serve as the best parameter for estimating the effective pore area of fabrics, regardless of their weave structure, and be useful in the treatment of fabric pores as orifices. To illustrate this, consider the determination of discharge coefficients as used by Blue and Robertson. A plain-weave fabric and a satin or twill having the same diameter/pitch ratio and percent projected open area would, on the basis of known previous performance, give different discharge coefficients at the same Reynold's number. In view of the results obtained here, though, there is reason to believe that if the discharge coefficients and Reynold's numbers were calculated using open areas based on the minimum pore areas, then the plain-weave, satin, and twill fabrics with equal textures and minimum pore areas might show more nearly equal discharge coefficients. That is to say, it is expected that a plain weave with a smaller diameter/pitch ratio than a satin (so that the minimum pore areas are equal) will have the same discharge coefficient and, correspondingly, have the same porosity, other factors being constant. Data are not available in the literature to permit evaluation of this hypothesis. The experimental work is rather straightforward and should first be conducted on wire screens and then later on actual fabrics.

Summary and Conclusions

A new technique has been developed for visually investigating the flow of fluids through fabrics. The method was applied and its potential usefulness demonstrated in an investigation to ascertain the effect of fabric weave on porosity. Four models were constructed of nearly constant d/p ratio to represent the

various types of possible combinations of yarns in a fabric pore, and were subjected to systematic photographic and visual investigation. The results of this work seem to warrant the following conclusions:

1. The visual investigation of flow through fabric-like structures proves to be a useful tool for studying certain types of fabric porosity. It may be used to determine velocity distributions and the streamlines resulting from fluid motion through a fabric.

2. The construction of the fabric pores has a decided influence on the pattern and area of the resultant jets.

3. The porosity of a fabric is largely determined by the minimum cross-sectional area of the jet, or effective pore area.

4. The effective pore area normally may be considered to be greater than the projected area except for the plain-weave pore type.

5. Except at very low Reynold's numbers, contraction of the jet causes the area available for the passage of fluids to be less than the minimum pore area proposed by Backer.

6. Due to the effect of pore construction on the jet, the effective pore area/minimum pore area ratio is very nearly the same for each pore type at Re = 400 and for the particular d/p ratio studied.

Literature Cited

1. Anon., *Heating and Piping* **15**, 53 (1943).
2. Backer, S., TEXTILE RESEARCH JOURNAL **18**, 650–8 (1948).
3. Backer, S., TEXTILE RESEARCH JOURNAL **21**, 703–14 (1951).
4. Blue, E. M., thesis, Mass. Inst. Technology, 1937 (unpublished).
5. Clayton, F. H., *J. Textile Inst.* **26**, T171–86 (1935).
6. Cowen, W., *J. Soc. Dyers Colourists* **55**, 290–302 (1939).
7. Draper, S., thesis, Mass. Inst. Technology, 1928 (unpublished) (through Sieminski, M. A., and Hotte, G. H., *Rayon Textile Monthly* **26**, 22–4 (1945)).
8. Eckert, B., and Pfluger, F., *Natl. Advisory Comm. Aeronaut., Tech. Mem.* No. 1003 (1942).
9. Erdman, F. S., *Cornell Eng.* **3**, 184–7 (1938).
10. Fage, A., and Preston, J. H., *J. Roy. Aeronaut. Soc.* **45**, 124–40 (1941).
11. Glauert, H., Hirst, D. M., and Hartshorn, A. S., *Aeronaut. Research Council, Tech. Rept.* T3234, R & M 1469 (1932).
12. Goldstein, S. (editor), "Modern Developments in Fluid Dynamics," Vol. I, Oxford, Clarendon Press, 1938.
13. Gregory, J., *J. Textile Inst.* **21**, T66–84 (1929).
14. Hance, L. H., thesis, Inst. Textile Technology, 1949 (unpublished).
15. Hauser, E. A., and Dewey, D. R., *J. Phys. Chem.* **46**, 212–13 (1942).
16. Huntington, R. L., *J. Chem. Education* **26**, 462–6 (1949).
17. Knudsen, M., *Ann. Physik* **28**, 75 (1909) (through Kennard, E. H., "Kinetic Theory of Gases," New York, McGraw-Hill Book Co., 1938).
18. Kowalke, O. L., *Ind. Eng. Chem.* **30**, 216–22 (1938).
19. Leaf, W. B., and Atchison, L. C., *J. Phys. & Colloid Chem.* **53**, 957–60 (1949).
20. Leva, M., and Weintraub, M., *Ind. Eng. Chem.* **43**, No. 1, 95 (1951).
21. Lewis, B., and Von Elbe, G., *J. Chem. Phys.* **11**, 75–97 (1943).
22. Lomax, J., *J. Textile Inst.* **36**, T60–6 (1945).
23. Marsh, M. C., *J. Textile Inst.* **22**, T56–63 (1931).
24. Prandtl, L., and Tietjens, O. G., "Applied Hydro- and Aeromechanics," New York, McGraw-Hill Book Co., 1934.
25. Rainard, L. W., TEXTILE RESEARCH JOURNAL **16**, 473–80 (1946).
26. Robertson, A. F., TEXTILE RESEARCH JOURNAL **20**, 838–57 (1950).
27. Sale, P. D., and Hedrick, A. F., *Natl. Bur. Standards (U. S.), Technol. Paper* 266, **18**, 529–46 (1929).
28. Schiefer, H. F., Cleveland, R. S., Porter, J. W., and Miller, J., *J. Research Natl. Bur. Standards* **11**, 441–52 (1933).
29. Sieminski, M. A., and Hotte, G. H., *Rayon Textile Monthly* **25**, 608–10 (1944).
30. Sieminski, M. A., and Hotte, G. H., *Rayon Textile Monthly* **26**, 22–4, 70–1, 111–16 (1945).
31. Taylor, G. I., *Aeronaut. Research Council, Tech. Rept.* 7345, R & M 2236 (1944).
32. Taylor, G. I., and Batchelor, G. K., *Rept. Memo. Aeronaut. Research Council, London* **2**, 1–29 (Mar. 1949) (through [21]).
33. Taylor, G. I., and Davies, R. M., *Aeronaut. Research Council, Tech. Rept.* 7614, R & M 2237 (1944).
34. Ullyott, P., *Trans. Am. Soc. Mech. Engrs.* **69**, 245–51 (1947).
35. Wakeham, H., and Spicer, N., TEXTILE RESEARCH JOURNAL **19**, 705–10 (1949).
36. Wallis, R. P., *Inst. Mech. Engrs. (London), J. and Proc.* **142**, P379–86 (1940).
37. Weller, R., *J. Applied Mechanics* **14**, 103–7 (1947).

(Manuscript received July 30, 1951.)

Molecular Theory of Damping in Fibers*

Taikyue Ree,† Mei Chio Chen,‡ and Henry Eyring**

University of Utah, Salt Lake City, Utah

Symbols Used in Parts I and II

a—sectional area of flow unit
A—sectional area of fiber
b—damping coefficient
b'—logarithmic decrement—*i.e.*, relative energy loss per cycle
c—internal friction, or gross viscosity, of the fiber
E—energy at maximum displacement in a cycle
ΔE—energy loss in a cycle
F—gross force acting on fiber across sectional area
ΔF—free energy for the dissociation of dashpot
$\Delta F^{\ddagger}$—activation free energy for flow process
$\Delta F_o^{\ddagger}$—activation free energy for flow process at frequency zero
$\Delta F_\nu^{\ddagger}$—activation free energy for flow process at frequency ν
g_1—spring constant of Maxwell spring
g_2—spring constant of straight spring
h—Planck constant
ΔH_i—dissociation heat of dashpot i
$\Delta H_i^{\ddagger}$—activation heat for flow process in dashpot i
k—Boltzmann constant
k'—specific rate constant
K—constant which is equal to $0.341 \times 10^{-8} c$
K'—constant which is equal to $(\pi/2)c$
l—length of fiber
Δl—elongation of fiber
m—mass of pendulum weight
n—ordinal number of period
n_1—number of Maxwell units in a flow unit
n_2—number of straight springs in a flow unit
n_3—number of bent springs in a flow unit
n_{1i}—number of dashpot, i, in a flow unit
r_o—radius of fiber
s—strain
s_o—strain impressed at time zero
s_s—strain on Maxwell spring
s_d—strain on dashpot
$\dot{s}$—rate of relative elongation
$\bar{\dot{s}}$—average of $\dot{s}$ through a period
$\ddot{s}$—second derivative of s with respect to time
S_n—amplitude at nth period
S_o—amplitude at zeroth period
ΔS_i—entropy for dissociation of dashpot i
$\Delta S_i^{\ddagger}$—activation entropy for flow process in dashpot i
t—time
T—absolute temperature
Y—Young's modulus
δ—phase angle by which friction force lags behind the displacement
η—dashpot viscosity; actually, friction constant of dashpot as a whole
η_o—dashpot viscosity at frequency zero
η_ν—dashpot viscosity at frequency ν
η_{io}—viscosity of dashpot i at frequency zero
η^*—true viscosity of dashpot
$\eta_{eff\,i}$—effective viscosity of dashpot i
λ—width of potential barrier
λ_1—distance between neighboring two positions where the molecular segment rests at equilibrium
λ_2—distance between two molecular layers, of which one layer moves with respect to the other
ν—frequency of vibration
ρ—ratio of the rate of displacement of the Maxwell spring to that of the conjugated dashpot
σ—area of dashpot
τ—period of vibration
$\bar{\tau}_i$—relaxation period of dashpot
ϕ—force acting on flow unit
ϕ_s—force acting on straight spring
ϕ_d—force acting on Maxwell unit
$\bar{\phi}_d$—average of ϕ_d through a period
ω—angular frequency in undamped free vibration
ω'—angular frequency in damped free vibration

* These two reports, Parts I and II, are based on Technical Reports No. XX and No. XXV, Research Contract N7-onr-45101, University of Utah, 1951.

† Research Professor of Chemistry, University of Utah.

‡ Graduate Student, Department of Chemistry, University of Utah.

** Dean of the Graduate School, University of Utah.

Part I: Vibrational Study of Saran Fibers

DURING the last decade, many papers and patent claims have appeared on polyvinylidene chloride plastics. The latter is widely known as Saran (a trade name of the Dow Chemical Company). A general survey on this plastic is given in the papers of Goggin and Lowry [3], Reinhardt [6], and Staudinger [7].

By the method of x-ray diffraction [2, 3, 5, 6, 7] the structure of Saran has been clarified a great deal, and its outstanding chemical and physical properties have been related to its structure.

The present work was undertaken to study the structure and the properties of Saran fibers from a different direction—*i.e.*, energy loss or internal friction accompanying the longitudinal free vibration of the fibers.

Experimental

Materials

The polyvinylidene chloride fibers (monofilaments) were supplied by Chicopee Manufacturing Corporation. In the present experiments a dyed green fiber of 15 mil diameter was used. By way of comparison, a gray and a heat-treated fiber were also used in the experiments reported in Part II. The heated-treated fiber is called "sample 9," and is the gray fiber (15 mil diameter) exposed at 220°F for 9 sec. under tension. The green and gray fibers are woven into screen cloths.

In every experiment a new sample was taken from the same stock. This procedure provides a common reference state for all samples used in the experiments.

Apparatus

The apparatus shown in Figure 1 was used in the study of the longitudinal vibration of the fibers. T is a transducer made by Statham Laboratory, Beverly Hills, California. Principally the G1-32 and G1-48 model types were used. This instrument is composed of a Wheatstone bridge wired with a strain-sensitive wire filament. If one pair of the arms of the Wheatstone bridge is lengthened, while the other is simultaneously shortened, the electrical balance which previously was established is altered so that an electrical current is caused to flow in the output circuit. This current intensity is proportional to the stress applied to the transducer. In the present experiment this current is amplified by a D. C. amplifier, A (Model BL-913, the Brush Development Co.). A magnetic Brush Penmotor inside the oscillograph, O, is driven by this amplified current, and thus the stress or strain imposed on the transducer is recorded on the chart paper in the oscillograph, which runs at a constant rate.

P in Figure 1 is a pendulum weight. Iron balls of different diameters were used. The masses of the weights are tabulated in Table II together with the vibrational Young's moduli, which will be mentioned later. The first column in Table II gives the weight number which represents the iron ball, and the second column gives the mass of the weight. This type of iron ball exhibits negligible air friction and executes a uniform motion compared to other forms of weights, such as cylinders and circular discs. A cathetometer was used for measuring the elongation of a fiber on appending the weight.

Procedure

A pin vise is used to attach a fiber to the pendulum weight and to the transducer. After a weight is hung on the fiber to be tested, 2 hrs. are allowed to elapse before the longitudinal vibration is imposed on the pendulum. During this period of waiting, the fiber is stretched and attains a uniform state corresponding to the stress bias. Referring to the check experiment, which will be mentioned later, this period of waiting is found to be long enough to get reproducible data.

The pendulum weight is pulled down by hand or by an electromagnetic device. When it is released it executes a damped oscillation. This motion of the pendulum is recorded on the chart paper. The best damped sine curve from several records is chosen.

If we plot the logarithm of the amplitude* of the curve, S_n, against the ordinal number of the period, n, we obtain a straight line. This straight line is expressed by the following equation:

$$\ln S_n = \ln S_o + b'n, \qquad (1)$$

* Half the distance between the highest and lowest points in a cycle of the damped motion is taken as the amplitude of the cycle.

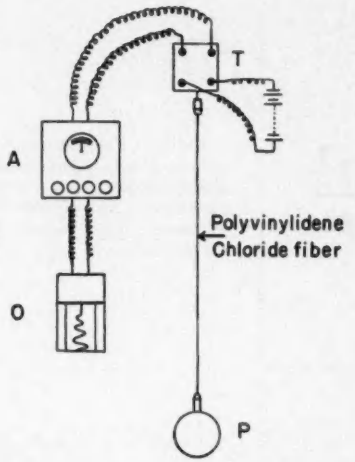

FIG. 1. *Apparatus.*

where S_o is the amplitude at the zeroth period, and b' is the slope of the straight line, which is commonly called the logarithmic decrement.

The frequency of vibration, ν, is measured by counting the number of cycles included in a certain interval of time.

All experiments were conducted at 25.5° ± 0.3°C, unless otherwise indicated.

Results

Time Effect.—The logarithmic decrements, b', and frequencies, ν, were measured after a fiber was stretched by a pendant weight for periods of 5, 10, 20, 40, 60, 80, and 100 min. The lengths of the fibers in these experiments were about the same, 255.0 ± 0.3 cm., and the same weight, No. VI-VII, and transducer, G1-48 type, were used throughout this set of experiments. It was found that the values of b' and ν were approximately independent of the preliminary stretching time. Therefore, we may conclude that the fiber attains virtually a stationary state within 5 min. after appending the weight. However, the fiber creeps still further, and the creep velocity does not become negligible until after a lapse of 90 min. Therefore, 2 hrs. were permitted to pass before the longitudinal vibration was imposed on the stretched fiber.

The b' Values and Frequencies.—The logarithmic decrement, b', and frequency, ν, change with the following variables: the mass, m, of the pendulum weight, and the length, l, the radius, r_o, and the ambient temperature, T (absolute), of the fiber. The values of b' and ν change also with the composition of the fiber and the conditions under which it was extruded and treated by heat or other means.

One example is tabulated in Table I, where the fiber was a green sample (15 mil) from the standard

TABLE I. SARAN, 15 MIL (GREEN SAMPLE); WEIGHT USED, No. VII

$$K = \frac{\left(\frac{b \times 10}{5 \times 2.303}\right)}{\left(\frac{2r_o}{\sqrt{ml}} \times 10^4\right)^2}$$

l (cm.)	$\left(\frac{2r_o}{\sqrt{ml}}\right)10^4$	$\nu/5$ (cycles/sec.)	$\frac{b}{(5\times2.303)}$	$\frac{b'}{2.303}$	K
8.0	5.575	2.63	0.505	0.192	0.162
7.4	5.801	2.70	0.586	0.217	0.174
7.0	5.954	2.78	0.594	0.214	0.168
6.3	6.286	2.94	0.529	0.180	0.134
5.9	6.493	3.11	0.628	0.202	0.149
5.3	6.860	3.23	0.659	0.204	0.140
4.9	7.140	3.36	0.766	0.228	0.150
4.3	7.623	3.70	0.736	0.199	0.127
3.7	8.218	3.85	0.716	0.186	0.106
3.2	8.815	4.21	0.880	0.209	0.113
2.6	9.801	4.41	1.107	0.251	0.115
2.1	10.88	4.62	1.256	0.232	0.106
14.0	4.219	2.02	0.341	0.169	0.192
11.8	4.600	2.17	0.343	0.158	0.162
10.7	4.825	2.27	0.402	0.177	0.173
10.1	4.962	2.44	0.432	0.177	0.175
9.5	5.123	2.48	0.461	0.186	0.176
9.0	5.260	2.54	0.478	0.188	0.173
247.6	1.003	0.472	0.0604	0.128	0.600
160.6	1.245	0.588	0.0800	0.136	0.516
107.3	1.523	0.719	0.100	0.139	0.431
64.2	1.970	0.926	0.105	0.139	0.271
31.8	2.797	1.32	0.188	0.143	0.240
21.8	3.379	1.61	0.261	0.162	0.229
20.3	3.501	1.67	0.267	0.160	0.218
19.3	3.594	1.72	0.285	0.165	0.221
18.2	3.695	1.79	0.313	0.175	0.229
17.2	3.802	1.85	0.343	0.185	0.237
16.1	3.935	1.88	0.306	0.162	0.198
5.0	7.044	3.33	0.670	0.201	0.135
4.8	7.205	3.38	0.646	0.191	0.124
3.5	8.438	4.00	0.784	0.196	0.110
2.7	9.621	4.31	0.927	0.215	0.100
2.2	10.66	4.90	0.985	0.201	0.0867
2.2	10.66	4.82	1.157	0.240	0.102
1.6	12.43	5.01	1.483	0.296	0.0960
48.1	2.27	1.05	0.140	0.133	0.272
25.7	3.11	1.49	0.238	0.159	0.246
5.5	6.72	3.33	0.780	0.234	0.204
1.5	12.83	5.55	1.58	0.284	0.0960
1.3	13.84	5.71	1.69	0.295	0.0883
1.1	15.03	6.00	1.65	0.275	0.0730

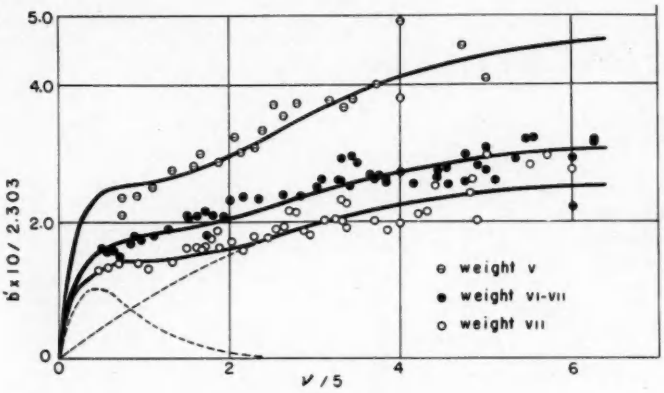

FIG. 2. *Comparison of theoretical curves with experimental curves. Dotted curves—*b′ vs. *ν curves corresponding to two different kinds of dashpots. Solid curves—Theoretical curves.*

spool, the pendulum weight was No. VII, and the transducer used was the G1-32 model type. Unless stated otherwise, the transducer used in all experiments in this report was of the G1-32 type. The fourth column gives the values of $b = b'\nu$, where b is the damping coefficient. The K values in the last column are the ratios of the quantities in the fourth column to the square of those in the second, as defined in the heading of Table II. The values of K will be discussed later. The b' values are plotted against frequencies, ν, in Figure 2. In this figure the b' values obtained using weights VI-VII and V under the same condition as for weight VII are plotted together. It is seen that b' does not change linearly with ν, and the heavier the weight, the lower the b' values.

The frequencies, ν, obtained using weights VII, VI-VII, and V are plotted against the factor $r_o/\sqrt{ml}$ in Figure 3. It is seen that the frequency changes linearly over a wide range of $r_o/\sqrt{ml}$ (from 0 to 1.05×10^{-3}), and the steeper the slope, the heavier the weight. Above the value 1.05×10^{-3}, the experimental points deviated downward from the straight line.

As will be seen later, the slope is proportional to the square root of Young's modulus (*cf.* equation (20)). The Young's modulus obtained by this method will be called the "vibrational Young's modulus." These values are tabulated in Table II. Observe that the heavier the weight, the higher Young's modulus.

Damping Coefficient, b.—The product of the logarithmic decrement, b', and the frequency, ν, is

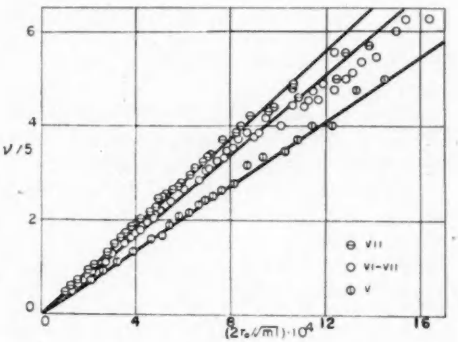

FIG. 3. *Dependence of frequency upon* $r_o/\sqrt{ml}$.

TABLE II. VIBRATIONAL YOUNG'S MODULUS

Weight No.	Mass of the weight (g.)	$Y \times 10^{-10}$ (dynes/cm.²)
VII	535.0	2.74
VI–VII	358.6	2.25
VI	226.5	1.75
V	130.5	1.47

equal to b according to the theory which will be propounded shortly (*cf.* equation (19)), and it is defined here as the damping coefficient. In Figure 4 the damping coefficients, b, in Table I are plotted against the factor $r_o/\sqrt{ml}$ together with the b values for weights V and VI–VII. It is seen from Figure 4 that the b values for the three weights are brought together in one curve, which falls precisely on the theoretical curve. A detailed description of the theoretical curve will be given later. This is a

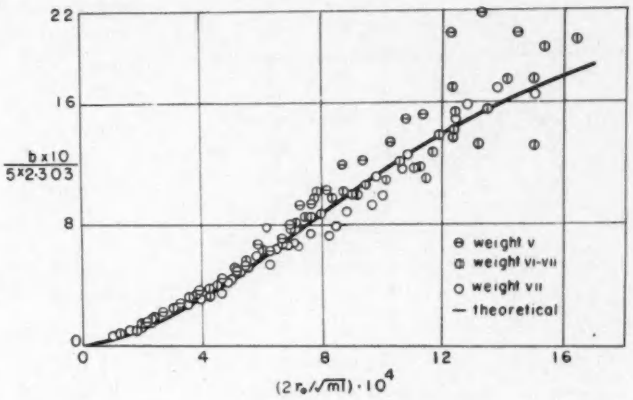

FIG. 4. *Damping coefficient* vs. $r_0/\sqrt{ml}$.

very interesting fact, considering that both b' and ν values are modified by the weights, but in opposite directions.

Theoretical Considerations

Derivation of the Equation of Motion

As the flow unit, we assume the following model (shown in Figure 5):

(*a*) The unit is composed of n_1 Maxwell units, n_2 straight springs,* and n_3 initially unstressed bent springs, all arranged in parallel.

(*b*) The bent springs come into action when the fiber is stretched by a sufficient force—*i.e.*, the bent springs are changed to straight springs. Therefore, the number of straight springs, n_2, increases by increasing the pendulum weights, while the number of bent springs, n_3, decreases.

(*c*) There are two kinds of Maxwell units† whose dashpot viscosities are η_1 and η_2. The numbers of the respective dashpots in the flow unit are n_{11} and n_{12}. Therefore, evidently, $n_1 = n_{11} + n_{12}$.

(*d*) The spring in the Maxwell unit moves with resistance which comes from the environment. Thus, we assume that the molecules are so intertwined that when the Maxwell dashpot moves, its spring is obliged to move a proportional distance.

Let the force acting on the flow unit be ϕ, and the forces acting on a spring and a Maxwell unit be ϕ_s and ϕ_d, respectively. Let the spring constant of the straight spring and the Maxwell spring be g_2 and g_1, respectively. Then, the following equation follows immediately:

$$\phi = n_2\phi_s + n_1\phi_d. \tag{2}$$

No force acts on the bent springs. Let the strain be s. Then the spring force, ϕ_s, is equal to $g_2 s$ according to Hooke's law. The rate of relative elongation, $\dot{s}$, is the sum of two terms: $\dot{s}_d$, the rate due to the dashpot, and $\dot{s}_s$, that due to the Maxwell spring. According to assumption (*d*), we can assume $\dot{s}_s = \rho\dot{s}_d$, where ρ is a constant. That is, the spring moves ρ times faster than the dashpot. Therefore, we have:

$$\dot{s} = (1 + \rho)\dot{s}_d. \tag{3}$$

According to Eyring's theory on creep and flow [1],

$$\dot{s}_d = 2k'\frac{\lambda}{\lambda_1}\sinh\frac{\phi_d\lambda}{2kT} \simeq k'\frac{\lambda^2}{\lambda_1}\frac{\phi_d}{kT}, \qquad = \phi_d/\eta, \tag{4}$$

where k' is the specific rate constant for the flow process, λ is the width of the potential barrier, and λ_1 is the distance between the neighboring two positions where the segment rests at equilibrium. From equations (3) and (4) we obtain

$$\phi_d = \eta\dot{s}/(1 + \rho). \tag{5}$$

* In Figure 5 the straight spring is represented by a Maxwell unit on which the force ϕ_s is acting. The dashpot of this Maxwell unit is held together so firmly that it does not move ordinarily.

† The mobile Maxwell units shown in Figure 5, on one of which the force ϕ_d is acting, consist of two types. To avoid confusion, the precise structure of these n_1 Maxwell units are not shown in Figure 5.

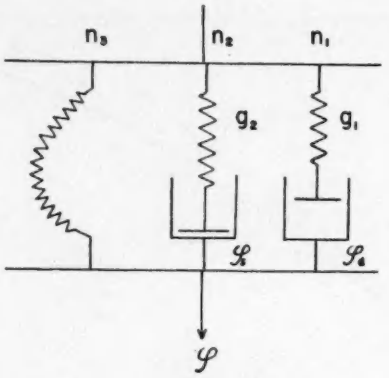

FIG. 5. *Molecular model for flow process.*

On the other hand, the force acting on the spring of the Maxwell unit, ϕ_d, is equal to $g_1 s_e$, where s_e is the strain on the spring due to this force. Therefore,

$$\phi_d = g_1 s_e = g_1 s\rho/(1 + \rho), \tag{6}$$

where the relations $s_e = \rho s_d$ and $s = s_e + s_d$ are used. From equations (5) and (6), ϕ_d is given as follows:

$$\phi_d = \frac{1}{2(1 + \rho)} (\eta\dot{s} + \rho g_1 s). \tag{7}$$

Force, ϕ, has the following relation:

$$\phi = aF/A = -aml\ddot{s}/A, \tag{8}$$

where a represents the sectional area of the flow unit, and F is the gross force acting on the fiber across the sectional area, A, of the latter. Taking into account that the dashpots are of two kinds, and substituting equations (7) and (8) into equation (2), we have*

$$-\frac{aml\ddot{s}}{A} = \frac{(n_{11}\eta_1 + n_{12}\eta_2)}{2(1 + \rho)}\dot{s} + \left\{ n_2 g_2 + \frac{\rho n_1 g_1}{2(1 + \rho)} \right\} s. \tag{9}$$

* Exactly speaking, the second term in equation (9) should be written in the following form:

$$\left\{ n_2 g_2 + \frac{\rho_1 n_{11} g_{11}}{2(1 + \rho_1)} + \frac{\rho_2 n_{12} g_{12}}{2(1 + \rho_2)} \right\} \frac{A}{aml} s,$$

where g_{11} and g_{12} are the spring constants for the springs attached to dashpots 1 and 2, respectively, and ρ_1 and ρ_2 are the previously defined quantities associated with each of these two springs. In equations (11) and (13), therefore, ρ and g_1 are considered as the mean values for ρ_1 and ρ_2 and g_{11} and g_{12}, respectively.

Arranging the terms of this equation, we obtain

$$\ddot{s} + 2b\dot{s} + \omega^2 s = 0, \tag{10}$$

where

$$b = \frac{n_{11}\eta_1 + n_{12}\eta_2}{4(1 + \rho)} \frac{A}{aml}, \tag{11}$$

$$\omega^2 = \frac{YA}{ml}, \tag{12}$$

$$Y \equiv \frac{1}{a} \left\{ n_2 g_2 + \frac{\rho n_1 g_1}{2(1 + \rho)} \right\}. \tag{13}$$

Equation (10) is known as the equation of a damped oscillation, and the solution of it is given as follows:

$$s = s_o \frac{\omega}{\omega'} e^{-bt} \sin(\omega' t + \delta), \tag{14}$$

where

$$\omega' = \sqrt{\omega^2 - b^2}, \tag{15}$$

$$\tan\delta \equiv \omega'/b. \tag{16}$$

The initial conditions, $s = s_o$ and $\dot{s} = 0$ (at $t = 0$), are used in obtaining the solution (equation (14)).

Because of the factor e^{-bt}, the amplitude of the motion decreases with time. The amplitude for the nth wave, S_n, is given by the following formula:

$$S_n = S_o e^{-nb\tau}, \tag{17}$$

where τ is the period of the vibration, and

$$S_o = s_o \frac{\omega}{\omega'} e^{-\frac{b\tau}{2}\left(\frac{1}{2} - \frac{\delta}{\pi}\right)}. \tag{18}$$

Equation (1) follows immediately by taking the logarithm of equation (17); from this we obtain the following relation:

$$b' \equiv b\tau. \tag{19}$$

Therefore, if the logarithm of the amplitudes is plotted against period number, n, a straight line is obtained. The logarithmic decrement, b', as is well known [8], is equal to $\Delta E/(2E)$, where $\Delta E/E$ is the relative energy loss per cycle.

The angular frequency of the damped vibration, ω', is equal to $(\omega^2 - b^2)^{\frac{1}{2}}$ (*cf.* equation (15)). However, ω' approaches very closely to ω if b is sufficiently small compared to ω. The latter condition is followed throughout the present experiment. Therefore, the frequency, ν, can be given by equation (12) with sufficient accuracy—*i.e.*, by

$$\nu \simeq \sqrt{\frac{Y}{4\pi}} \frac{r_o}{\sqrt{ml}}, \tag{20}$$

where A is substituted by πr_o^2.

It was found that equation (20) is strictly followed over a long range of the variation of $r_o/\sqrt{ml}$ (*cf.* Figure 3).

From equations (11), (19), and (20), we obtain

$$b' = \frac{\pi^2 \nu}{(1+\rho)Y} \sum_{i=1}^{2} n_{1i}\eta_i, \qquad (21)$$

where the subscript i stands for the dashpots 1 and 2, and summation is taken over these two. Therefore, b' must be proportional to frequency. This, however, is not the case, as is seen from Figure 2. The reason for this will be considered below.

Energy Loss and Viscosity as a Function of Frequency

In deriving the hyperbolic sine law, equation (4), Eyring assumed that an applied stress to a deformable material distorts the potential curve for the flow process. The validity of this formula was shown by Eyring, Halsey, White, Stein, Holland, Katz, Tobolsky, and Reichardt [4] for creep, stress relaxation, and constant rate of stretching. For a periodic vibrational stretching, another factor enters. The activation free energy, $\Delta F^{\ddagger}$, is no longer constant, but is a function of frequency. The reason for this will be considered below.

The force, ϕ_d, acting on a dashpot works not only to distort the potential curve, but also to reduce the activation free energy, as shown in Figure 6, where the latter is reduced by an amount

$$\delta(\Delta F^{\ddagger})_\nu = \Delta F_o^{\ddagger} - \Delta F_\nu^{\ddagger},$$

where $\Delta F_o^{\ddagger}$ and $\Delta F_\nu^{\ddagger}$ are the activation free energies at the frequencies zero and ν, respectively. This kind of consideration is quite probable considering that bonds between molecules (dashpots) are partly in the dissociated state when they are forced to vibrate. In the extreme case, with an infinite frequency and sufficient amplitude, all these bonds might be broken. Thus, the fiber structure will attain an amorphous state. The amount of $\delta(\Delta F^{\ddagger})_\nu$ may be put equal to $\alpha\bar{\phi}_d\lambda/2$, where this amount of work is done on the average to the bond by force $\bar{\phi}_d$. $\bar{\phi}_d$ is the average of ϕ_d through a period τ, and α is a factor relating the change in the potential surface to the average deforming potential. The factor α can be put equal to 1, by assuming that the distance between two successive equilibrium positions does not change appreciably by this kind of activation. Because of the reduction of the activation free energy, the viscosity decreases according to the following expression:

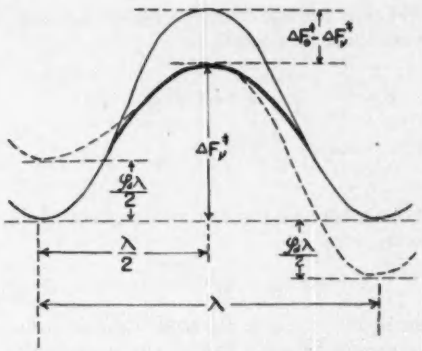

FIG. 6. *Potential energy barrier for a flow process in vibrational condition.*

$$\eta_\nu = \frac{h\lambda_1}{\lambda^2} e^{\frac{\Delta F_\nu^{\ddagger}}{kT}} = \eta_o e^{-\frac{\bar{\phi}_d\lambda}{2kT}}, \qquad (22)$$

where η_ν and η_o stand for the viscosities at the frequencies ν and zero, respectively; according to equation (4), η_o is given as follows:

$$\eta_o = \frac{kT\lambda_1}{k'\lambda^2} = h\frac{\lambda_1}{\lambda^2} e^{\Delta F_o^{\ddagger}/kT}. \qquad (23a)$$

The force, $\bar{\phi}_d$, in equation (22) is equal to $\eta_\nu\bar{s}/(1+\rho)$, as equation (5) shows. However, the following equation may be used as the first-order approximation:*

$$\eta_\nu = \eta_o e^{\frac{-\eta_o\bar{s}\lambda}{2(1+\rho)kT}}. \qquad (23b)$$

Generally, the nth derivation of s given by equation (14) with respect to time is given by the following equation:

$$\frac{d^n s}{dt^n} = s_o \frac{\omega^{n+1}}{\omega'} e^{-bt} \sin\{\omega' t - (n-1)\delta\}.$$

* This approximation has the following basis: The exact equation for η_ν is

$$\eta_\nu = \eta_o e^{\frac{-\eta_\nu\bar{s}\lambda}{2(1+\rho)kT}} \equiv \eta_o e^{-\alpha'\eta_\nu}.$$

From this equation,

$$\ln\left(\frac{\eta_\nu}{\eta_o}\right) = -\alpha'\eta_\nu.$$

Expand the left-hand term and take only the first term of this, because $|(\eta_\nu - \eta_o)|/\eta_o \ll 1$. We then obtain equation (23b), where the exponential factor in the latter is assumed to be a small quantity. This assumption is true in fact.

The time average through a period, $\bar{s}$, is obtained by the following procedure:

$$\bar{s} = \frac{2s_o\omega^2}{\tau\omega'}\int_0^{\tau/2} e^{-bt}\sin\omega' t\,dt$$

$$= \frac{s_o\omega'}{\pi}\left(1 + e^{-\frac{b\tau}{2}}\right) \simeq s_o(4\nu - b) \simeq 4s_o\nu. \quad (24)$$

If we substitute $\bar{s} = 4s_o\nu$ into equation (23b), we obtain

$$\eta_\nu = \eta_o e^{-\frac{2s_o\eta_o\lambda\nu}{(1+\rho)kT}}. \quad (25)$$

That is, the viscosity decreases if the frequency of vibration is raised. This is the phenomenon of thixotropy. In the extreme case, where ν is infinite, the viscosity becomes equal to zero.

Substituting equation (25) into equations (11) and (21), we obtain

$$b = \frac{\pi kT}{8s_o\lambda a}\left(\sum_{i=1}^{2} n_{1i}\bar{\tau}_i e^{-\bar{\tau}_i\nu}\right)\frac{r_o^2}{ml}, \quad (26)$$

$$b' = \frac{\pi^2 kT\nu}{2s_o\lambda a\,Y}\sum_{i=1}^{2} n_{1i}\bar{\tau}_i e^{-\bar{\tau}_i\nu}, \quad (27)$$

where

$$\bar{\tau}_i \equiv \frac{2s_o\eta_{io}\lambda}{(1+\rho)kT}. \quad (28)$$

η_{io} denotes the viscosity of the dashpot i under a static condition. Before going further to show the validity of equations (26) and (27), it is advisable to consider the meanings of Y and $\bar{\tau}$ given by equations (13) and (28), respectively.

Young's Modulus and Relaxation Period

The equation (10) of the damped oscillation can be derived by a simple classical mechanical consideration. Equation (29a) follows immediately:

$$F/A = Ys + c\dot{s}, \quad (29a)$$

where Y is Young's modulus in dynes/cm.^{2}, and c is a constant. The dimension of the constant c is the same as for viscosity; it is called the internal friction or gross viscosity of the fiber. The first term on the right-hand side of equation (29a) comes from Hooke's law, considering the fiber as a perfect spring. The second term is a friction force which accompanies the movement of the fiber due to the pendulum weight. By substituting $F = -ml\ddot{s}$ into equation (29a) and arranging the terms, we obtain equation (10), using the following identities:

$$2b = \frac{cA}{ml}, \quad (29b)$$

$$\omega^2 = \frac{YA}{ml}. \quad (29c)$$

Comparing equation (29c) with equation (12), we see that Y, as given by equation (13), is Young's modulus of the fiber. Thus, we can obtain Y from equation (20).

As mentioned above, the total quantity, b_i, is the sum of b_1' and b_2', which are due to dashpots 1 and 2, respectively. If the derivative of b_i' with respect to frequency is put equal to zero, we obtain from equation (27) $\nu_{max} = 1/\bar{\tau}_i$. ν_{max} is the frequency at which b_i' is a maximum. Thus, the dimension of $\bar{\tau}$ is time. Therefore, this quantity is called the relaxation time.

Testing the Theory

From equation (26) we have

$$K' \equiv \frac{b}{(r_o/\sqrt{ml})^2} = \frac{\pi kT}{8s_o\lambda a}\sum_{i=1}^{2} n_{1i}\bar{\tau}_i e^{-\bar{\tau}_i\nu}. \quad (30)$$

First, consider the meaning of the quantity K', defined by the identity in equation (30). From equation (29b), we see that $K' = \pi c/2$—*i.e.*, K' is $\pi/2$ times the internal friction of the fiber, c. K' is also related to the quantity K, defined by the formula at the top of Table I—*i.e.*, $K' = 4.606 \times 10^8 K$. Thus, the internal friction, c, is equal to $2.932 \times 10^8 K$. In Figure 7, the logarithm of the K values in Table I are plotted against frequency. It is seen that the internal friction changes greatly with the frequency.

As equation (30) shows, if there is only one kind of dashpot, then the relation between $\log_{10} K'$ and ν must be linear. From Figure 7, it is seen that the curve is linear except at low frequency, where it rises sharply. This indicates that there are at least two kinds of dashpots.

In order to obtain the parameters corresponding to the two dashpots, two tangents are drawn to the log K *vs.* ν curve in Figure 7. One is drawn so that as much of the high-frequency portion of the curve as possible coincides with the tangent. The other is drawn tangent to the low-frequency part of the curve. The tangents are called tangent 1 and tangent 2, respectively. The corresponding dashpots are dashpot 1 and dashpot 2. From the slopes

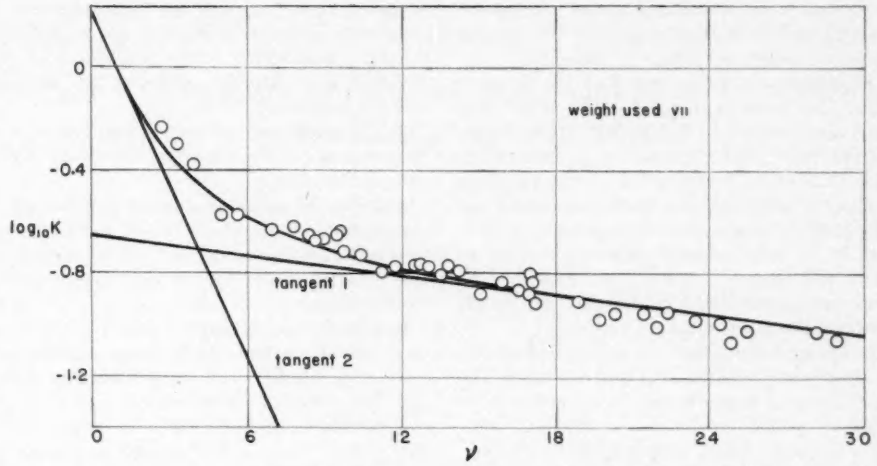

FIG. 7. *Saran, 15 mil (green sample): $\log_{10}$ K vs. frequency, where* $K = \left(\frac{b \times 10}{5 \times 2.303}\right) \Big/ \left(\frac{2r_o}{\sqrt{ml}} \times 10^4\right)^2$.

of the two tangents, $\bar{\tau}_1$ and $\bar{\tau}_2$ are determined—0.0299 and 0.500 sec., respectively.

From the y intercepts, we obtain

$$\frac{\pi kT}{8s_o\lambda}\frac{n_{11}\bar{\tau}_1}{a} = 4.61 \times 10^8\, e^{-1.50}, \qquad (31)$$

$$\frac{\pi kT}{8s_o\lambda}\frac{n_{12}\bar{\tau}_2}{a} = 4.61 \times 10^8\, e^{0.438}. \qquad (32)$$

If we take the values $s_o = 0.01$ and $\lambda = 5$ Å., which will be discussed later, we obtain $n_{11}/a = 1.06 \times 10^{14}$ and $n_{12}/a = 4.41 \times 10^{13}$. These quantities are the concentrations of dashpots 1 and 2, respectively.

Thus, we have all the data for the parameters entered in equations (26) and (27). These data were fixed using the experimental data obtained by using weight VII. In order to test our theory, b' and b were calculated for all of the weights used in the present experiments, using the data, $\bar{\tau}_i$ and n_{1i}/a, obtained above.

The values b_1' and b_2' for weight VII were calculated by using equation (27), and are represented by the dotted lines in Figure 2. The solid curve for weight VII was obtained by summation of the two dotted curves. By the same procedure, the solid curves for weights V and VI-VII were obtained. In every case, the agreement between theory and experiment is satisfactory.

The values for b were calculated by a similar procedure, using equation (26), and are represented by the solid curve in Figure 4. In this case, the b value is independent of the weight. In fact, all of the b values obtained for different weights are distributed around the theoretical curve.

Effective Viscosity

From equation (28), $\eta_{10}/(1+\rho)$ and $\eta_{20}/(1+\rho)$ are calculated as 1.23×10^{-6} and 2.06×10^{-5}, respectively. Unfortunately, the factor ρ is not available from the present experiments or from any others. Therefore, for the time being, it is put equal to zero.

The viscosity calculated under this assumption will be called the "effective viscosity," η_{eff}. The meaning of the η_{eff} will now be considered.

The three-element system which is composed of a spring in parallel with a Maxwell unit changes to a Voigt system which is composed of a spring in parallel with a dashpot when the factor ρ is put equal to zero. This Voigt model, instead of the three-element system, may be used for the vibrational kinetics. For this purpose, however, the viscosity of the Voigt model must be much smaller than that of the three-element system; otherwise, the mobility of the Maxwell-unit spring cannot be explained. Although this Voigt model cannot explain the initial sudden stretching in creep experiments, it is substituted successfully for the three-element system in phenomena other than creep

with the precaution mentioned above. Therefore, the viscosity which is calculated under the assumption $\rho = 0$ is called the "effective viscosity."

From equation (28), the width of the potential barrier, λ, can be estimated to be 5.10^{-8} cm. This figure is nearly equal to the distance (4.86 Å.) between the two CH_2 groups of the polyvinylidene chloride chain [1]. On these CH_2 groups rest the two CCl_2 groups belonging to another molecule, thus making polar bonds (*i.e.*, dashpots) which will be broken in the flow process. Therefore, λ is set approximately equal to 5 Å. The quantity s_o in equation (28) is the initial stretch per unit length, which is usually about 0.01.

Although we have called η as given by equation (23a) "viscosity," this requires qualification. The relation between true viscosity, η^*, and η is as follows:

$$\eta^* = \frac{\phi_d/\sigma}{\lambda_1 \delta_d/\lambda_2} = \frac{\phi_d}{\delta_d}\frac{\lambda_2}{\sigma\lambda} \simeq \frac{\eta}{\sigma},$$

where σ is the area of a dashpot, and λ_2 is the distance between two molecular layers, of which one layer moves with respect to the other. Therefore, η may be considered as the frictional constant of the dashpot as a whole. The area, σ, is estimated to be $(5.10^{-8})^2$ for convenience. Then, the effective viscosities at 25°C for dashpots 1 and 2, respectively, are as follows:

$$\eta_{\text{eff}\,1} = 4.92 \times 10^{8} \text{ dyne-sec./cm.}^2$$

$$\eta_{\text{eff}\,2} = 8.22 \times 10^{9} \text{ dyne-sec./cm.}^2$$

Summary

1. Polyvinylidene chloride fiber (Saran, dyed green) was tested by longitudinal free vibrations.

2. The relative energy loss (the logarithmic decrement), b', and the internal friction (the gross viscosity of the fiber) were determined at 25.5°C over a wide range of frequencies (from 1.75 to 31.5 cycles per sec.). Both quantities changed with frequency.

3. Young's moduli were determined by the vibrational method.

4. The flow unit involves three types of parallel units: n_1 Maxwell units; n_2 springs (actually, the so-called "pure" springs are Maxwell units with practically immobile dashpots); and n_3 initially unstretched, bent springs. The dashpots of the mobile Maxwell units further subdivide into dashpots 1 and 2, respectively.

5. The viscosities of the dashpots change with the frequency of the vibration. A theory of thixotropy is formulated.

6. With the assumptions stated in (4) and (5), above, the equations for b' and $b = b'v$ (the damping coefficient) were derived. The theoretical b' and b values agreed satisfactorily with the experimental values.

7. The relaxation times, $\bar{\tau}_1$ and $\bar{\tau}_2$, for the dashpots 1 and 2, respectively, were determined as follows: $\bar{\tau}_1 = 0.0299$ sec.; $\bar{\tau}_2 = 0.500$ sec.

8. The effective viscosities, $\eta_{\text{eff}\,1}$ and $\eta_{\text{eff}\,2}$, of the two dashpots, respectively, were found to have the values: $\eta_{\text{eff}\,1} = 4.92 \times 10^{8}$ dyne-sec./cm.^{2}; $\eta_{\text{eff}\,2} = 8.22 \times 10^{9}$ dyne-sec./cm.^{2}.

9. The number of dashpots per unit area in the flow unit were 10.6×10^{13} and 4.41×10^{13} for dashpots 1 and 2, respectively.

Literature Cited

1. Eyring, *J. Chem. Phys.* **4**, 283 (1936).
2. Fuller, *Chem. Rev.* **26**, 143 (1940).
3. Goggin and Lowry, *Ind. Eng. Chem.* **34**, 327 (1942).
4. Halsey, White, and Eyring, TEXTILE RESEARCH JOURNAL **15**, 295 (1945); Halsey and Eyring, *ibid.*, **15**, 451 (1945); **16**, 13, 124, 329, 335 (1946); Katz, Halsey, and Eyring, *ibid.*, **16**, 284, 378 (1946); Stein, Halsey, and Eyring, *ibid.*, **16**, 53 (1946); Holland, Halsey, and Eyring, *ibid.*, **16**, 201 (1946); Reichardt, Halsey, and Eyring, *ibid.*, **16**, 382 (1946); Reichardt and Eyring, *ibid.*, **16**, 635 (1946); Tobolsky and Eyring, *J. Chem. Phys.* **11**, 125 (1943).
5. Natta and Rigamonti, *Atti Acad. Lincei* **24**, 381 (1936).
6. Reinhardt, *Ind. Eng. Chem.* **35**, 422 (1943).
7. Staudinger, *British Plastics* **19**, 381 (Sept. 1947).
8. Zener, "Elasticity and Anelasticity," University of Chicago Press, 1948, p. 63; Thomson, "Mechanical Vibrations," New York, Prentice-Hall, 1948, p. 53.

(*Manuscript received July 23, 1951.*)

Part II: The Effect of Temperature and Heat Treatment on the Energy Loss in Saran

USING the same method and the same apparatus as described in Part I of this series, the effect of temperature and heat treatment on the energy loss, as well as on Young's modulus, was studied. Weight No. VII was used throughout the experiment unless stated otherwise. For the samples used in the present report, refer to Part I, the section on Experimental Materials (p. 790).

Experimental

Relative Energy Losses

The relative energy losses (the logarithmic decrements), b', of the green sample at different temperatures are plotted against frequency in Figure 1. The temperatures at which the experiments were conducted are 42.0°, 33.8°, 14.8°, 3.5°, and −1.2°C. The curve for 25.5°C was reproduced from Figure 2 of Part I. It is seen that by lowering the temperature the b' value rises, while it decreases at temperatures below 14.8°C. In Figure 2, the b' values at the frequency 20 cycles per sec. are plotted against the reciprocals of the absolute temperatures. We thus see that there is a temperature at which the b' value attains a maximum; in Figure 2, this temperature is around 10.2°C.

For metals, a maximum of the energy loss with temperature has been found by many authors [3]. However, as far as we know, no case has been reported showing a maximum for high-polymeric substances.

In Figure 1, we see that the b' values at −1.2°C show a maximum at the frequency 13.5 cycles per sec. The observed decrease of the b' values at frequencies higher than 13.5 cycles per sec. is greater than the experimental error. The existence of the maximum in the b' values at −1.2°C is direct evidence for the theory presented in Part I.

Young's Moduli

The frequencies observed for the green sample were plotted against values of $r_o/\sqrt{ml}$, as in Figure 3 of Part I. The vibrational Young's moduli at different temperatures are calculated from the slopes of the straight lines as in Part I. The Y values (dynes per sq. cm.) are tabulated in Table I and are plotted against temperature in Figure 3 (curve A). The Young's modulus increases with decreasing temperature. This increase in the Y values is sharper in the lower temperature range, below 17°C, than in the higher range above it. This result is in accord with that obtained by Moll and LeFevre [2]. They named this temperature the "cold point," which was a function of the kind and content of the plasticizers. According to their results, the cold points appeared in the range from −12° to 15°C for Saran B.

On the other hand, Young's modulus was determined by measuring the elongation, Δl, after a weight had been appended to a fiber for 2 hrs. This is also the time when the vibration was imposed on the fiber. Young's modulus was calculated by the equation $Y = (F/A)/(\Delta l/l)$. l is the length of the fiber at a relaxed state. The Young's modulus obtained by this method is here called the "static" value.

A green sample of 15 mil diameter was used, the length of which ranged from 100 to 250 cm. A mean Y value was taken out of more than five data for each weight at 25.5°C. These mean values are tabulated in the second column of Table II.

Young's modulus was also determined by another method, which is quite different from both of the methods described above. A fiber was stretched for 2 hrs. by appending a weight. Let l' be the length of the stretched fiber. Then impose an additional weight, Δm. Let $\Delta l'$ be the additional elongation immediately after* the additional stress was impressed. The modulus was calculated by

* In this experiment, it was too difficult to read the elongation immediately after the additional bias. Usually, 8 or 10 sec. elapsed before the first reading was taken. After that, it was still creeping gradually, reaching an almost stationary state after 5 min. It seemed that the main additional elongation was achieved within 5 sec. after the additional stress. Thus, in the calculation of Young's modulus from the additional stress and strain, we used the elongation at 10 sec. after an additional weight had been appended to the fiber.

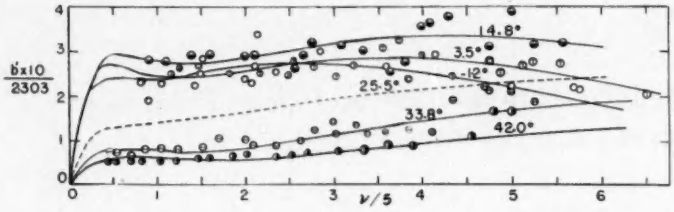

FIG. 1. b′ vs. *frequency. Solid curves are theoretical.* ◒, 14.8°C. ⊕, 3.5°C. ○, −1.2°C. ⊖, 33.8°C. ◑, 42.0°C.

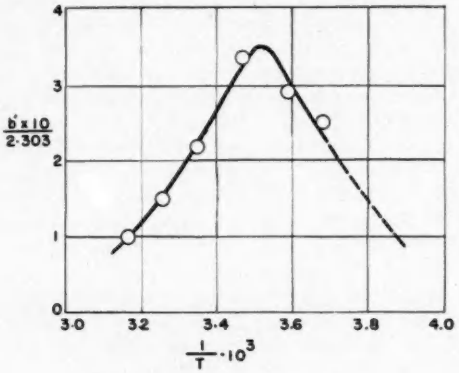

FIG. 2. b′ *at 20 cycles per sec.* VS. *reciprocal temperature.*

TABLE I. VIBRATIONAL YOUNG'S MODULI AT VARIOUS TEMPERATURES; WEIGHT USED, 535.0 G.

$$\nu = \sqrt{\frac{Y}{4\pi}}\frac{r_o}{\sqrt{ml}}$$

Sample	Temperature (°C)	$Y \times 10^{-10}$ (dynes/cm.²)
Green	−1.2	8.70
Green	3.5	7.45
Green	14.8	3.81
Green	25.5	2.75
Green	33.8	2.39
Green	42.0	2.27
Gray	25.5	3.07
Sample 9	25.5	2.45

TABLE II. STATIC YOUNG'S MODULI OF GREEN SARAN AT 25.5°C

Weight	$Y \times 10^{-10}$ dynes/cm.² (from fotal stretching)	$Y \times 10^{-10}$ dynes/cm.² (from additional stretching)
VII	0.735	2.38
VI-VII	0.710	1.90
VI	0.737	1.51
V	0.704	1.14

the equation $Y = (g\Delta m/A)/(\Delta l'/l')$, where g is the gravitational constant. The additional bias, Δm, was so adjusted that the additional strain would be about 1%. The results obtained by this method are tabulated in the third column of Table II.

All of the Young's moduli obtained by the three different methods mentioned above are plotted in Figure 4 against weight appended. The striking facts are: the Young's moduli obtained by the vibrational and additional-stress methods are higher than the static modulus; the former values change linearly with the weight appended; the static modulus is practically independent of the weight.† The reason will be considered later.

The Results for Gray Samples

The b' values obtained for a gray sample and for sample 9 at 25.5°C are plotted against frequency, ν, in Figure 5. The dotted line indicates the corresponding values for the green sample in Part I. Young's moduli for the gray fiber and sample 9 were determined by the method mentioned above, and are tabulated in Table I with those for the green sample.

Theoretical Considerations

Calculation of the Parameters

By the same method as in Part I, the molecular parameters were calculated; these are tabulated in Table III.

Using the values in Tables I and III, the values of b' at different temperatures can be calculated from equation (27) of Part I. The results are shown in Figure 1 by the solid curves. The agreement between the theory and experiment at each temperature is excellent.

† The Young's modulus of Saran B at 25°C obtained by Moll and LeFevre [2] is 1.22×10^6 lbs./sq. in., which is equal to 0.815×10^{10} dynes/cm.². This value is comparable with our mean value of static Young's modulus, 0.735×10^{10} dynes/cm.².

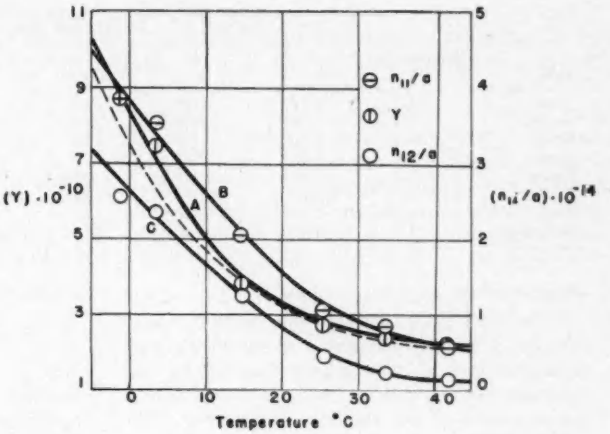

FIG. 3. *Young's modulus and concentration of dashpots* vs. *temperature.*

Activation Heats and Activation Entropies

From equation (23a) and (28) in Part I, we obtain

$$\ln(\bar{\tau}_i T) = \frac{\Delta H_i^{\ddagger}}{kT} - \frac{\Delta S_i^{\ddagger}}{k} + \ln\frac{2h\lambda_1 s_o}{(1+\rho)\lambda k}, \quad (1)$$

where the substitution $\Delta F^{\ddagger} = \Delta H^{\ddagger} - T\Delta S^{\ddagger}$ was made. The values $\log(\bar{\tau}_2 T)$ and $\log(\bar{\tau}_1 T)$ are plotted against the reciprocal of the absolute temperature in Figures 6 and 7, respectively. The linearity between $\log(\bar{\tau}_i T)$ and $1/T$ is as predicted by equation (1). The quantity ρ is assumed to be a constant in the range of the temperatures. The activation heats, $\Delta H_1^{\ddagger}$ and $\Delta H_2^{\ddagger}$, for dashpots 1 and 2, respectively, were calculated from the slopes of the straight lines in Figures 7 and 6 as follows:

$$\Delta H_1^{\ddagger} = 6.58 \text{ kcal.}$$

$$\Delta H_2^{\ddagger} = 1.38 \text{ kcal.}$$

Under the assumption that $\rho = 0$ and $\lambda \simeq \lambda_1$, the activation entropy, $\Delta S_i^{\ddagger}$, can be calculated from equation (1). The values are as follows:

$$\Delta S_1^{\ddagger} = -40.27 \text{ e.u.}$$

$$\Delta S_2^{\ddagger} = -63.49 \text{ e.u.}$$

The absolute values of the above activation entropies are the lowest possible since, as equation (1) shows, the absolute magnitude of $\Delta S_i^{\ddagger}$ increases with ρ, reaching infinity when $\rho = \infty$. Even these entropies are very large negative values. This means that as the dashpots are freed from the neighboring molecules during the activation process, an over-all tightening in the immediate medium occurs, and that the energy needed for this process constitutes the main part of the activation free energy. This is especially true for dashpot 2.

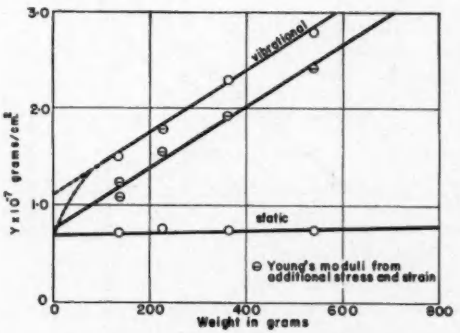

FIG. 4. *Young's moduli* vs. *weight.*

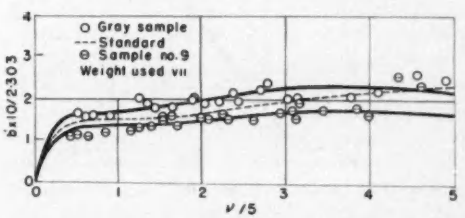

FIG. 5. *Energy loss* vs. *frequency.*

TABLE III. MOLECULAR PARAMETERS

Sample	Temperature (°C)	$\bar{\tau}_1 \times 10$ (sec.)	$\bar{\tau}_2$ (sec.)	$n_{11}/a \times 10^{-14}$	$n_{12}/a \times 10^{-14}$	$\eta_{10}/(1+\rho) \times 10^{6}$	$\eta_{20}/(1+\rho) \times 10^{5}$	n_{11}/n_{12}
Green	−1.2	0.730	0.684	3.85	2.57	2.74	2.57	1.50
Green	3.5	0.587	0.596	3.53	2.35	2.24	2.40	1.50
Green	14.8	0.479	0.532	2.04	1.26	1.90	2.11	1.62
Green	25.5	0.299	0.500	1.06	0.441	1.24	2.06	2.40
Green	33.8	0.155	0.446	0.853	0.236	0.656	1.89	3.61
Green	42.0	0.138	0.422	0.572	0.152	0.600	1.83	3.76
Gray	25.5	0.578	0.620	1.08	0.454	7.49	8.02	2.38
Sample 9	25.5	0.578	0.620	0.628	0.276	7.49	8.02	2.28

Dissociation Heats of the Dashpots

From Table III we see that the concentration of dashpots 1 and 2 decreases with increasing temperatures—that is, the dashpots disappear by dissociation. In Figure 8, $\log (n_{1i}/a)$ is plotted against the reciprocal of the absolute temperature. The upper and lower straight lines are for dashpots 1 and 2, respectively.

Suppose a dashpot, A, dissociate into its products, B and C. Then the concentration of A is given as follows:

$$[A] = [B][C]e^{\frac{\Delta F}{RT}} = [B][C]e^{-\frac{\Delta S}{R}+\frac{\Delta H}{RT}}, \quad (2)$$

where ΔF, ΔH, and ΔS are the thermodynamic quantities defined as usual for the dissociation equilibrium. We assume that the product [B][C] is not increased significantly through the small dissociation of A. In this case, equation (2) gives

$$\ln [A] = \text{constant} - \frac{\Delta S}{R} + \frac{\Delta H}{RT}. \quad (3)$$

In Figure 8, the logarithm of the concentrations of the dashpots, $\log (n_{1i}/a)$, are plotted against the reciprocal of the absolute temperature. We see that a linear relationship between these two quantities is followed approximately as equation (3) predicts. The upper and lower straight lines in Figures 8 are for dashpots 1 and 2, respectively.

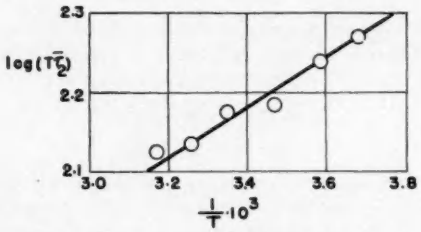

FIG. 6. *Determination of activation heats for the flow process of dashpot 2.*

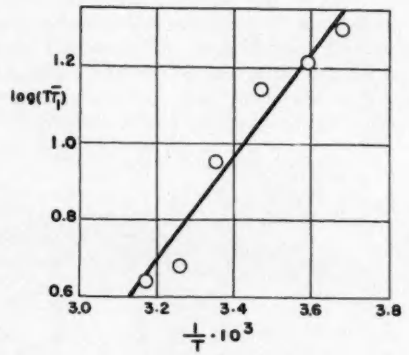

FIG. 7. *Determination of activation heats for the flow process of dashpot 1.*

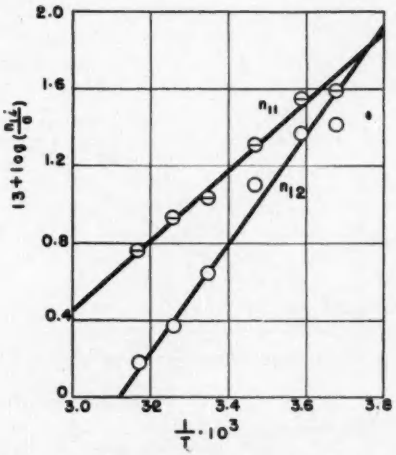

FIG. 8. *Determination of dissociation heats of dashpots 1 and 2.*

From the slopes of these lines, the dissociation heats, ΔH_1 and ΔH_2, of the dashpots can be calculated as follows:

$$\Delta H_1 = 5.51 \text{ kcal.}$$

$$\Delta H_2 = 12.6 \text{ kcal.}$$

The Effect of Weight and Temperature on Young's Modulus

The weight-dependence of the vibrational Young's modulus is obvious from equation (13) of Part I—*i.e.*, the vibrational Young's modulus, Y, is a function of the number of springs, n_2, which increases with the force (the pendulum weight) applied to the fiber. The number of springs, n_2, may reasonably be expected to be a linear function of the weight. Consequently, the vibrational modulus must likewise increase linearly with the weight. This anticipation is justified by the straight line drawn through the experimental points in Figure 4. It is uncertain whether or not for light weights the line curves to reach the static value at zero weight.

The static Young's modulus, which is constant irrespective of the weight, is lower than the vibrational modulus because in the relaxed state there are many bent springs.

In the stress-increment method, the state of the fiber and the standard from which the stress and strain are measured are exactly the same as in the vibrational method. Consequently, Young's modulus from this method is near the vibrational value. If we could measure the instantaneous elongation after the additional weight is added, the modulus from the stress-increment method would undoubtedly be exactly the same as that for the vibrational method.

It is well known [1] that the dynamic Young's modulus is higher than the static modulus for frequencies higher than those used here. Although we observe this same result, it is for a different reason.

In Figure 3, the observed values of n_{11}/a and of n_{12}/a (see Table III) are plotted against the temperature as curves B and C, respectively. The Young's modulus curve, A, is approximately parallel with both curves B and C—*i.e.*, equation (13) of Part I is obeyed. The dashed curve in Figure 3 is the mean value of the concentration of the two dashpots. The Young's modulus curve, A, closely overlaps the dashed curve.

The Maximum Energy Loss

As can be seen from equation (27) of Part I, the relative energy loss, b', is a complicated function of temperature. This is because, as seen above, the quantities Y, n_{1i}, $\bar{\tau}_i$, and $\eta_{i\infty}$ are functions of temperature. For simplicity, consider now the case where only one kind of dashpot works, and assume further that n_{1i}/Y is approximately independent of temperature. Differentiating equation (27) with respect to $1/T$, and setting the result equal to zero, we obtain the following condition for the maximum:

$$\frac{1}{T_{max}} = \frac{k}{\Delta H_i^{\ddagger}} \ln \frac{\Delta H_i^{\ddagger}}{k\beta\gamma}, \tag{4}$$

where

$$\left.\begin{aligned} \beta &= \frac{2s_\infty \lambda \nu}{k} \\ \gamma &= h\frac{\lambda_1}{\lambda^2} e^{-\frac{\Delta S_i^{\ddagger}}{k}} \end{aligned}\right\}. \tag{5}$$

At such a high frequency as 20 cycles per sec., only dashpot 1 works. If we therefore substitute $\Delta H_1^{\ddagger}$ and $\Delta S_1^{\ddagger}$, obtained before, as well as the assumed values for s_∞, λ, and λ_1 into equations (4) and (5), we obtain $1/T_{max} = 15.9 \times 10^{-3}$, which is five times larger than the observed value, 3.5×10^{-3}. This is not surprising since the calculation is oversimplified. If we take into account that the quantities Y and n_{1i}/a in equation (27) are temperature-dependent, then the maximum condition becomes so complicated that only a trial-and-error method is available for solving for $1/T_{max}$. The result, of course, approaches the observed value. The detailed description, however, will not be given here. In any case, the existence of the maximum energy loss at a specific temperature is a necessary consequence of equation (27). The physical significance is as follows:

When the temperature is rising, the friction constant, $\eta_{i\infty}$, in equation (28) decreases. Consequently, the energy loss decreases with increasing temperature. The quantity $\eta_{i\infty}$ increases with decreasing temperature, and so increasing the energy loss. However, when the temperature is too low, the number of dashpots decreases because they stick together too firmly. Eventually the number of dashpots reaches zero as the temperature approaches absolute zero. Consequently, the energy loss decreases again with decreasing temperature. Thus, we understand the existence of a temperature of maximum energy loss.

The Effect of Heat Treatment

The molecular parameters for the gray fiber and sample 9 are tabulated in Table III together with those of the green sample. The following interesting facts were observed:

(1) The relaxation periods, $\bar{\tau}_1$ and $\bar{\tau}_2$, of the two dashpots are the same in these two samples; consequently, the constants $\eta_{10}/(1+\rho)$ and $\eta_{20}/(1+\rho)$ relating to their viscosities are the same.

(2) The dashpot concentrations, n_{11}/a and n_{12}/a, are decreased due to the heat treatment by factors of 1.72 and 1.64, respectively. Thus, we see that the heat treatment decreases the number of dashpots without changing their nature.

It is noteworthy that the concentrations, n_{11}/a and n_{12}/a, of the two dashpots are about the same in the green and in the gray samples. However, the constant $\eta_{10}/(1+\rho)$ is 6.04 times larger for the gray sample than for the green one, and $\eta_{20}/(1+\rho)$ is 3.89 times larger for the gray sample than for the green one. Thus, we see that in Figure 5 the higher b' values in the gray sample than in the green are due to the higher viscosities in the former. The difference in the viscosities in the gray and green samples is due to the difference in the structure of the two samples. Different plasticizers were used in the two fibers. This may possibly cause some difference in the polymerization as well as in the crystallinity.

Summary

1. The relative energy losses in Saran fibers were measured at −1.2°, 3.5°, 14.8°, 25.5°, and 42.0°C by a method of longitudinal free vibrations.

2. The relaxation periods, viscosities, and concentrations of dashpots were determined at the various temperatures.

3. The activation heats and activation entropies for the flow process and the heats of dissociation of the dashpots were determined.

4. A maximum in the energy loss with temperature was found. This temperature was 10.2°C for the frequency of 20 cycles per sec.

5. This maximum in energy loss with temperature was explained using the theory propounded in Part I by the authors.

6. The vibrational and static Young's moduli were determined. The moduli increased sharply below 17°C. This is apparently due to some second-order transition which occurred at 17°C.

7. Heat treatment reduces the number of dashpots without changing the nature of the remaining ones.

Acknowledgment

We wish to express our appreciation to the Chicopee Mills Manufacturing Corporation and to the Dow Chemical Company for support of this project. We also are indebted to the Research Committee of the University of Utah for a fellowship to one of us (M.C.C.). Our thanks are also due to the Office of Naval Research for the use of certain equipment. We wish to thank Dr. Carlyle Harmon and Dean C. J. Christensen for valuable advise throughout the course of the investigation.

Literature Cited

1. Kuhn, Künzle, and Preissmann, *Helv. Chim. Acta* **30**, 307 (1947).
2. Moll and LeFevre, *Ind. Eng. Chem.* **40**, 2172 (1948).
3. Zener, "Elasticity and Anelasticity," University of Chicago Press, 1949.

(*Manuscript received July 23, 1951.*)

Quantitative X-Ray Studies of Order in Amorphous and Crystalline Polymers*

Scattering from Various Polymers and a Study of the Glass Transition in Polystyrene and Polymethyl Methacrylate

Samuel Krimm† and Arthur V. Tobolsky‡

Contribution of Textile Research Institute and Frick Chemical Laboratory, Princeton University, Princeton, New Jersey

Abstract

The application of a Geiger counter spectrometer to the quantitative study of the scattering from amorphous and crystalline polymers has been investigated, and this technique has been shown to be very well suited to this purpose. The experimental technique used is described. The following polymers have been studied, in order to gain some insight into the structure and order characterizing the amorphous and crystalline regions: hexadecane, polyisobutylene, natural rubber, polystyrene (oriented and unoriented), polymethyl methacrylate, polytrifluorochloroethylene, octacosane, polyethylene, polytetrafluoroethylene, and various natural keratins. The scattering patterns are analyzed for their structural implications.

It has been found that the x-ray diffraction patterns of polystyrene and polymethyl methacrylate change as these materials are heated through and above the region of their second-order transition. It is shown that these changes are interpretable in terms of definite changes in structure of the polymeric chains. The bearing of these results on the nature of the glass transition in these materials is discussed.

THE USE of x-ray diffraction as a tool in studying the structure of crystalline solids is well known. It is not appreciated quite so generally for obtaining information about less ordered structures, such as gases, liquids, and amorphous solids. The scattering of x-rays by amorphous materials does yield, however, very definite, if somewhat limited, information about the structures of these substances. This is of especial interest in the study of high polymers, in which substances we almost always encounter some disordered material along with the highly ordered crystalline regions. Recognition of this fact almost immediately brings two questions to mind: what is the nature of the disordered regions, and what fraction of the material do they constitute? These problems are important because of the very close relationship between the structure and texture of the polymer, on the one hand, and the physical and mechanical behavior which we observe and utilize, on the other hand. The present study is an effort to shed some light on the answers to these questions for a few typical polymers.

In the present paper we consider the scattering from various amorphous and crystalline polymers, with the view of determining the type of information which can be obtained from the diffraction pattern concerning the structures of these materials and the type of order present. This includes a study of the diffraction patterns of some of the materials as a function of temperature, particularly in the range of the glass, or "second-order," transition.

Experimental Procedure

The most generally convenient method for detecting diffracted x-rays is by means of the photographic

* This article is based upon a thesis submitted by Samuel Krimm in partial fulfillment of the requirements for the degree of Doctor of Philosophy at Princeton University.

† Research Fellow of Textile Research Institute; presently DuPont Postdoctoral Fellow at the Department of Physics, University of Michigan, Ann Arbor, Mich.

‡ Staff member, Textile Research Institute. Present address: Department of Chemistry, Princeton University.

film. This method is not eminently suited, however, to quantitative work, primarily because of the very careful standardization of intensity calibration and of film handling and development which is demanded. The length of exposure required also does not ordinarily make it feasible to follow changes in the diffraction pattern with time. Because of the desirability of having a sensitive and quantitative detector, and also in order to be able to follow time changes in the diffraction pattern, it was decided to use a Geiger counter to record the diffracted x-rays. A brief description follows of the spectrometer and of the pertinent techniques used.*

Copper radiation was used throughout in most of the work monochromated by reflection from a pentaerythritol crystal. In some instances nickel-filtered radiaton was used. In order to permit more accurate compensation for variations in the x-ray tube output than was possible with the voltage-regulated input to the x-ray machine, the beam issuing from the opposite port of the x-ray tube was monitored with a second pentaerythritol crystal and another Geiger counter. In this way, intensity fluctuations were effectively kept down to 0.5% to 1.0%. Following the monochromator, the beam was collimated by a Soller slit, 130 mm. long with lead sheets 0.08 mm. thick spaced 0.8 mm. apart, and a pair of adjustable lead jaws which limited the vertical divergence of the beam. The resulting irradiated sample area was about 3 mm. × 6 mm. Between this Soller slit and the sample, provision was made for accurately inserting into the beam a set of nickel filters and a fine pinhole collimating slit. These were used to get an accurate measure of the incident-beam intensity and of absorption by the sample. This x-ray absorption method for determining thickness was shown to be accurate to within about 1% by comparing thickness determinations of pure nickel and aluminum sheets with micrometer measurements. During the scanning of the diffraction pattern, this set of filters and pinhole slit were removed from the beam.

The sample was mounted inside a temperature-controlled oven, the beam entering and leaving through cellophane windows. Heaters and a thermoregulator enabled control of the temperature to within about ± 0.5°C. The clamps holding the sample were part of an orientation jig, contained within the oven, which enabled the sample to be elongated as well as rotated in the plane perpendicular to the x-ray beam, both adjustments being possible from outside the oven. This rotation permitted a determination of crystallite orientation in the sample since, by fixing the radial position of the Geiger counter at the Bragg reflection and rotating the sample so that its center of rotation coincided with the point of penetration of the x-ray beam, the intensity distribution around a halo or Debye-Scherrer ring could be determined. The external control of these motions made it possible to operate at above room temperatures. When the sample was in the form of a solid film of polymer, it was mounted directly between the clamps and could then be maintained at the initial length or elongated at will. Liquids were contained in a small mica-window cell which was attached to the upper clamp, thus allowing positioning in the beam. Fibers were mounted in a special frame which could then be attached to the orientation jig, thus permitting them to be elongated and rotated as above. The jig and clamping arrangement were so constructed that a sample could be removed from the x-ray beam without disturbing its elongation or orientation. This enabled the incident-beam intensity to be measured during the scanning of the diffraction pattern, when it was so desired. The sample thicknesses were usually less than the optimum thickness for maximum diffracted energy in order to permit easier clamping and elongation, and to diminish differential errors due to radiation scattered at angles slightly different from that of the Geiger counter setting.

The Geiger counter measuring the diffracted-beam intensity was mounted so that it could be moved in a horizontal plane along a graduated circle, the axis of rotation being the sample position. The counter setting could be adjusted to values of 2θ to within $\pm 0.05°$ (θ = Bragg angle). The spectrometer quadrant was calibrated by means of the strong diffraction lines of a number of standard materials, employing the Bragg law, $n\lambda = 2d \sin \theta$, where λ is the wave length of the x-rays, n the order of the reflection, and d the lattice spacing. This calibration indicated that the quadrant readings of 2θ were accurate to within the above error in setting the Geiger counter. Provision was also made for adjusting the vertical elevation of the counter. Attached to the counter, and moving with it, were a Soller slit of dimensions identical to those of the

* A description of the complete Geiger counter spectrometer will be published in *Review of Scientific Instruments.*

first collimating Soller slit, and a pair of adjustable lead jaws for vertical collimation. The output of this Geiger tube, and also that of the monitoring Geiger tube, was fed into a commercial decimal scaling unit, which gave a direct reading of the number of counts recorded. A relay circuit and electrical timer permitted both scalers to be started and stopped simultaneously. The counting period used at each quadrant setting was 1 min.

The readings thus obtained were corrected in the following way before being used to plot the diffraction curve. After correction for the normal background count of the Geiger tubes, the diffraction reading was divided by that of the monitor. This result was divided by the corresponding ratio for the pinhole-collimated transmitted beam, thus giving a ratio of diffracted beam to transmitted beam. This transmitted-beam value, $I_{2\theta=0}$, is not the same as the beam intensity transmitted by the sample; it is, however, proportional to it. From the above ratio the air scattering was subtracted, since it had also been related to the same transmitted-beam intensity. When the mica-window cell was used, the scattering from the empty cell was deducted. The values thus obtained were then corrected for relative absorption by the sample and by the exit cellophane window [20], which includes correction for coincidence losses due to the relatively high counting rates on the main beam. Correction was also made for polarization of the beam by the monochromating crystal and by the sample. These results represent the corrected diffraction readings (neglecting temperature corrections), $I_{2\theta}/I_{2\theta=0}$, and were plotted to give the diffraction curve. No correction was made for incoherent scattering in this phase of the work.

In the cases where different masses of a given material were in the same x-ray beam and it was desired to base the resulting diffraction curves on the same scattering mass, the above diffraction readings were corrected by means of the ratio of ρt values of the samples, determined from the x-ray absorption measurements made at the beginning and end of each run (ρ is the density and t the thickness of the sample, the product being determined from the absorption law $I = I_o e^{-\mu_m \rho t}$, where μ_m is the mass absorption coefficient of the material). It is easily shown that the scattered intensity from crystalline and amorphous materials is proportional to their respective ρt values, provided extinction effects are inappreciable and samples are compared in which the radial density distribution functions for the amorphous regions are not too different. When it was desired to compare the total integrated scattering from different polymers, the integrated intensities were reduced to the same basis by means of the atomic scattering factors [21].

Scattering from Various Polymers

Amorphous Polymers

Hexadecane.—Present views on polymer structure consider that the amorphous regions are characterized by a random arrangement of the long-chain molecules. In fact, many writers have thought of the amorphous regions as approaching the type of structure present in liquids—*viz.*, a long-range disordered structure which is continually changing as a result of thermal motions. Of course, a completely random arrangement of the atoms in the amorphous regions is precluded by the impenetrability of atoms, by the presence of primary valence forces between adjacent atoms in the chain, and by the restraining influence on chains of cross-links and crystallites, when the latter are present. It is nevertheless useful to examine the scattering from a liquid in order to determine how closely that of amorphous materials approaches it. A liquid whose molecules are similar to those of the solid is desirable, and therefore hexadecane was chosen for examination.

A radial scan of the scattering from hexadecane is shown in Figure 1. It shows a pronounced halo with a peak at about $2\theta = 19.1°$, corresponding to a Bragg spacing of 4.64 Å., and a less intense halo

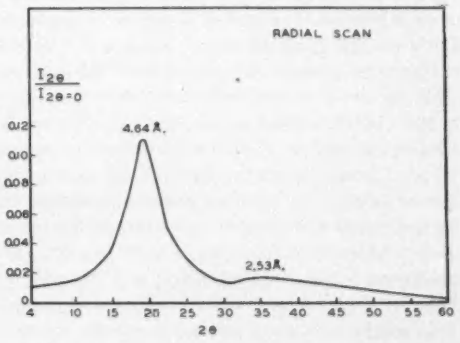

FIG. 1. *Radial scattering curve for hexadecane.*

whose peak is at about $2\theta = 35.5°$, which corresponds to a Bragg spacing of 2.53 Å. (Although the Bragg equation is not strictly applicable to calculating spacing from a liquid diffraction pattern—the calculated spacings being somewhat smaller than the true distance between scattering centers—the Bragg spacings may be taken as a close enough approximation for qualitative purposes.) It must be pointed out that although this diffraction curve indicates the presence of concentrations of scattering matter at distances of about 4.64 and 2.53 Å. from any given atom, it doesn't yet furnish quantitative information about the number of atoms at each distance, nor even indicate that the maximum concentrations are at these distances. In order to obtain this information, a Fourier analysis of the curve must be performed [20]. This has been done by Warren [44], who has shown that for normal paraffins containing up to ten carbon atoms the chains are essentially straight in the liquid and approximately parallel to each other over short distances. The 19.1° peak is shown to correspond to an interchain spacing—*i.e.*, it represents an average distance of closest approach between carbon atoms in different molecules.

In so far as these results are applicable to liquid hexadecane, it is seen that although all possible orientations occur in the liquid, a certain amount of order persists over short distances because of the requirement of roughly parallel alignment imposed by the condition of fairly dense packing. It is important to observe that the conditions required by the equation giving the intensity of scattering from amorphous materials—*viz.*, a spherically symmetrical radial distribution function and a random molecular orientation—are satisfied despite the existence of a nonrandom local orientation in the immediate neighborhood of a given molecule. This is true because the smallest portion of liquid from which it is possible to obtain a measurable intensity of scattered radiation still contains a large number of molecules, so that the regions of local arrangement occur with all possible orientations. Therefore, the average molecular orientation over the entire assemblage may be considered as a random one. Should the regions of local order show a preferred orientation, the above conditions would not be satisfied, and the predicted intensity distribution would probably not be realized. This will be seen to be the case when the scattering from oriented amorphous polymers is considered.

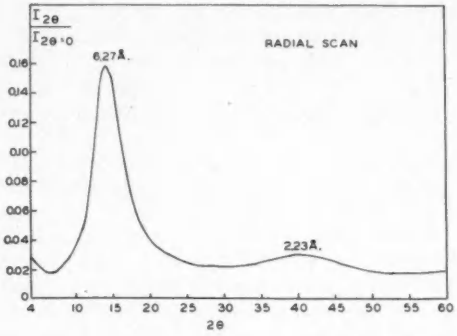

FIG. 2. *Radial scattering curve for polyisobutylene.*

Polyisobutylene.—This polymer is amorphous in the unstretched state at room temperature, as is shown by the radial scan in Figure 2. The viscosity average molecular weight of this sample is about 2,800,000. This rubbery polymer crystallizes upon stretching, and gives one of the sharpest and most detailed fiber patterns known so far among polymers. The crystal structure is quite complicated [14] and has not yet been unambiguously determined.

The amorphous pattern shows a pronounced halo of about $2\theta = 14.1°$, and a less intense halo at about $2\theta = 40.0°$, corresponding to Bragg spacings of 6.27 and 2.23 Å., respectively . It is seen that the interchain spacing in polyisobutylene is much larger than that in hexadecane, a fact which is understandable when it is realized that half of the hydrogens of a straight chain have been replaced by methyl groups. The larger size of the latter prevents the chains from approaching each other as closely as is possible in the case of a straight-chain hydrocarbon. The 6.27 Å. halo also appears to be sharper than the corresponding 4.64 Å. halo of hexadecane, the width at half-maximum intensity being 5.0° in the former case and 5.9° in the latter (the experimental conditions were the same in both cases). This appears to indicate a more definite interchain concentration of scattering matter in polyisobutylene.

Natural Rubber.—Rubber is a polymer of isoprene. It is amorphous in the unstretched state at room temperature, giving a diffraction pattern such as that in Figure 3. The azimuthal scan represents the intensity distribution around the halo, $\phi = 0°$ being the equator and $\phi = 90°$ being the meridian of the diffraction pattern. The scattering shown in

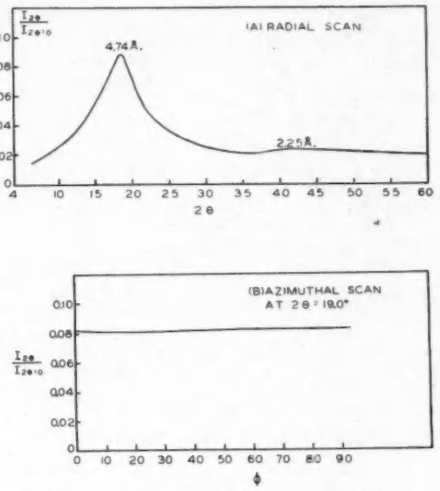

FIG. 3. *Scattering curves for unstretched vulcanized Hevea.*

Figure 3 is from a sample of vulcanized Hevea. When stretched or frozen, the pattern indicates the presence of crystalline regions interspersed in the amorphous matrix.

The peaks in the amorphous diagram correspond to Bragg spacings of about 4.74 and 2.25 Å. A Fourier analysis of the diffraction of amorphous rubber has been performed [39]. The results indicate that the x-ray pattern can be accounted for by the usual chain-molecule picture of rubber, without the necessity of making any specific assumptions as to mutual orientation of the chains. Because of this, however, the analysis of the amorphous pattern yields practically no information as to relative orientation of chains or as to whether the individual chains are coiled or straight. Since no assumptions are necessary in the analysis, the information obtained is definite. Because no assumptions are made, however, the information is limited; in other words, the radial density distribution resulting from the Fourier analysis cannot uniquely determine a structure when complex molecules are involved.

An effort was made to obtain an oriented amorphous sample of rubber by stretching and then heating a sample. Most samples broke under this treatment. One, however, was stretched 315% and heated to 95°C and the diffraction pattern was obtained. This did not indicate any orientation of the amorphous regions, as evidenced by the intensity distribution in the azimuthal scan.

Polystyrene.—Polystyrene is a glassy polymer which gives an x-ray diffraction pattern characteristic of amorphous solids. The scattering curve of a piece of unoriented polystyrene at room temperature is shown in Figure 4(A). Azimuthal scans around each of the two halos indicated no orientation whatsoever—*i.e.*, the intensity was uniform around each halo. The first two prominent peaks correspond to Bragg spacings of 8.84 and 4.67 Å., respectively. It is not known why the value of the inner halo spacing is less than that usually reported —*viz.*, about 10Å. A diffraction photograph of the material, taken with filtered radiation, gave an inner halo spacing of about 9.8 Å. The inner halo which we measured at 8.84 Å. has been interpreted [23] as arising from interchain interferences, mainly on the basis of the fact that this halo is not present in the scattering diagram of monomeric styrene, whereas the 4.67 Å. halo is. This interpretation is not unreasonable, since it would be expected that the bulky phenyl side-groups would prevent the close approach of neighboring chains and would account for the presence of this large-spacing interchain interference. The scattering curve of benzene also shows only one halo, corresponding to a Bragg spacing of 4.7 Å. [42], thus lending more support to the interpretation of the 8.84 Å. halo as resulting from interchain interferences.

The corresponding assignment of the 4.67 Å. halo is not quite as clear-cut, but the evidence seems to point to its being due in part to intramolecular interferences such as those between the phenyl groups on the chain. The corresponding halo in benzene has been subjected to a thorough analysis [24, 34, 42], including a Fourier analysis, with the conclusion that it arises from inter-ring interferences in directions perpendicular to the ring. The determination of the structure of crystalline benzene [16] confirms this viewpoint and makes it probable that the halo in polystyrene arises from the same effects. It is possible, however, that contributing to this halo in polystyrene are also some intermolecular distances such as those representing the distance of closest approach between the outer carbon atoms of a phenyl group in one chain and the backbone atoms of a neighboring chain.

In an effort to elucidate further the nature of the two prominent halos in the scattering curve, an in-

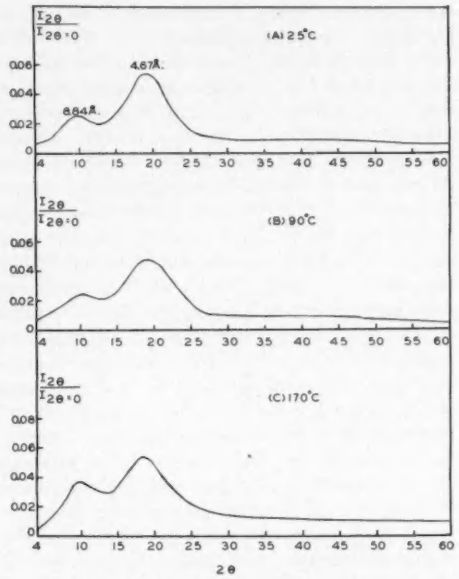

FIG. 4. *Radial scattering curves for unoriented polystyrene at several temperatures.*

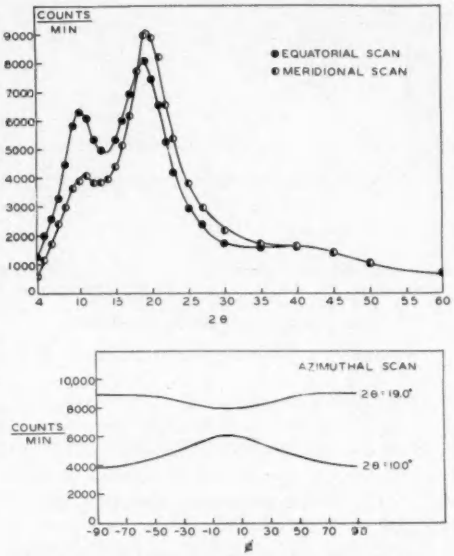

FIG. 5. *Scattering curves for oriented polystyrene—fast-cooled.*

vestigation of oriented polystyrene was undertaken. When heated to above about 80°C, polystyrene can be stretched to more than 100% of its original length [6]. Although the sample remains oriented after cooling, as shown by strong birefringence and marked anisotropic mechanical properties, the material does not crystallize. This is apparently due to the very irregular geometrical shape and structure of the chains, as well as to a certain amount of branching. Although Mark [30] states that it has been impossible to obtain an orientation in the amorphous diagrams, Katz [23] and Fuller [19] claim that polystyrene can be oriented and the effect observed by the splitting of the inner halo into two arcs. Observation of x-ray orientation for crazed polystyrene has also been reported [36]. It was decided to investigate this in the hope of detecting this orientation.

The sample used had been elongated about 300% at 93°C and then cooled rapidly. In order to pick up more easily any possible effects, filtered radiation was used. The curves, shown in Figure 5, have not been corrected for absorption and polarization. The sample was mounted with the orientation direction vertical, so that the equatorial scan is in a plane perpendicular to the direction of elongation of the sample. For purposes of comparison, a diffraction photograph of this sample is shown in Figure 6. Three points are evident. First, the halo maxima in the meridional scan are shifted slightly with respect to the maxima in the equatorial scan. The latter occur at the same angles as for unoriented polystyrene, corresponding to Bragg spacings of 8.84 and 4.67 Å.;

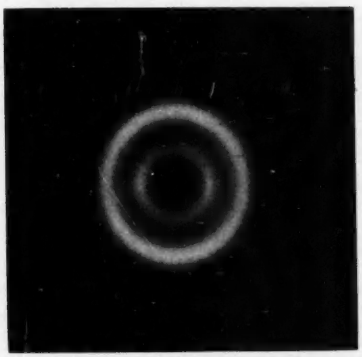

FIG. 6. *Diffraction photograph of sample reported in Figure 5—axis of stretching vertical.*

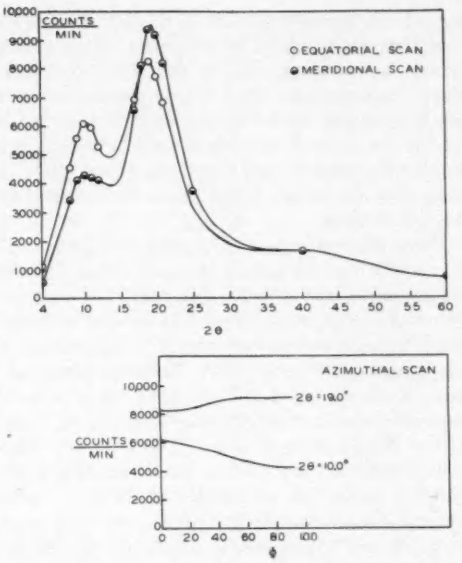

FIG. 7. *Scattering curves for oriented polystyrene—slow-cooled.*

the corresponding maxima in the meridional scan give Bragg spacings of 8.35 and 4.57 Å. Second, the two curves coincide at scattering angles greater than $2\theta = 40°$. Third, the azimuthal scans of both halos indicate an orientation effect. If the degree of orientation, O, is expressed by an equation of the form

$$O = \frac{180° - \beta}{180°}, \qquad (1)$$

where β is the width in degrees of the azimuthal peak at half-maximum intensity, then the orientation of the inner halo is 0.60 and that of the outer halo is 0.33.

It has been found that the mechanical properties of oriented polystyrene depend on the rate at which the sample is cooled after being oriented [31], the idea being that fast cooling preserves the orientation more effectively than slow cooling. It was decided, therefore, to investigate the diffraction pattern of a sample similar in previous history to the former one except that it had been cooled slowly after being oriented. The results, shown in Figure 7, were also obtained with filtered radiation, and are seen to be similar to the curves obtained from the rapidly cooled sample. The peak shift, however, is not the same, the inner halo in this case remaining unchanged and the outer shifting to a Bragg spacing of about 4.61 Å. The curves again coincide beyond $2\theta = 40.0°$, and the orientation, as indicated by the azimuthal scans, is similar. The numerical values, as calculated from equation (1), are 0.54 and 0.33 for the inner and outer halos, respectively, indicating less orientation in this sample than in the rapidly cooled specimen.

We see, therefore, that it is possible to obtain x-ray diffraction evidence of orientation in polystyrene. Not only is there such evidence in the splitting of the inner halo, but the outer halo is also observed to undergo splitting. It is thus seen that it is possible to orient amorphous regions in polymers. Recently [29], evidence has been obtained for the orientation of the amorphous regions in polyvinyl alcohol; we have also obtained evidence of orientation of amorphous regions in polyethylene [26]. Discussion on the possible interpretation of the scattering from unoriented and oriented polystyrene will be deferred until the effect of temperature on the diffraction pattern has been noted (see section on Glass Transition).

Polymethyl Methacrylate.—Polymethyl methacrylate is a polymer which at room temperature is similar to polystyrene in that it is glassy. Its diffraction pattern is also typical of those of amorphous solids, and is shown in Figure 8(A). This material is also unoriented. Two prominent halos occur at Bragg spacings of about 6.60 and 2.92 Å. The first undoubtedly arises from interchain interferences, the large spacing resulting from the bulkiness of the $-COOCH_3$ side-group. This group is probably slightly coiled up rather than extending to its maximum length perpendicular to the carbon-chain backbone, since the chain cross section in the latter case is at least about 9 Å., whereas the maximum spacing, as indicated by a modification of Bragg's equation, which would account for this peak, is 8.25 Å. The 2.92 Å. halo most probably arises from intramolecular interferences, although the effect of intermolecular interferences cannot yet be entirely eliminated. The scattering from the oxygen atoms undoubtedly contributes to this peak. The spacing between the two oxygen atoms in each ester group is about 2.25 Å., whereas the distance between oxygen atoms in neighboring ester groups will vary from 2.54 Å. upwards, depending on the folding of the main chain and thus on the rotation of these groups with respect to each other. Any dipole effect in the

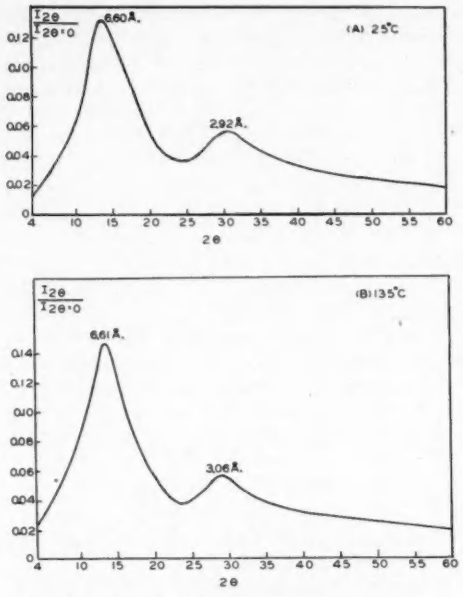

FIG. 8. *Radial scattering curves for polymethyl methacrylate at different temperatures.*

ester group would tend to orient neighboring groups as near to each other as geometrically possible, and this, together with the 2.25 Å. spacing within each group, might easily result in an average distance between oxygens of 2.92 to 3.62 Å. Of course, intramolecular distances between carbon atoms also contribute to this peak.

Polytrifluorochloroethylene.—Another example of a polymer which appears glassy at room temperature and is presumably amorphous is polytrifluorochloroethylene. A radial scattering curve from this material is shown in Figure 9(A). Peaks occur at angles corresponding to Bragg spacings of about 14.7, 5.53, and 2.25 Å. There are a number of unique features about this pattern. First is the rather large spacing of 14.7 Å., which, although of small intensity, is beyond experimental error. Second, the 5.53 Å. peak is quite sharp compared to the usual halos encountered in the liquids and amorphous polymers studied thus far. The half-maximum width is 2.5°, as compared with 5.9° for hexadecane and 5.0° for polyisobutylene. In fact, one is inclined to consider this peak as resulting from crystalline diffraction rather than from amorphous scattering. If the crystallites were very small, the diffraction peak could easily be broadened to the extent shown in the figure. Third, this peak has a definitely asymmetrical shape, very suggestive of a superposition of a crystalline diffraction peak on an amorphous halo. It appears difficult to analyze this pattern in terms of the usual amorphous diagram because of the almost crystalline order indicated by the 5.53 Å. peak.

When this material is heated above room temperature, the diffraction pattern changes, as indicated by the scattering curves in Figures 9(B) and 9(C) at 70° and 135°C, respectively. It is seen that the peaks in the scattering curve at 25°C corresponding to spacings of 5.53 and 2.25 Å. retain the same positions in the curves at 70° and 135°. The relative intensities also remain practically the same, being 2.82 at 25°C, 2.86 at 70°C, and 2.80 at 135°C. The peak at 14.7 Å. in the 25°C scan appears to have shifted to a spacing of 9.81 Å. in the 70°C scan, where it is also relatively less intense. It is not present in the 135°C pattern. It should be remembered that these three scattering curves are based on the same mass of material in the beam. A new peak ap-

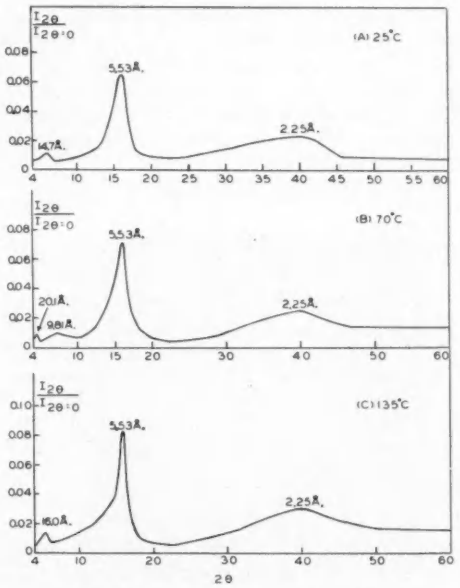

FIG. 9. *Radial scattering curves for polytrifluorochloroethylene at various temperatures.*

pears in the 70°C pattern at a Bragg spacing of about 20.1 Å. and is shifted in the 135°C scan to a spacing of about 16.0 Å. This peak was not evident in the 25°C scan, which had been started at $2\theta = 2.0°$. A striking feature of the series of scans in Figure 9 is the progressive sharpening of the 5.53 Å. peak as the temperature is raised. The half-maximum widths at 25°, 70°, and 135°C are 2.5°, 2.1°, and 1.5°, respectively. It also appears as if the 2.25 Å. halo becomes more symmetrical with increasing temperature.

No evidence of a "second-order transition" seems to have been found yet in this material, which is also very susceptible to supercooling and the formation of metastable amorphous states [8]. Its melting point is above 150°C, and it thus appears that the above results indicate a recrystallization of the material as it is heated. This is very similar to the phenomena occurring in quenched polyamides [7]. The uncertainty concerning the previous history of this sample makes an interpretation of the scattering patterns for this material difficult.

Crystalline Polymers

Octacosane.—For a better understanding of the scattering from polycrystalline polymers, the diffraction pattern of a crystalline paraffin was investigated. The scattering from octacosane was studied from $2\theta = 4°$ to $2\theta = 60°$; curves for the scattering between $2\theta = 10°$ and $2\theta = 30°$, in which range the diffraction peaks occur, are shown in Figure 10. The material is the commercial product put out by Eastman Kodak, and it melts at about 61°C. Scattering curves were obtained at 26°, 56°, 59°, 65°, and 150°C, and are shown in Figure 10 drawn to the same scale and based on equal scattering masses.

The two prominent peaks in the room-temperature scan occur at Bragg spacings of 4.15 and 3.74 Å. They represent the (110) and (200) crystal reflections, respectively [13, 32]. The 4.15 Å. peak occurs also in the 56° and 59°C scans. It can be seen that as the material is heated near its melting point an increasing amount of liquid or amorphous material is formed. This is indicated by the halos in the scans at 56° and 59°C. At 65°C the material is completely melted. The halos in the patterns at 59° and 65°C correspond to a Bragg spacing of 4.59 Å.; that in the 150°C scan is at a Bragg spacing of 4.77 Å. It appears from the scattering curves that the major change accompanying the transition in crystal

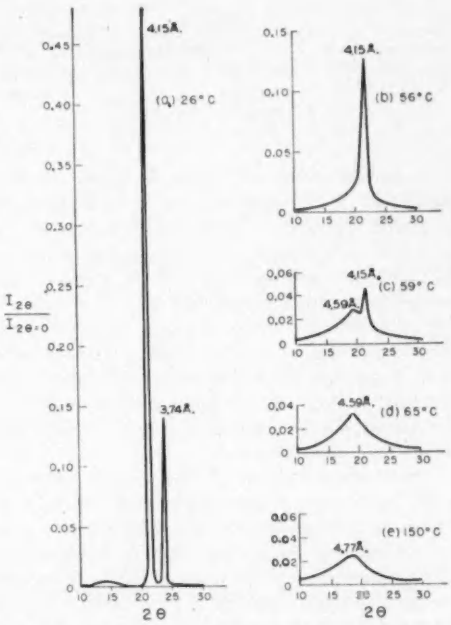

FIG. 10. *Scattering from octacosane at various temperatures.*

structure, which is believed to result from the onset of rotation about the long-chain axes [33] and occurs at about 54°C in octacosane [38], is the disappearance of the (200) reflection. It is interesting to compare the halo spacings of 4.59 and 4.77 Å. with that in hexadecane—*viz.*, 4.64 Å. The presence of the 4.59 Å. spacing at temperatures just above and below the melting point agrees with the idea that a certain amount of incipient order is retained when these substances melt—*i.e.*, over a very short range in the liquid the chains are practically parallel to each other. The longer chains of octacosane, and the fact that the scattering pattern was obtained very near the melting point, probably account for the smaller average spacing in this case (4.59 Å.) than in hexadecane (4.64 Å.). The 4.77 Å. halo in the 150°C scan is a manifestation of the larger average intermolecular spacings resulting from enhanced thermal motions.

In order to check the assumption often made of equality of scattering from equal masses of crystalline and amorphous polymer, the integrated intensities obtained from the scattering curves of octaco-

TABLE I

Curve in Figure 10	Temp. (°C)	Integrated intensity $2\theta = 4°–60°$	$2\theta = 10°–30°$	(110)+(200)
(a)	26	0.448	0.433	0.398
(d)	65	0.509	0.331	
(e)	150	0.518	0.332	

sane, part of which are shown in Figure 10, were compared. The results are shown in Table I, the integrated intensities being the areas under the respective components. The paraffin was in all cases enclosed in a mica-window cell, the powder being packed in at room temperature as closely and uniformly as possible (correction was made, of course, for the scattering due to the mica). The scattering in the crystalline diffraction pattern was investigated out to $2\theta = 60.0°$, and no other diffraction peaks of any measurable intensity were found. A diffraction photograph confirmed this.

The values for 65° and 150°C may be considered equal within the experimental error which is involved in determining ρt and obtaining the areas underneath the curves by means of a planimeter. Their difference is of the order of 1.5%. The value for the crystalline scattering is significantly different, the difference being at least 12%. It should be noted that this difference would be greater if the amorphous scattering beyond $2\theta = 60.0°$ were considered, since, whereas there is a fair amount of amorphous scattering in this region, there is little or no crystalline scattering. The only serious possible error in the result could be in the ρt determination of the crystalline material, since the area of the beam used during scattering was larger than that used for the absorption measurement, and it might be possible to pick out a nonrepresentative volume for the absorption determination. It is felt, however, that this error was not very serious in view of the tightness and uniformity of packing of the sample and the 1 mm.² area of the sample irradiated by the pinhole slit. The conclusion to be drawn from the above data is that although for this paraffin the scattering from crystalline and amorphous regions is of nearly the same "efficiency" (the ratio being about 0.88 if the total crystalline scattering curve is considered and 0.78 if only the sum of the (110) and (200) peaks is taken), equal masses of the two constituents do not scatter the same total integrated intensity.

It is interesting to note that the scattered intensity from the liquid octacosane at 65° and 150°C is very nearly the same although the two curves are of

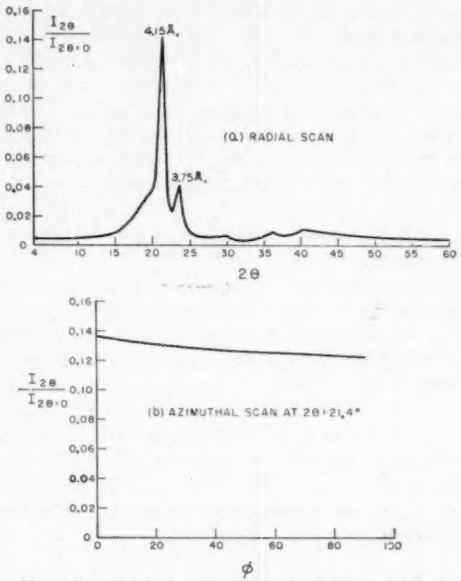

FIG. 11. *Scattering from unoriented polyethylene at 25°C.*

different shape; the widths of the halos at half-maximum intensity are 6.7° and 7.3° at 65° and 150°C, respectively, and the ratio of the halo maxima for these temperatures is 1.17. This serves to emphasize the greater significance of the integrated as compared to the peak intensity, and also indicates that the small changes in local structure in amorphous materials will affect the integrated scattered intensity much less than the intensity at any particular value of 2θ.

Polyethylene.—Polyethylene is a translucent, waxy-appearing polymer which melts at about 115°C to either a very viscous liquid or a rubbery material, depending on the molecular weight. It is thought to consist of long chains of CH_2 groups, although there is evidence from infrared spectra [17, 43] indicating the presence of about one methyl group to every fifty CH_2 groups. A typical x-ray diffraction pattern of an unoriented sample at room temperature is shown in Figure 11. Prominent crystalline diffraction peaks occur at Bragg spacings of 4.15 and 3.75 Å. and correspond to the (110) and (200) reflections, respectively. The three other small peaks at angles of about 30°, 36°, and 40° are also crystalline interferences. The structure has

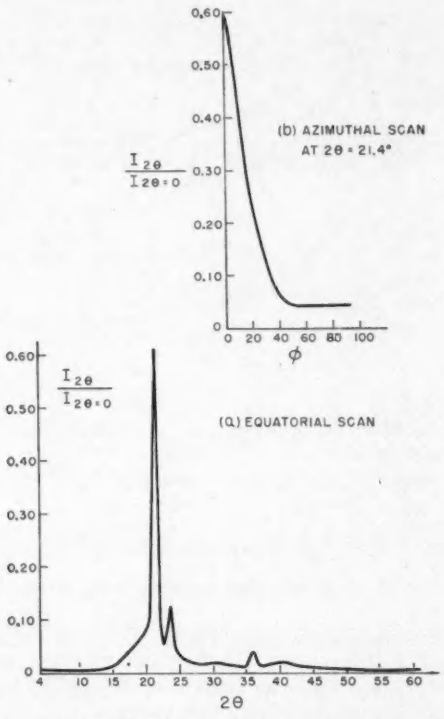

FIG. 12. *Scattering from oriented polyethylene.*

been shown to correspond to an orthorhombic unit cell with $a = 7.40$ Å., $b = 4.93$ Å., and $c = 2.534$ Å. [15]. It can also be seen that there is a certain amount of amorphous material present, since the (110) and (200) reflections are superimposed on a broad liquid-like halo. The crystalline pattern exhibits peaks of the same spacings as those in octacosane, which serves to confirm our ideas of the crystal structure of polyethylene.

The crystallites in polyethylene can be oriented by stretching the material. At low elongations the direction of preferential orientation is at an angle to the direction of stretching [11, 26], whereas at high elongations the crystallites line up in the direction of elongation. Figure 12 shows the diffraction curve at room temperature of a sample of polyethylene stretched 100% at 90°C. It can be seen that the material shows a high degree of orientation, being 0.845 as determined from the (110) peak by means of equation (1).

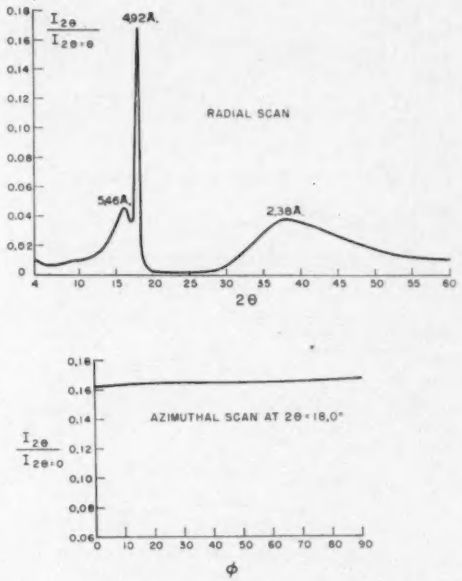

FIG. 13. *Scattering from polytetrafluoroethylene.*

Polytetrafluoroethylene.—When all the hydrogens in polyethylene are replaced by fluorine atoms, the polymer polytetrafluoroethylene (Teflon) results. It also possesses a composite crystalline-amorphous structure, as is shown by the diffraction curve in Figure 13. A prominent crystalline diffraction peak occurs at a Bragg spacing of 4.92 Å., with amorphous halos at spacings of 5.46 and 2.38 Å. The unit cell has not yet been worked out, but it appears that the chains are spaced farther apart than in polyethylene. This is especially true of the amorphous regions, which in polyethylene give a halo at about 4.53 Å. The behavior of this polymer as a function of temperature (its melting point is in the neighborhood of 300°C) has not yet been thoroughly investigated; the material appears to undergo a room-temperature transition which is believed to be a change in crystal structure [35].

Keratin.—The main constituent of skin, nails, horn, hair, and feathers is the protein designated as keratin. Although its exact structure is not yet definitely known, it is known to be a long-chain polypeptide of amino acids, among which are arginine, cystine, leucine, proline, valine, and tyrosine

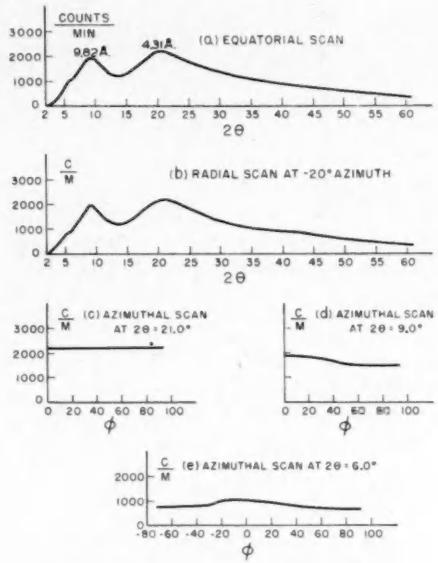

FIG. 14. *Scattering from merino horn.*

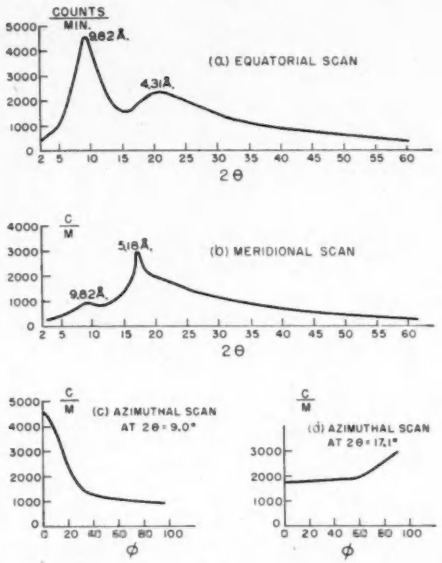

FIG. 15. *Scattering from unstretched hog bristle.*

[27]. Since it occurs in many materials in what seems to be a crystalline form, the first efforts to elucidate its structure were through an interpretation of its x-ray diffraction pattern, particularly in wool, where it was found that the structure is altered by stretching [2–5, 9, 28, 45]. This has led to the postulation of two keratin structures, an extended or β form and a folded or α form. Although the general features of the β form are agreed upon, the exact nature of the folding in the α form is still in dispute. The work described below was undertaken mainly in order to characterize the x-ray diffraction pattern of keratins as determined by a Geiger counter spectrometer and compare it with diffraction by simpler amorphous and polycrystalline polymers.

The diffraction curves of the keratins were obtained with filtered radiation because the intensity of crystal-monochromated radiation diffracted by the samples was very small. Correction was made for air scattering, but not for absorption in the sample (which was very small) or for polarization. All scans were obtained at room temperature and humidity. The curves in Figure 14 are from a piece of merino horn, obtained by machining a small uniform strip from the horn. Peaks occur in the radial scans at Bragg spacings of 9.82 and 4.31 Å. The 4.31 Å. halo shows no evidence of orientation, but the 9.82 Å. peak does give some evidence of orientation of this spacing. Attempts to obtain a diffraction pattern from stretched horn failed because the sample broke, although thoroughly water-soaked previous to elongating.

Figues 15 to 18 show the diffraction patterns of Russian hog bristle, both unstretched and at various elongations. The unstretched material gives a diffraction photograph which is a typical "α-pattern." The fibers were elongated by slow stretching and relaxing in steam. After attaining the elongation, excess surface water was removed from the fibers, which were then suspended in a stream of air in order to attain room humidity. The scans were usually obtained 3 to 4 hrs. after the elongation. In attaining the higher elongations many fibers broke; this accounts for the lower intensities in these patterns. In the pattern of the unstretched material, peaks occur in the equatorial scan at spacings of 9.82 and 4.31 Å., and in the meridional scan at spacings of 9.82 and 5.18 Å. When the material is stretched 50%, the equatorial scan indicates the

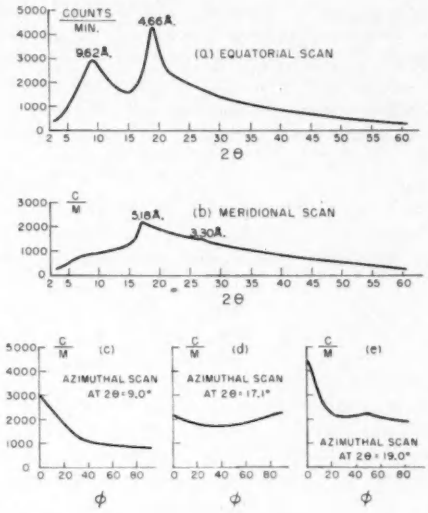

FIG. 16. *Scattering from hog bristle—stretched 50%.*

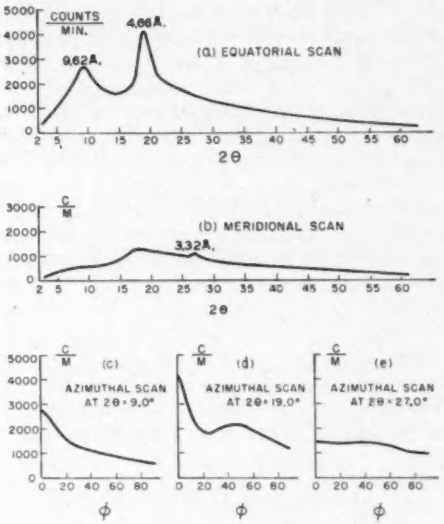

FIG. 17. *Scattering from hog bristle—stretched 78%.*

presence of a new spacing of 4.66 Å., and a slight shift of the first peak to a spacing of 9.62 Å. The 5.18 Å. peak is still present in the meridional scan, but is of lower relative intensity, and there is a faint indication of a peak at a spacing of 3.30 Å. The intensity of the latter peak increases as the material is stretched further, whereas that of the 5.18 Å. peak decreases, having disappeared at 78% elongation. At 95% elongation the meridional spacing is 3.36 Å. The change in the meridional spacing on stretching, as well as the appearance of a new equatorial spacing, has been the basis of the proposed change in structure from a folded to an extended polypeptide chain, since it can be shown that the repeat distance along an extended polypeptide chain is about 3.3 Å. The efforts have been concerned mainly with fitting a fold to the 5.18 Å. repeat distance present in the unstretched material.

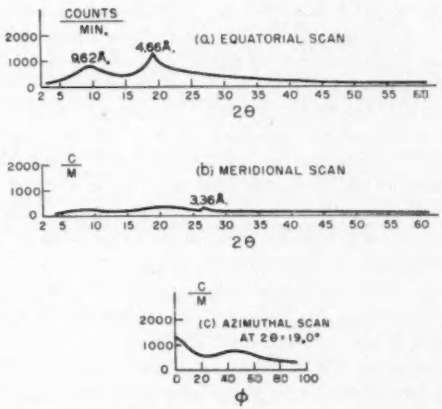

FIG. 18. *Scattering from hog bristle—stretched 95%.*

The scattering from unstretched and stretched Cotswold wool is shown in Figures 19 and 20, respectively. The spacings and their changes with elongation are the same as for the hog bristle, except for the presence of peaks in the wool diagram at spacings of about 5.90 and 25.2 Å., the latter being more intense in the stretched fibers. The fibers were stretched after soaking in water. It is rather interesting to note that whereas the intensity relationships of the halos in the equatorial scan are the same in unstretched hog bristle and wool, this does not appear to be the case for the stretched materials. The change in relative intensity of the peaks

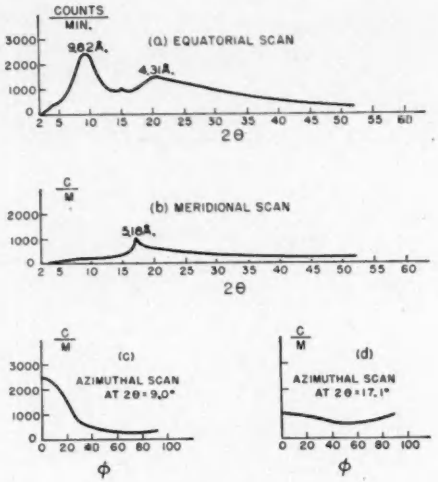

FIG. 19. *Scattering from Cotswold wool—unstretched.*

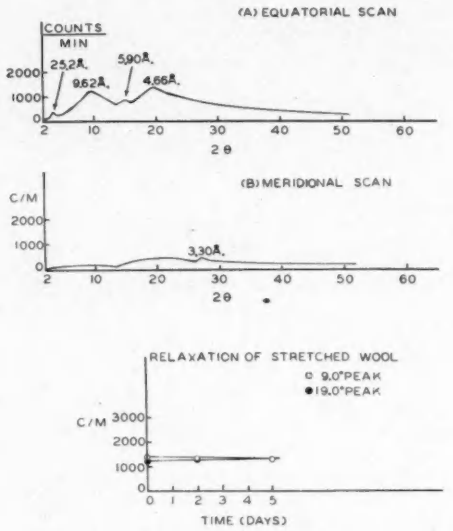

FIG. 20. *Scattering from Cotswold wool—stretched 60%.*

with time in the stretched-wool diagram appears to indicate some relaxation effects.

Although the radial scans of the above keratins show peaks which are very similar to the type observed in amorphous polymers, the corresponding azimuthal scans indicate a fairly high degree of orientation which is not usually found in amorphous materials. This type of fiber diagram has been interpreted on the basis of small crystallite size—that is, although a fairly large number of repeat distances occurs along the fiber axis, the number perpendicular to it is small. This reduction in crystallite size will lead to broadening of the reflections, presumably the effect observed here. This conclusion is also reached by a more careful consideration of scattering by individual molecular chains and small groups of molecular chains [22]. The diffuseness of the patterns also appears to indicate scattering by an amorphous component, but it is difficult to separate clearly the effects of the two constituents.

The Glass Transition in Polymers

It is a well-known phenomenon that many high-polymeric materials undergo a more or less abrupt change in many physical properties at a certain temperature, or in a small range of temperatures about this point. Since at this temperature a discontinuity has been found in the first derivatives of such primary thermodynamic properties of the material as volume and heat content, the transition has been termed one of the "second order" and the temperature designated as the "second-order transition temperature" [10]. It is also known as the "glass transition temperature," since the substance usually changes from a liquid or rubbery solid to a glassy solid [25]. Whereas there is general agreement that polymers undergo this type of transformation, there is still significant disagreement concerning the origin and nature of this transition. Presumably, as the material is cooled through the transition region, certain degrees of freedom characteristic of the liquid or rubbery solids are "frozen in," thus, for example, no longer contributing to the thermal expansion and specific heat, and also resulting in a change in other physical properties. The mechanism of this freezing-in is the point of dispute. Two entirely different mechanisms are possible: the equilibrium or thermodynamic freezing-in of a degree of freedom, and the dynamic or relaxation freezing-in. Kauzmann [25] concisely differentiates between the two as follows: "The thermodynamic mechanism arises from a structural change in the system or from the quantum-mechanical discreteness of its energy levels;

it is an equilibrium phenomenon. The relaxation mechanism, on the other hand, is a consequence of a deficiency in the experimental procedure; it results from changing the external forces acting on the system and then making measurements before the system has had time to re-establish complete thermodynamic equilibrium with its changed surroundings."

The prevailing opinion during recent years has been that the transition is only an apparent one and can be explained as a dynamic or rate phenomenon. This has been true especially in the case of polystyrene [1, 18, 40]. Experimental evidence for lactoprene, however, has seemed to indicate that the stretching mechanism changes in the transition region [41]. It seemed desirable, therefore, to investigate possible changes in the x-ray diffraction patterns of such materials in this temperature region, in order to relate such information to the above views. Polystyrene and polymethyl methacrylate were investigated for this purpose.

Polystyrene

The diffraction patterns of a sample of unoriented polystyrene were obtained at a series of temperatures between room temperature and 200°C. The glass transition in polystyrene occurs at about 81°C, the temperature depending on the molecular weight of the material. The material used here has an estimated viscosity average molecular weight of 300,000 to 400,000. At temperatures above 90°C the sample was exposed in a mica-window cell in order to eliminate any possible flow or orientation effects. Crystal-monochromated radiation was used. The scattering curve was obtained only after the sample had been kept for at least half an hour at the temperature in question. Most curves were recorded after heating the sample from room temperature to the temperature at which the measurement was made; in one case, however, a scattering curve was redetermined at room temperature after the sample had been heated to 135°C. Since the result was practically the same as the original room-temperature determination, it may be assumed reasonably well that the sample was at equilibrium at each of the temperatures.

The scattering curves at 90° and 170°C are shown in Figures 4(B) and 4(C). It can be seen that the ratio of the peak intensities of the two halos is different at the two temperatures. This has also been noted by Sebrell [37]. If a plot is made of the ratio of the two peak intensities as a function of temperature, the curve in Figure 21 is obtained. It can be seen that this ratio is essentially constant until about 90°C, at which point it falls to a lower value, which is then constant above about 160°C. It was also observed that the positions of the two peaks remain practically constant until about 160°C. Table II indicates the changes taking place. It thus apears that a fairly definite structural change takes place in polystyrene within the temperature range of about 90° to 160°C, a change which is not entirely explained by the thermal expansion of the material. The increased intensity of the inner halo with respect to the outer halo indicates a change in the number of atoms at this average distance from a given carbon atom. Although the exact change cannot be determined except by a Fourier analysis of the scattering curve, it is worth-while considering in a semiquantitative manner a possible interpretation of the scattering curves and the changes undergone when the material is heated or stretched.

The assignment of the inner and outer halos of unoriented polystyrene to inter- and intramolecular interferences, respectively, is supported by the scattering curves of oriented polystyrene. If we attribute the inner halo to distances such as those between the carbon atoms in the backbones of neighboring chains, then, by orienting these chains preferably along the direction of stretching, we would expect an increase in scattering in the equatorial plane. This is precisely what is found. Furthermore, any orientation of the main chains along the direction of stretching must result in a preferred orientation of

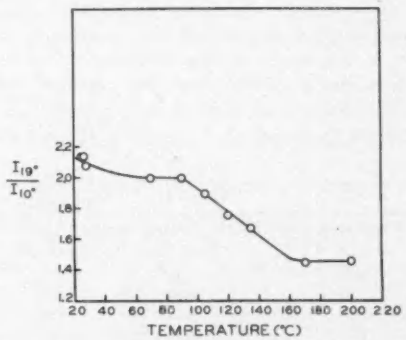

FIG. 21. *Ratio of intensities of two halos as a function of temperature for unoriented polystyrene.*

the phenyl side-groups perpendicular to this direction. If the outer halo results in part from interferences between phenyl groups, then we should expect it to indicate greater scattered intensity at the meridian. Moreover, if intermolecular interferences such as those between phenyl groups and neighboring chains also contribute to this halo, since their orientation is opposite to that of the phenyl groups, we should expect the two effects to work in opposite directions and produce a halo whose orientation is small and is a compromise between these two effects. This appears to be the case, and the indication is that the scattering from the phenyl groups outweighs that due to the comparable intermolecular distances. It is worth noting in this connection that if the above ideas are true, then we should expect small changes in the orientation of the material to affect the intensity distribution of the inner halo more than that of the outer halo. Comparison of the angular half-widths of the peaks in the azimuthal scans in Figures 5 and 7 shows this to be the case. A word is required about the origin of the 4.67 Å. halo. If part of it arises from inter-phenyl-group interferences, then we would expect these groups to be the ones which are separated by three chain carbon atoms, since phenyl groups on every other carbon atom are 2.54 Å. apart (assuming head-to-tail configurations), whereas alternate phenyl groups are spaced 5.08 Å. apart along a straight zig-zag chain. The average spacing will, of course, be determined by the amount of coiling in the chain.

In terms of these ideas, a not too unreasonable interpretation is possible of the behavior of unoriented polystyrene as a function of temperature. As the scattering curves in the region of about 90° to 160°C indicate, increasing temperature causes a relative increase in the 8.84 Å. population as compared to the density of atoms at the 4.67 Å. distance, without significantly altering these spacings. There also appears to be an absolute increase in the scattering in the inner halo (*cf.* Figures 4(B) and 4(C), which are reduced to the same scattering mass). This seems to point to a change in the configuration of the chain such that neighboring chains are able, on the average, to maintain a more regular distance of separation from one another over a longer length of chain. Only a Fourier analysis of the curves would indicate the magnitude of this possible tendency toward a slightly more regular intermolecular arrangement. It is, however, quite possible that the initial effect of increased temperature will be to permit greater rotation about bonds, which, because of the particular structure of polystyrene, results on the average in greater uniformity of cross section along larger portions of the chain and, therefore, in the possibility of a slightly more regular packing of neighboring chains. Further increase in temperature then results in expansion by means of increase of intermolecular spacing, as is indicated by the data in Table II. The fact that the inner halo average spacing then increases more than the outer halo spacing, both absolutely and relatively, seems to substantiate the belief that the outer halo arises in part from intramolecular interferences. It is significant that Fox and Flory [18] report a change in slope of the specific volume-temperature curves for polystyrene fractions at about 160°C, in addition to the usual more abrupt change at the transition point. This coincides with the present findings that the mechanism of expansion of the material is different above and below about 160°C.

TABLE II

Temperature (°C)	Bragg spacing (Å.) Inner halo	Outer halo
26	8.84	4.67
70	8.84	4.67
90	8.84	4.67
135	8.84	4.67
170	9.03	4.77
200	9.50	4.92

The scattering curves of polystyrene as a function of temperature indicate that the material is passing through various equilibrium configurational structures in the temperature range of about 90° to 160°C. If the above interpretation of this phenomenon is correct—*viz.*, its connection with increased rotational freedom at higher temperatures—it would suggest that the glass transition in polystyrene is associated with the temperature at which the barriers to rotational freedom are overcome. Therefore, it would seem justified to consider the part of the transition connected with rotational freedom to be of the equilibrium type [12], in that below the transition only a hindered rotation is possible, independent of how long one waits before making measurements on the system.

Polymethyl Methacrylate

Polymethyl methacrylate undergoes a glass transition in the neighborhood of 62°C. It was decided

to investigate its scattering far above this transition, and in Figure 8(B) the diffraction curve at 135°C is shown. The peaks correspond to Bragg spacings of 6.61 and 3.06 Å., compared to 6.60 and 2.92 Å. for the corresponding halos in the 25°C scan. The ratio of the peak intensities of the inner and outer halos is 2.61 at 135°C, compared with 2.36 at 25°C, the intensity of the outer peak being the same in both cases. Thus, the increase in temperature is accompanied by no change in the average spacing of the inner halo, but by a small increase in the average concentration of atoms at this distance. At the same time, the spacing of the outer halo increases, the concentration remaining the same.

In so far as these effects are definite, they could be interpreted as follows. If the outer halo results in part from intramolecular interferences between oxygen atoms, then it should be expected that as the temperature is increased the average separation might change as a result of rotation effects, but the average concentration of these scattering centers would remain the same. This is what is found. Since the spacing is increased with increasing temperature, an agent which will tend to cause greater rotation about bonds, we can infer that at room temperature the —$COOCH_3$ groups are maintained at a smaller average separation, most probably as a result of the interaction between the dipole moments of these groups. As the temperature is increased, the thermal agitation will counteract the orienting effect of these dipoles and result in an increased spacing between the diffracting centers.

If the inner halo arises from intermolecular interferences, then the conclusion to be drawn from the scattering curves is that the average spacing between chains remains practically the same, but the concentration of these scattering distances increases with rise in temperature. This phenomenon seems to be very similar to that occurring in polystyrene —*i.e.*, increased rotation in the chain has resulted in a more uniform cross section and therefore in the possibility of better packing over longer chain distances. This does not necessarily imply any tendency toward crystallization. The same average randomness exists, and the bulky side-groups still prevent efficient packing and disposition of forces required for crystallization. Nevertheless, on a micro-scale the chains are able to maintain a more regular disposition with respect to each other than was possible at lower temperatures, where geometrical arrangements of groups along a given chain were not quite as random and therefore the packing could not, on the average, be as effective as at the higher temperatures. It thus seems as if the transition from the glassy to the rubbery state, and vice versa, is accompanied by small, but quite definite, average changes in structure of the polymeric chains.

Acknowledgment

The authors are indebted to the Office of Naval Research (Contract Nos. N7-onr-374, Nonr-09000, and Nonr-09001) for its support of the part of this research carried out by the junior author. The latter also wishes to acknowledge the assistance furnished by a Textile Research Institute Fellowship during the coarse of this work.

The authors are indebted to Mr. Bryce Maxwell for furnishing the samples of oriented and unoriented polystyrene.

Literature Cited

1. Alfrey, T., Goldfinger, G., and Mark, H., *J. Applied Phys.* **14**, 700 (1943).
2. Astbury, W. T., and Bell, F. O., *Nature* **147**, 696 (1941).
3. Astbury, W. T., and Sisson, W. A., *Proc. Roy. Soc. (London)* **A150**, 533 (1935).
4. Astbury, W. T., and Street, A., *Trans. Roy. Soc. (London)* **A230**, 75 (1931).
5. Astbury, W. T., and Woods, H. J., *Trans. Roy. Soc. (London)* **A232**, 333 (1933).
6. Bailey, J., *India Rubber World* **118**, 225 (1948).
7. Baker, W. O., in "Advancing Fronts in Chemistry," Vol. I, New York, Reinhold Publishing Corp., 1945, p. 105.
8. Baker, W. O., private communication.
9. Bear, R. S., *J. Am. Chem. Soc.* **66**, 2043 (1944).
10. Boyer, R. F., and Spencer, R. S., in "Advances in Colloid Science," Vol. II, New York, Interscience Publishing Co., 1946, p. 1.
11. Brown, A., *J. Applied Phys.* **20**, 552 (1949).
12. Buchdahl, R., and Nielsen, L. E., *J. Applied Phys.* **21**, 482 (1950).
13. Bunn, C. W., *Trans. Faraday Soc.* **35**, 482 (1939).
14. Bunn, C. W., in "Advances in Colloid Science," Vol. II, New York, Interscience Publishing Co., 1946, p. 95.
15. Bunn, C. W., and Alcock, J. C., *Trans. Faraday Soc.* **41**, 317 (1945).
16. Cox, E. G., *Proc. Roy. Soc. (London)* **A135**, 491 (1932).
17. Fox, J. J., and Martin, A. E., *Proc. Roy. Soc. (London)* **A175**, 208 (1940).
18. Fox, T. G., and Flory, P. J., *J. Applied Phys.* **21**, 581 (1950).

19. Fuller, C. S., *Chem. Revs.* **26**, 143 (1940).
20. Gingrich, N. S., *Revs. Modern Phys.* **15**, 90 (1943).
21. Hermans, P. H., and Weidinger, A., *J. Polymer Sci.* **4**, 709 (1949).
22. James, R. W., "The Optical Principles of the Diffraction of X-Rays," London, G. Bell and Sons, Ltd., 1948.
23. Katz, J. R., *Trans. Faraday Soc.* **32**, 77 (1936).
24. Katzoff, S., *J. Chem. Phys.* **2**, 841 (1934).
25. Kauzmann, W., *Chem. Revs.* **43**, 219 (1948).
26. Krimm, S., and Tobolsky, A. V., *J. Polymer. Sci.* **7**, 57 (1951).
27. Lindley, H., *Nature* **160**, 190 (1947).
28. MacArthur, I., *Nature* **152**, 38 (1943).
29. MacGillavry, C. H., *Rec. trav. chim.* **69**, 509 (1950).
30. Mark, H., in "Chemistry of Large Molecules," New York, Interscience Publishing Co., 1943, p. 53.
31. Maxwell, B., private communication.
32. Muller, A., *Proc. Roy. Soc.* (*London*) **A120**, 437 (1928).
33. Muller, A., *Proc. Roy. Soc.* (*London*) **A138**, 514 (1932).
34. Pierce, W. C., *J. Chem. Phys.* **5**, 717 (1937).
35. Rigby, H. A., and Bunn, C. W., *Nature* **164**, 583 (1949).
36. Sauer, J. A., Marin, J., and Hsiao, C. C., *J. Applied Phys.* **20**, 507 (1949).
37. Sebrell, L. B., *Ind. Eng. Chem.* **35**, 736 (1943).
38. Seyer, W. F., Patterson, R. F., and Keays, J. L., *J. Am. Chem. Soc.* **66**, 179 (1949).
39. Simard, G. L., and Warren, B. E., *J. Am. Chem. Soc.* **58**, 507 (1936).
40. Spencer, R. S., and Boyer, R. F., *J. Applied Phys.* **17**, 398 (1946).
41. Stein, R. S., Krimm, S., and Tobolsky, A. V., TEXTILE RESEARCH JOURNAL **19**, 8 (1949).
42. Stewart, G. W., *Phys. Rev.* **33**, 889 (1929).
43. Thompson, H. W., and Torkington, P., *Proc. Roy. Soc.* (*London*) **A184**, 3 (1945).
44. Warren, B. E., *Phys. Rev.* **44**, 969 (1933).
45. Woods, H. J., *Proc. Roy. Soc.* (*London*) **A166**, 76 (1938).

(*Manuscript received May 1, 1951.*)

The Felting of Wool as Related to the Elastic and Swelling Behavior of the Fiber*

Herman Bogaty, Arnold M. Sookne, and Milton Harris

Harris Research Laboratories, Washington, D. C.

Introduction

Sufficient advance in the theory of the mechanism of the felting of wool has been made in recent years so that there is general agreement as to the contribution of such factors as the frictional and mechanical properties of the wool fiber. Thus, it is now recognized that in order for felting to be possible, a fiber must possess a surface scale structure, must be easily stretched and deformed, and must possess the power of recovery from deformation. A considerable amount of attention has been given to the relationship between the felting of wool and the frictional properties of the fiber [4, 7, 8, 9, 10, 11, 14, 15, 19, 20]. On the other hand, the role of the elastic behavior of the fiber in felting has not been widely investigated since Speakman, Stott, and Chang [20] noted the importance of the mechanical properties of the fiber in felting, based on a comparison of the milling behavior of wool in solutions of differing pH and in soap at various temperatures. Liu, Speakman, and King [13] discussed the relationship between the milling of fabrics dyed with large amounts of dye and the recoverability of the fibers from extension.

In the course of an investigation of the shrinkage of wool which is now in progress in these laboratories, a study of felting in solutions of a variety of organic and inorganic reagents was undertaken. The properties of the fiber in these solutions were also determined, and these exhibited a wide range of behavior. Thus, it was possible to compare the felting shrinkage of the wool and the single-fiber properties over a wide range of conditions. It is the purpose of this paper to present the results of these

* This work constitutes a part of the Army Quartermaster program on the shrink-resistance of wool for military clothing, which is under the supervision of the National Research Council Committee on Textile Finishing Research.

studies, including several of the general functional relationships developed between fiber behavior and the felting of wool top.

Materials and Methods

The wool used throughout this work was from a single ball of a commercial wool top of 64's grade Australian. Felting shrinkage of the top was determined in various reagents by a top-shrinkage test, previously described [3], which involves tumbling lengths of the wool top in 1 l. of liquid and measuring the length changes occurring as a function of time of tumbling; this test has been shown to relate to the felting shrinkage in conventional machine-laundering of fabrics made from top treated for shrink-resistance. The use of this simple procedure facilitated the accumulation of the shrinkage data, only relatively small quantities of liquid and of wool being required.

Mechanical measurements were made with a single-fiber autographic extensometer employing a resistance strain gage [6]. Generally, 2-in. fibers were used, and these were extended 20% and retracted, both at a rate of 30% per min. These measurements were first made in water and then in the reagent under study, the use of this calibrated fiber technique enabling the calculations of relative work for extension, or the 20% index. From each load-extension curve, the resilience of the wet fiber, defined as the ratio of the work recovered from extension to that required for extension, was determined.

The swelling of the fiber in the various reagents relative to the equilibrium diameter in water was determined microscopically through the use of a cell in which water could be replaced by the liquid being investigated. Ten fibers mounted on a slide were measured at three to five points along the length in contact with water, after which the reagent under study was allowed to flow through the cell. The slide was marked so that measurements could be repeated at the same points on the fiber. The relative-diameter values reported herein are the ratios of the fiber diameter in a given medium to that in water; the measurement can be repeated on a given system to within 0.02 unit in the range studied.

Results and Discussion

The top shrinkage in various reagents after 4 min. and after 10 min. of wet mechanical action are presented in Table I. Swelling and mechanical properties are also included for most of the systems studied.

Many of the neutral salts,—*e.g.*, the chlorides of sodium, potassium, and calcium—are seen to depress the felting of wool in proportion to the concentration of salt present. The solutions of calcium chloride appear to be more effective in depressing felting than sodium chloride solutions when they are compared on the basis of molarity. However, felting in solutions of both of these salts is not very different when the comparison is made on the basis of ionic strength. Depression of felting also occurs with the isopropanol solutions, the top shrinkage decreasing as the concentration of alcohol increases. These materials exert a deswelling action on the fiber, the diameter in the reagent being less than in water, and the felting shrinkage in the reagent being less than that in water in all cases in which this deswelling occurs. The decrease in relative fiber diameter is accompanied by a corresponding increase in stiffness of the fiber, as shown by the larger values for work required for extension; and the retractile ability of the fiber is lowered, as indicated by the decreased resilienee. The action of these solutions on the mechanical and swelling behavior of wool comes about through osmotic effects [18], and it may be said that in these media the wool is in a relatively "drier" atmosphere than in water. The lowered feltability in "dry" media is consistent with experience that dry wool is difficult to felt, as it is also in dry-cleaning solvents.

In contrast, acids, some organic reagents, and certain salts which swell wool all act to promote felting, the increased swelling being reflected in decreased work for extension and markedly greater resilience.

The addition of small amounts of acid to concentrated salt solutions is seen to decrease feltability even below that in the solutions containing equivalent amounts of salt only, although the presence of acid does not appear to affect the deswelling action of the salt significantly. The work required for extension is lowered in the acid-salt mixture as compared with that in a solution of salt alone, but, at the same time, the fiber retracts from extension more sluggishly, resulting in decreased resilience. The mechanical behavior of wool in concentrated salts containing acid has been discussed elsewhere [17].

In a general way, therefore, it can be seen that wool felts more readily in media that swell the fiber, and that felting is inhibited in reagents which hinder fiber swelling. The over-all relationship between top shrinkage and relative fiber diameter is plotted in Figure 1. As might be expected from the close relationship between fiber swelling and extensibility,

TABLE I. FELTING SHRINKAGE OF WOOL TOP AND MECHANICAL AND SWELLING PROPERTIES OF SINGLE FIBERS IN VARIOUS REAGENTS

Reagent	Top shrinkage (%) 4 min.	Top shrinkage (%) 10 min.	Relative fiber diameter*	Relative work for 20% extension†	Fiber resilience‡
H_2O	28	47	1.00	1.00	0.49
KCl, 4*M*	21	34	.98	1.14	.38
NaCl, 1*M*	29	46	—	—	—
3*M*	21	40	—	1.03	.45
5*M*	19	34	.96	1.25	.35
Sat.	12	26	—	1.30	.32
$CaCl_2$, 1.6*M*	24	39	.96	1.25	.40
3*M*	6	13	—	—	—
LiCl, 1*M*	30	49	—	—	—
5*M*	18	35	—	—	—
LiBr, 1*M*	34	50	—	—	—
5*M*	29	48	1.02	.80	.54
KI, 5*M*	29	45	1.03	—	—
KCNS, 1*M*	35	50	—	—	—
5*M*	39	53	1.02	.69	.62
HCl, 0.1*M*	35	52	1.03	.59	.68
HCOOH, 2%	38	54	1.03	.72	.66
9%	43	58	1.06	.67	.71
20%	45	59	1.08	.55	.75
Phenol, 5% (pH 7)	44	55	—	.62	.72
10% (pH 8)	56	68	1.26	.31	.89
Urea, 1*M* (pH 7)	31	48	—	—	—
5*M* (pH 7)	41	55	1.05	.83	.59
4*M* KCl + 0.01*M* HCl	13	27	.97	.96	.33
4*M* KCl + 0.1*M* HCl	18	34	.98	.91	.34
5*M* NaCl + .1*M* HCl	12	23	—	—	—
5*M* NaCl + .01*M* HCl	10	20	.95	1.18	.24
3*M* NaCl + .1*M* HCl	19	34	—	—	—
Sat. NaCl + 0.1*M* HCl	10	19	—	1.10	.24
Sat. NaCl + 0.1*M* HOAc	11	21	—	—	—
Sat. NaCl + 0.05*M* H_2SO_4	12	21	—	—	—
i-PrOH, 99%	4	8	.86	**	—
89%	15	25	.92	1.97	.23
84%	17	37	—	1.33	.31
49%	35	54	1.03	1.05	.48

* Ratio of fiber diameter in the reagent to that in water.
† Ratio of work to extend fiber 20% in reagent to that required in water.
‡ Ratio of work recovered to that required for 20% extension in the reagent.
** Fibers could not be extended 20% in this medium without breaking.

a similar curve is obtained when the top shrinkage is plotted as a function of work for extension (Figure 2). These curves describe good general relationships, especially when the variety of systems included is considered. In fact, no swelling system has been found in which felting is retarded, nor a deswelling system in which shrinkage is accelerated.

Detailed examination of some of the results, however, reveals several cases in which the swelling or the extensibility does not reflect the observed felting behavior. Thus, in concentrated lithium bromide solutions the fibers are swollen and exhibit corresponding low values of work for extension, yet increased felting over that in water is not found, as might be expected from the relationships shown in Figures 1 and 2. Similarly, the work-for-extension and relative-diameter values in the acid-salt solutions would predict equal or enhanced shrinkage over those in solutions containing salt alone, whereas the observed felting is substantially lower. The results

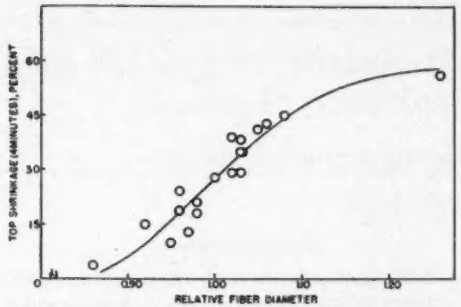

FIG. 1. *The relationship between felting of wool top and the swelling of fibers in various reagents (fiber diameter in $H_2O = 1.0$).*

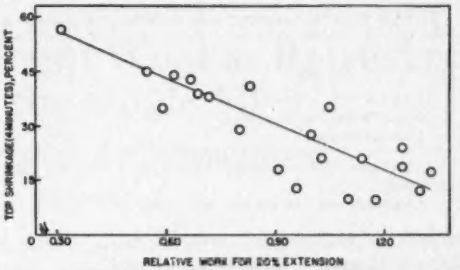

FIG. 2. *The relationship between felting of wool top and the relative work for extension of fibers in various reagents.*

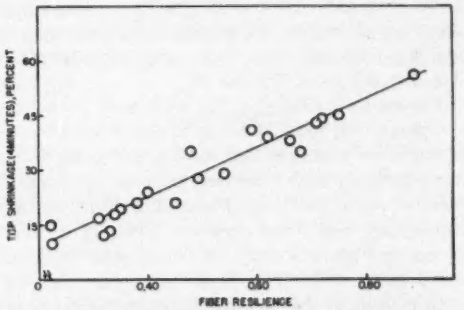

FIG. 3. *The relationship between felting of wool top and the resilience of fibers in various reagents.*

in Table I for the acid-salt mixtures indicate that a more precise functional relationship might be found between the top shrinkage and the fiber resilience in the wet state; this is shown in Figure 3.

The resilience of the fiber in any of the solutions shows very good correlation with the felting behavior. The felting behavior exhibited by the wool in the various solutions, as shown by the top-shrinkage values, ranged from 6%, similar to that for well-processed, shrink-resistant, commercial wool in water, to 56% shrinkage in 4 min., which represents an extremely rapid rate of felting—about twice that of untreated wool in water. It therefore appears that a very close relationship exists between felting and the elastic properties of the single fiber, although it is impossible to state that this is a cause-and-effect condition. In any event, the linear relationship plotted in Figure 3 enables the prediction of the felting behavior from the single-fiber properties with a surprisingly high degree of precision. Thus, the simple function $S = 70R - 6$, where S is the top shrinkage in 4 min. and R is the fiber resilience, enables the calculation of the top shrinkage from the fiber measurements to within 2 top shrinkage %, on the average, of the observed values given in Table I, which is within the experimental error of the shrinkage determination. An even simpler relationship, $S = 55R$, gives calculated values of the top shrinkage which differ from the observed values given in Table I by only 3%, on the average. Similar correlations may be obtained using the top-shrinkage values at 10 min. These are surprisingly simple functions for such a complex phenomenon as felting.

These results indicate that reagents which promote rubber-like behavior and increased fiber resilience increase the feltability of wool. This appears to be the principle of acid fulling. The results suggest avenues for further investigation in the direction of reducing felting through modification of the medium, as well as through modification of the wool, in such a way as to produce less swellable or less rubbery fibers. This has been attempted through the deposition of resins *in situ* [1, 12], and by the use of cross-linking agents of many kinds [2, 5].

It was considered desirable to demonstrate that the felting behavior of wool, as indicated by the top-shrinkage test, could be affected by modification of the elastic behavior of the fiber itself, as well as by changing the medium surrounding the fiber. Previous work [18] had shown that wool dyed to saturation with an acid dye exhibited elastic properties similar to those of dry fibers, and Liu, Speakman, and King [13] indicated that the dyeing of wool with large amounts of dye is effective in decreasing the fiber resilience and feltability.

Accordingly, calibrated fibers and top-shrinkage specimens were dyed to equilibrium with Orange II by the procedure described by Smith and Harris [16]. In essence, this consists in dyeing the wool

TABLE II. MECHANICAL AND FELTING PROPERTIES IN 0.1*M* HCl OF WOOL DYED TO SATURATION WITH ORANGE II

Sample	Top shrinkage (%) 4 min.	Top shrinkage (%) 10 min.	Relative work for 20% extension*	Fiber resilience†
Dyed wool	18	32	1.95	0.21
Wool "dyed" without dye	32	49	1.00	.59
Untreated wool	32	49	—	.62

* Ratio of work required to extend dyed fiber in 0.1*M* HCl to that required to stretch untreated fiber in the same medium (20% index).

† Ratio of work recovered to that required for 20% extension in the reagent.

in a 0.1*M* HCl solution with an excess of dye at 45°–50°C, using a large liquor-to-wool ratio. Dyeing was continued for 24 hrs., a time sufficient to insure attainment of equilibrium. A set of controls was run simultaneously, omitting the dye from the bath. Since the dye is quite readily displaced from the wool at higher pH values, fiber measurements and top-shrinkage tests were made in 0.1*M* HCl. The data are given in Table II.

During the tumbling of the dyed wool in the top-shrinkage test, some bleeding of dye occurs, so that it might be expected that the top-shrinkage values are slightly too high. In view of this fact, the agreement of these data with those of Table I is quite satisfactory, and if the values of Table II were inserted in Figure 3, they would be seen to fit the curve quite well. This result provides additional confirmation of the validity of the relationship between felting and fiber resilience, and demonstrates that modification of felting may be achieved by fiber modification as well as through modification of the medium surrounding the fiber.

Summary

1. The felting of wool top in a number of types of solutions has been determined. The feltability is seen to vary approximately directly with the fiber swelling in each reagent and inversely with the work for extension of the wet fiber.

2. There is a close linear relationship between the felting shrinkage of wool top and the resilience of the single fiber in the wet state. The linear relationship between felting shrinkage and resilience of the wet fiber makes possible the estimation of feltability from the single-fiber properties with surprisingly high precision.

3. Changes in felting behavior may be produced by modification of the fiber properties as well as through changes in the medium. Fibers dyed to saturation with Orange II exhibit elastic behavior similar to that for undyed fibers in a poor-felting solution, and are shown to felt correspondingly slowly.

Acknowledgment

Grateful acknowledgment is made to Miss Martha L. Markovich, to Mrs. Virginia A. Moran, and to Miss Nancy J. Tucker for assistance in making many of the measurements reported.

Literature Cited

1. Barr, T., and Speakman, J. B., *J. Soc. Dyers Colourists* **60**, 238 (1944).
2. Barr, T., and Speakman, J. B., *J. Soc. Dyers Colourists* **60**, 335 (1944).
3. Bogaty, H., Frishman, D., Sookne, A. M., and Harris, M., TEXTILE RESEARCH JOURNAL **20**, 270 (1950).
4. Bohm, L., *J. Soc. Dyers Colourists* **61**, 278 (1945).
5. Capp, C. W., and Speakman, J. B., *J. Soc. Dyers Colourists* **65**, 402 (1949).
6. Dart, S. L., and Peterson, L. E., TEXTILE RESEARCH JOURNAL **19**, 89 (1949).
7. Gralén, N., and Olofsson, B., TEXTILE RESEARCH JOURNAL **17**, 488 (1947).
8. Harris, M., and Frishman, D., *Am. Dyestuff Reptr.* **57**, P52 (1948).
9. Lindberg, J., TEXTILE RESEARCH JOURNAL **18**, 470 (1948).
10. Lindberg, J., and Gralén, N., TEXTILE RESEARCH JOURNAL **18**, 287 (1948).
11. Lipson, M., and Howard, P., *J. Soc. Dyers Colourists* **62**, 29 (1946).
12. Lipson, M., and Speakman, J. B., *J. Soc. Dyers Colourists* **65**, 390 (1949).
13. Liu, W. T., Speakman, J. B., and King, P. E., *J. Soc. Dyers Colourists* **55**, 183 (1939).
14. Martin, A. J. P., *J. Soc. Dyers Colourists* **60**, 225 (1944).
15. Mercer, E. H., *J. Council Sci. Ind. Research* **18**, 185 (1945).
16. Smith, A. L., and Harris, M., *J. Research Natl. Bur. Standards* **19**, 81 (1937).
17. Sookne, A. M., Bogaty, H., and Harris, M., TEXTILE RESEARCH JOURNAL **21**, 479 (1951).
18. Sookne, A. M., and Harris, M., *J. Research Natl. Bur. Standards* **19**, 535 (1937).
19. Speakman, J. B., Chamberlain, N. H., Menkart, J., *J. Textile Inst.* **36**, T91 (1945).
20. Speakman, J. B., Stott, E., and Chang, H., *J. Textile Inst.* **24**, T273 (1933).

(Manuscript received September 4, 1951.)

The Felting of Shrink-Resistant Wool as Related to Some Properties of the Single Fiber*

Arnold M. Sookne, Herman Bogaty, and Milton Harris

Harris Research Laboratories, Washington, D. C.

Introduction

The felting behavior of wool in many solutions has been shown to be related to the stress-strain behavior of the fibers in those media [2]. A simple relationship of this type may be stated as

$$S = a + b\,R,$$

where S is the shrinkage in a simple top-felting test under arbitrary conditions [1], R is the work recovered from extension of the fiber as a fraction of the work of extension, and a and b are constants. This equation was found to hold for untreated wool tops in a wide variety of reagents. The extent of shrinkage of wool which has been subjected to a chemical antifelting treatment would also be expected to be influenced by the nature of the felting medium, depending upon the extent to which the wool has been modified in processing. Much of the study of fiber properties in relation to the feltability of shrink-resistant wool has heretofore emphasized the importance of the surface of the fiber. Thus, it has been clearly established that chemical treatments for conferring shrink-resistance to wool which involve the use of active chlorine result in a decrease in the directional frictional effect of the single fibers (see [7], for example). It has been postulated that this change in the frictional properties of the fibers, which is generally a decrease in the difference between the with-scale and the anti-scale friction, is responsible for the antishrink effect, and that the effectiveness of the shrink-resistance resulting from treatment is inversely proportional to the residual directional frictional effect. It would seem, therefore, that the felting behavior of wool top in any given solution might be expressed in terms of both the frictional and the elastic properties of the single fibers. By controlled treatment of the wool with aqueous solutions of active chlorine, wool top of several levels of shrink-resistance can be obtained. Through a study of the felting of these tops in several solutions of widely differing types and of the elastic and frictional properties of the fibers in these same solutions, it was hoped that a unified picture of the felting in terms of both single-fiber properties would emerge. It is the purpose of this paper to present the results of this study.

Experimental

Fibers from a single ball of a commercial 64's grade wool top were calibrated in five solutions of widely different types by extension to 20% at a rate of 30% per min. using a single-fiber autographic extensometer [3]. After retraction, the fibers were relaxed, and their frictional properties were measured in both directions (with and against the scales) and in the same five solutions using the Fiber Friction Meter [5]. The reagents in which the fibers were equilibrated prior to the measurement of the single-fiber mechanical and frictional properties included water, 0.1M HCl, 9% HCOOH, 4M KCl, and 4M KCl + 0.01M HCl. These solutions have been shown [2] to affect the felting and elastic behavior of wool profoundly, the solutions ranging from very good to very poor felting promoters.

The calibrated fibers were inserted in lengths of wool top which were subjected to a commercial type of treatment for shrink-resistance [4] which involves rapid processing with a mildly alkaline sodium hypochlorite solution, followed by removal of the excess reagent with sodium bisulfite. By adjustment of the concentration of available chlorine in the bath, five levels of shrink-resistance were obtained. The treatments designated below as "control," A, B, C, and D represent wool processed with 0%, 0.3%, 0.6%, 1.0%, and 1.2% of available chlorine, respectively.

After treatment the fiber properties were determined in the five solutions listed above, and the level of feltability was determined by means of the top-

* This work constitutes a part of the Army Quartermaster program on the shrink-resistance of wool for military clothing, which is under the supervision of the National Research Council Committee on Textile Finishing Research.

TABLE I. SHRINKAGE AND ELASTIC AND FRICTIONAL PROPERTIES IN VARIOUS MEDIA OF WOOL TOP TREATED FOR SHRINK-RESISTANCE TO VARYING DEGREES

Treatment	Medium	Top shrinkage (%) 4 min.	Top shrinkage (%) 10 min.	Fiber resilience*	Frictional properties† μ_1	μ_2	$\mu_1 - \mu_2$
Control	H_2O	23	38	0.48	0.52	0.28	0.24
A	H_2O	9	30	.43	.49	.32	.17
B	H_2O	8	22	.47	.49	.35	.14
C	H_2O	2	7	.45	.50	.42	.08
D	H_2O	1	3	.47	.65	.60	.05
				Mean .46			
Control	0.1M HCl	34	54	0.64	0.54	0.27	0.27
A	0.1M HCl	20	40	.63	.48	.29	.19
B	0.1M HCl	12	32	.64	.52	.35	.17
C	0.1M HCl	3	5	.61	.49	.39	.10
D	0.1M HCl	1	5	.61	.70	.61	.09
				Mean .63			
Control	9% HCOOH	38	56	0.66	0.55	0.28	0.27
A	9% HCOOH	29	48	.69	.56	.33	.23
B	9% HCOOH	20	41	.65	.51	.36	.15
C	9% HCOOH	5	14	.69	.54	.48	.06
D	9% HCOOH	1	5	.64	—	—	—
				Mean .67			
Control	4M KCl	15	28	0.37	0.49	0.27	0.22
A	4M KCl	3	10	.37	.42	.26	.16
B	4M KCl	5	13	.37	.44	.32	.12
C	4M KCl	0	3	.34	.44	.33	.11
D	4M KCl	0	3	.35	.66	.56	.10
				Mean .35			
Control	4M KCl + 0.01M HCl	11	22	0.36	0.52	0.28	0.24
A	4M KCl + 0.01M HCl	2	9	.33	.50	.33	.17
B	4M KCl + 0.01M HCl	4	11	.35	.55	.40	.15
C	4M KCl + 0.01M HCl	2	6	.34	.51	.39	.10
D	4M KCl + 0.01M HCl	2	4	.32	.63	.60	.03
				Mean .34			

* Ratio of the work recovered from extension to 20% to the work required for extension.
† μ_1 and μ_2 are the coefficients of friction in the anti-scale and with-scale directions, respectively.

shinkage test [1]. The complete data therefore include top shrinkage, frictional measurements, and elastic properties in five media for each of five levels of shrink-resistance. Since previous studies [2] demonstrated that the most satisfactory correlation between felting and elastic behavior was found with the use of work recovery as the independent variable, only this parameter is reported herein.

The results are summarized in Table I.

Discussion

The retractile ability of the fibers in a given medium is seen to be unimpaired by the degree of shrink-resistance. The mean values of the resilience of the fiber in each of the solutions, defined as the ratio of the work recovered to that required for 20% extension, are given in Table I, and the top shrinkage is plotted against the fiber resilience in Figure 1. This graph confirms the linear functional relationship noted previously for untreated wool, and indicates that the same type of relationship holds for mildly chlorinated wool. When the level of treatment approaches complete shrink-resistance, the slopes of the lines approach zero, as in the case of treatments C and D.

The tabulated values for the coefficients of friction indicate the manner of change with increasing level of treatment. The value of μ_1, anti-scale coefficient,

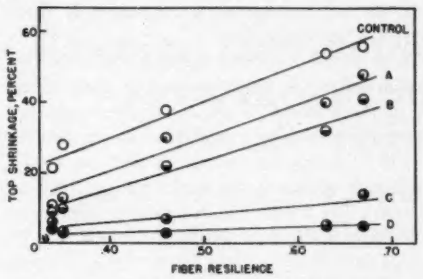

FIG. 1. *The relationship between felting of wool top treated with solutions of NaOCl and the resilience of the fibers in various reagents. (Letters denote levels of treatment described in the text.)*

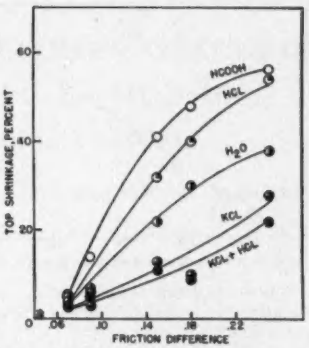

FIG. 2. *The relationship between felting of wool top treated with solutions of NaOCl and the frictional properties of the fibers in various reagents.*

is substantially constant at about 0.5 for all but the highest level of treatment, irrespective of the nature of the solution in which the measurement is made. The with-scale coefficient, μ_2, increases progressively with increasing felt-resistance, such that the friction difference decreases and approaches zero. One may average the values for each treatment, neglecting the relatively small differences observed due to the effect of the solution on the measurement. The mean friction differences calculated in this way for the control and treatments A, B, C, and D were found to be 0.25, 0.18, 0.15, 0.09, and 0.07, respectively. The top shrinkage is plotted against these averaged values of friction difference in Figure 2. This graph indicates that the wool is substantially unfeltable when the friction difference is brought to a low value by the chlorination, irrespective of the felting medium. When the wool is untreated or only mildly chlorinated, the fiber-friction difference is relatively high, as is the top-shrinkage value. Despite the fact that these high friction differences are virtually identical in the various solutions, the observed shrinkage values appear to depend upon the nature of the solution for untreated or mildly treated wool.

Considering the results plotted in Figures 1 and 2 together, one may view the situation in the following manner: When top is subjected to felting in various solutions, if the level of treatment is low, the resilience of the fiber controls the extent of shrinkage. The shrinkage is low in solutions in which fiber resilience is low, and high in solutions in which the fibers exhibit good recoverability. When the wool has been subjected to an adequate shrink-resistance treatment, the difference in with-scale and anti-scale friction coefficients begins to vanish. In these cases, the nature of the solution or the elastic behavior of the fibers is unimportant, the residual directional frictional effect limiting the felting to a low value.

Since the shrinkage is a function of resilience (at constant level of treatment) and a function of friction difference (in a given medium), one should be able to relate the shrinkage in any medium to measurements of single-fiber friction and stress-strain properties. Such a very general relationship is shown in Figure 3, in which top shrinkage is shown as essentially a linear function of the product of friction difference and fiber resilience. It should be noted that similar relationships hold when other frictional parameters are employed—*e.g.*,

$$(\mu_1 - \mu_2)/(\mu_1 + \mu_2) \quad \text{or} \quad \left(\frac{1}{\mu_2} - \frac{1}{\mu_1}\right).$$

This is a remarkably simple functional relationship for such a complex phenomenon as felting. The linear plot enables prediction of the shrinkage of top from the two types of fiber properties under a wide variety of circumstances of treatment and felting medium. Although the relationship is drawn as a straight line in Figure 3, a better fit of the observed points could actually be obtained with a sigmoid curve. This latter fact is consistent with experience. The limiting shrinkage in the top test is of the order of 60%–70%, even with long-continued tumbling, so that the curve should be expected to flatten at the upper end. Similarly, at the low end of the curve, where felting is slow and friction difference is the

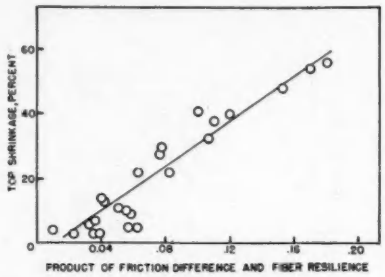

FIG. 3. *The relationship between felting of wool top treated with solutions of NaOCl and the product of friction difference and fiber resilience.*

controlling element, measurement of both top shrinkage and friction difference is subject to larger error. One could state that below certain low values of friction difference and top shrinkage the wool is not feltable for all practical purposes, and hence this region of the curve is flat. In the middle region the slope is a maximum, and the shrinkage behavior is most sensitive to changes in medium or level of treatment.

From this generalized relationship one may observe that unshrinkability may be achieved through reduction of the friction difference, as with chemical treatments, or through modification of the elastic properties of the fiber. This latter approach is commonly utilized in cleansing wool with dry-cleaning solvents; in such media wool shows poor resilience and little felting. With respect to the treatment of wool, the deposition of resins *in situ* would be expected to operate in this manner; the recent work of Lipson and Speakman [6], for example, is of interest in this connection.

It is noteworthy that the highest level of treatment, D, gives frictional coefficients which differ considerably from the others. Thus, as one increases the level of chlorination, μ_1 is virtually constant and μ_2 increases slowly and steadily. Upon going from treatment C to treatment D, the frictional coefficients increase markedly, although the improvement in shrink-resistance is not very great. It is noted that this level of treatment corresponds to the point at which the 20% index begins to depart appreciably from the 0.9–1.0 range. By usual commercial standards, the top represented by treatment D would be considered as overtreated.

Some of the preceding discussion assumes that the friction-difference values are substantially independent of the medium in which the measurements are made. While this is a reasonable assumption for the present systems, the results do indicate small, but consistent, effects of the media on the friction difference. The values for the friction difference tend to be high in the same media for which ease of extension and resilience are high. It is not possible from these data to determine whether these results are due to the test method, in which the extensibility of the fibers plays a part, or whether intrinsically the fiber "friction" is greater in swelling media.

Summary

The feltability of wool treated to various degrees of shrink-resistance by a commercial type of wet-chlorination process has been determined in solutions of widely different types. The shrinkage behavior has been shown to be related in a simple manner to the single-fiber elastic properties (fiber resilience) and to the fiber frictional properties measured in the same reagents. A simple linear function of the form $S = a + bFR$, where S = top shrinkage, F = friction difference, R = fiber resilience, and a and b are constants, enables the prediction of the feltability of the wool from the single-fiber properties under a wide variety of circumstances of treatment and felting medium.

Literature Cited

1. Bogaty, H., Frishman, D., Sookne, A. M., and Harris, M., TEXTILE RESEARCH JOURNAL **20**, 270 (1950).
2. Bogaty, H., Sookne, A. M., and Harris, M., TEXTILE RESEARCH JOURNAL **21**, 822 (1951).
3. Dart, S. L., and Peterson, L. E., TEXTILE RESEARCH JOURNAL **19**, 89 (1949).
4. Frishman, D., and Harris, M., U. S. Patent 2,466,695, April 12, 1949; assigned to Harris Research Laboratories.
5. Frishman, D., Smith, A. L., and Harris, M., TEXTILE RESEARCH JOURNAL **18**, 475 (1948).
6. Lipson, M., and Speakman, J. B., *J. Soc. Dyers Colourists* **65**, 390 (1949).
7. Mercer, E. H., *J. Council Sci. Ind. Research* **18**, 188 (1945).

(Manuscript received September 4, 1951.)

Chemical Substitution in Fibrous Cotton and Resistance of Substituted Cotton to Microbiological Deterioration

Charles F. Goldthwait, Edmund M. Buras, Jr., and Albert S. Cooper

Southern Regional Research Laboratory, New Orleans, Louisiana*

Abstract

The resistance for months to deterioration by microorganisms (in soil burial) of suitably acetylated fibrous cottons, some with only one-third of the hydroxyl groups substituted, depends upon the distribution of the acetyl groups as well as upon the total number of such groups present.

Under usual conditions of acetylation, according to the literature, reaction takes place first in the amorphous cellulose, starting at the most accessible places. According to the present experimental acetylations and special dyeing tests, the reaction, which is probably confined at first to the amorphous cellulose, takes place along fibers in various segments and throughout cross sections rather than as a layer increasing in thickness from the surface inward. At one-third substitution the amorphous cellulose is converted to triacetate; the cotton fiber still contains about two-thirds of the original cellulose, which is present as crystalline material surrounded by acetylated cellulose. The swelling capacity of the cotton in water is greatly reduced.

While the mode of attack by microorganisms is not completely understood, they apparently begin at the most readily accessible amorphous cellulose. From the literature and from the present experiments, protection by partial acetylation is believed to be due to the blocking of hydroxyl groups, the filling of spaces between chains in the amorphous cellulose, and the suppression of swelling. It represents a general method of rendering cellulose unsuitable, or at least inaccessible, as a food for microorganisms.

A relatively low degree of partial saponification may detract greatly from the rot-resistance of a well-protected acetylated cotton owing to the restoration of amorphous cellulose, with loss of blocking groups and a restoration of swelling capacity.

Partial methylenation by treatment with formaldehyde may impart a moderate degree of rot-resistance, which seems best explained as being due to the suppression of swelling by cross-linking. Formaldehyde-containing resins which impart rot-resistance apparently act similarly.

The evidence obtained indicates that the amorphous cellulose is the part which is normally attacked, and that its ability to swell in water may be a more important factor in microbiological attack than is commonly recognized.

The use of dyeing has been exemplified for qualitative tests to supplement other evidence regarding substitution and the composition and properties of substituted cottons.

THE GREAT RESISTANCE of suitably acetylated cottons to attack by microorganisms is recognized [8, 10, 19]. The resistance normally increases with the degree of substitution, or acetyl content, but since the fiber as a whole may become highly resistant even though the cellulose is only partially reacted, the resistance must be even more dependent upon the distribution of the acetyl groups in the cellulose than upon their number. In the course of many preparations at the Southern Regional Research Laboratory of partially acetylated yarn and cloth, which were subjected to soil-burial tests, necessary requirements of processes for obtaining products of exceptionally high mildew- and rot-resistance have become recognized. The indications from these experiments and from work with partially methylenated cotton are that the rot-resistance depends very largely upon the reaction taking place in the amorphous portion of the cotton cellulose and upon the consequent suppression of swelling of the fiber.

* One of the laboratories of the Bureau of Agricultural and Industrial Chemistry, Agricultural Research Administration, U. S. Department of Agriculture.

Nature of the Acetylated Cottons

We are concerned mainly with acetylations whose products remain in partially substituted fibrous form as textiles. The most attention will be given herein

to cottons acetylated under the conditions usually employed at the Southern Regional Research Laboratory [6, 10], or in the same general manner. Similar processes, or the steps in the processes, have been employed by others, although they have not always been applied to the partial acetylation of cotton textiles.

The cellulose acetylated in the present work was ordinary (undegraded) cotton. Two principal methods of acetylation were employed, described here only in very general terms: (1) pretreating cotton by soaking for 4 hrs. or more in glacial acetic acid, acetylating with a mixture, usually of about one-fourth acetic anhydride and three-fourths glacial acetic acid, with perchloric acid present as catalyst to 0.1% or 0.15% of the mixture, washing in water, and drying with heat; (2) preswelling cotton in water or in acetic acid containing about 20% of water, displacing water from the cotton by strong acetic acid followed by acetic acid containing the perchloric acid catalyst, then acetylating in anhydride, washing, and drying with heat. In the first method, one-third of the hydroxyl groups are substituted at room temperature within about 1 hr., and in the second, with the cotton preswollen, within 1 to 2 min. These processes will be referred to as the "first" and the "second" methods.

The products studied came not only from small laboratory preparations, but also from 5- to 10-lb. lots of yarn or from 50- to 150-yd. lots of cloth from pilot-plant production. No distinction is necessary on the basis of size of lot; the samples of high resistance to microbiological attack are considered representative of possible commercial products.

Recent Views in the Literature *

Fibrous Cellulose Reactions

Recent writers are in general agreement on reactions like the fibrous acetylation of native cotton. These reactions are not only heterogeneous, between a liquid and a solid substance, but the solid consists of two constituents, crystalline and amorphous cellulose, which are present in a submicroscopically mixed form, although in a continuous structure. While frequently spoken of as "surface" reactions, most fibrous acetylations are not conducted under conditions suitable for true surface reaction, which, as defined for example by Timell [20], would result in a layer of a homogeneous product on the outside of the fiber. Rather, ". . . more recent investigations indicate that the amorphous material is converted both earlier and more rapidly than the crystalline."

Heuser and coworkers [15] say that esterification proceeds in a heterogeneous manner on fibrous cellulose, the hydroxyl groups reacting as they gradually become accessible to the reagents. If the reaction is interrupted before completion, "the substituting groups are, in many cases, nonuniformly distributed over the chain molecules."

Studies by Vermaas and Hermans [21] on acetylation and deacetylation of model viscose filaments showed nonuniformity of reaction even though the product appeared to be homogeneous under the microscope and conditions seemed to be the most favorable for initial uniform surface action. They stated that the degree of substitution at a given time and place on a fiber is a function of accessibility. Hence, the amorphous cellulose is acetylated first, and the cellulose in the crystalline regions is acetylated relatively little until the amorphous cellulose is nearly converted to triacetate.

Happey [12, 13] summarized results from extensive experiments on the acetylation of regenerated and native fibers by mixtures of glacial acetic acid and acetic anhydride, with sulfuric acid as catalyst. He said that in the mode of acetylation which is typical, in the main, whether by the fibrous or the solution method, the acetylation mixture gains access to the fiber by way of regions opened up in its amorphous portions by pretreatment; acetylation of these takes place along with that of intercrystalline surfaces of the cellulose; and in the initial stages of the reaction most of the crystalline cellulose remains unsubstituted. Cellulose triacetate thus formed in the amorphous regions is swollen quite readily by the acetylation medium, so that fresh cellulose surfaces are exposed, and penetration into the more crystalline portions is assisted by progressive swelling and acetylation. The acetylation reaction appears to occur in this way mainly in the amorphous and intercrystalline parts of the fiber up to a combined acetic acid content of 30% (21%–22% acetyl), which is also the point at which one-third of all the hydroxyl groups are reacted.

The coincidence that the most valuable properties of partially acetylated cotton are pronounced when the hydroxyl groups in the cellulose are about one-

* References present mainly recent views, and these can be consulted for earlier references for points on history and priority.

third reacted, and that one-third of the hydroxyls (the primary) are distinctly different from the rest, may have led earlier writers to believe that a true cellulose monoacetate, with one acetyl group present in each glucose unit, was possible. However, papers which take into account the structural features that are the most widely accepted for native cellulose do not indicate any possibility that any one hydroxyl group alone can become reacted throughout a cellulose fiber, and then the next most reactive. In fact, Heuser [14] stated "It is impossible to produce mono- or di-substituted cellulose esters that can be regarded as homogeneous compounds."

X-ray diffraction diagrams of partial acetates also indicate that the amorphous cellulose reacts before the crystalline cellulose because there is no change in the x-ray diagram, which is that of native crystalline cellulose, up to an acetic acid content of 30% [12].

Properties of Acetylated and Partially Deacetylated Products

Partial deacetylation decreases rot-resistance and changes other significant properties of acetylated cottons. Hence, recent views on deacetylation, or saponification, are pertinent.

Happey [12, 13] indicated that deacetylation proceeds in much the same manner as the opposite reaction, acetylation. At the beginning of the saponification of cellulose triacetate by alkali, the latter penetrates into the less crystalline regions and they are converted back to cellulose. Penetration may continue into the body of the fiber, to the surfaces of the crystallites, and ultimately to their interiors. Since removal of acetyl groups reduces the cross sections of cellulose chains, partial saponification restores the most readily accessible amorphous portions of the fiber to something like their former state so that they can swell again in water and become readily penetrable to dyes.

Also, with model viscose filaments of a degree of substitution of about 2.3, saponification took place, according to Vermaas and Hermans [21], more readily in the regions of easier accessibility. Hence, a given degree of acetylation reached by acetylating directly may correspond to an entirely different distribution of acetyl groups from that present when the same degree is obtained by saponification from an acetate of higher substitution. That is, the most readily accessible amorphous portions, well covered by acetyl groups in the first product, are the ones from which the acetyl groups have been removed in the saponified product. That the effect is in the amorphous cellulose is indicated by a rapid increase in swelling capacity with partial saponification, up to about the normal amount for the original fibers. This swelling behavior is the reverse of that during acetylation, when the swelling capacity of fibers is progressively reduced by the substitution of hydroxyl groups until the amorphous cellulose is reacted, but this capacity changes little more as the reaction proceeds into the crystalline regions.

Corresponding with the loss of direct dyeing capacity by cellulose during partial fibrous acetylation, as hydroxyl groups are blocked and swelling is reduced, there is restoration of some of this dyeing capacity after even very little saponification [12]. There are apparently large enough spaces in the regenerated cellulose of the partially saponified acetate, when swollen in the dye bath, for the entry of dye molecules, which are then taken up on hydroxyl-rich areas of accessible intercrystalline surfaces.

Deterioration of Cellulose by Microorganisms

Although the process of deterioration of cellulose by either bacteria or fungi is not fully understood, some of the initial effects are visible in the microscope, and have been discussed in recent papers. Bacteria act at points where they are present on the fiber surface, and degrade away the cellulose to form hollowed-out areas. They do not penetrate at once to the center of the fiber, but etch the surface so that it appears roughened or pitted [11, 17]. While fungi have been observed many times to penetrate into the lumens of cotton fibers, there is a difference of opinion [11] as to whether all fungi act in this way. Any fungi which degrade cellulose without penetrating would act on the outside, like bacteria, since the modes of attack are similar in that digestion of cellulose apparently occurs only at the immediate point of contact between organism and cotton fiber, when the required amount of moisture is present, and when the temperature is favorable. Abrams [1] and Greathouse [11] described similar microscopically visible attack, which was made more apparent by removal of degraded cellulose at attacked areas by means of sodium hydroxide.

The probability that the attack begins in the amorphous cellulose, the part which is the most accessible to chemical reaction, has been recognized, but may have had less emphasis than it deserves. Siu [17] said that it seems quite certain that the amorphous portions of cotton fibers are more readily attacked by

microorganisms than the crystalline areas; and Greathouse [11] mentioned the importance of the internal surface that is accessible to the enzymes and noted that the proportions of the crystalline and amorphous forms of cellulose should be a factor in the rate of dissolution by enzymic action. A recent British publication [5] indicates that the attack of microorganisms on cotton "consists of the preferential removal of the amorphous cellulose of the interlacing fringes of the micelles. Loss of strength then results."

The closely related property of the swelling of cellulose in water, the seat of which is commonly accepted as being mainly the amorphous region, seems to have had still less attention. Greathouse [11] implied that swelling is a factor, but, in general, no clear distinction seems to have been made between simple swelling in water while attack is going on and previous swelling with chemical agents. Possibly, the importance of simple swelling seems so obvious that it is generally regarded as being understood. At least, the need for relatively large amounts of moisture for the growth of fungi and bacteria on cotton means that the cotton is considerably swollen when it is attacked by them.

Since the final effect of attack is commonly regarded as largely hydrolysis, and the final products as sugars which the microorganisms can utilize, efforts have been made [1, 11, 18] to determine whether fungi can subsist on acetyl-substituted sugars such as might be expected to result from the hydrolysis of cellulose acetate. The answer is not yet clear. Greathouse [11], in suggesting that the resistance of cellulose acetate is due to chemical blocking of the hydroxyl groups, commented that the availability of sugars to microorganisms is decreased by chemical substitution in their hydroxyl groups. Hence, the blocking of hydroxyls may have effects in addition to that on swelling. Probably, it is safe to agree with Barker [3] that the acetylation of cellulose represents a method of rendering it unsuitable as a food substance for the organisms, although there is still some question as to whether the cellulose is actually rendered unsuitable or whether it is merely inaccessible.

Experimental Observations and Discussion

Acetylation and Saponification

The most important observations in the present work were the retention of most of their strength by suitably acetylated cottons when buried in active soils for 6 months to a year [10], and the failure of certain other acetylated cottons, although of supposedly high enough acetyl content, to show similar high resistance.

One cause of such failure is the lack of sufficient reaction throughout the cotton, which is often due to tight twist or weave with consequent poor penetration, even though the average acetyl content may be sufficient. Such defects have been readily shown by a special dye test (see Methods section, below) in which well-acetylated areas are colored by an acetate yellow, unacetylated areas by a direct blue, and poorly acetylated areas to an intermediate green. Extensive experience has shown that acetylated cottons of 20% to 30% acetyl content, which take the full yellow color of the acetate dye, can be expected to have excellent rot-resistance, while materials that show appreciable amounts of blue or green can be expected to break down prematurely. Frequently, the blue-yellow dyeing test will allow a better prediction of response to soil burial than will the analysis for amount of acetyl.

Another possible cause of low rot-resistance is partial saponification by alkali. In tests simulating repeated severe laundering, acetylated cottons which before the laundering would not color with the direct blue dye in the usual test took up appreciable amounts afterward; in soil-burial tests these cottons lost strength to a degree entirely out of proportion to the decreased amounts of acetyl. For example, a cloth sample containing 23.3% acetyl retained 89% of its strength after soil burial, but when tested after the acetyl had been reduced by saponification to 20.5%, the cloth retained only 20% of its strength. On the other hand, a sample which was acetylated directly to the same level (20.7%) as the partially saponified sample and dyed the full yellow shade retained 80% of its strength during the same test.

The effects of saponification were especially striking in a series of acetylations by the second method. Samples with 23% to 41% acetyl retained full strength after soil burial for 6 months, but a similar sample with 37% acetyl which was saponified back to 23% was completely destroyed in 2 weeks. That the two materials with the same acetyl content (23%) were entirely different in behavior is unquestionably due mainly to a difference in the distribution of the acetyl groups.

Saponification to 23% acetyl content was accompanied by two other significant changes from the

original properties: the yellow-dyeing rot-resistant fiber became green-dyeing as well as rot-susceptible; there was a restoration of swelling capacity. For example, the swelling of an untreated cotton yarn was represented by 38% water retention in the centrifuge test [22], that of the product of direct acetylation to 23% acetyl content was 23% (retention), but that of the cotton whose 23% acetyl was reached by saponification was 32%.

It follows from saponification experiments that there may be limitations to the use of partially acetylated cotton for articles intended to be mildew-resistant which require frequent or severe laundering or exposure to other alkaline conditions. Also, other special properties may be impaired.

Low resistance of some partially acetylated cottons, especially if they are of low acetyl content, is explained partly by nonuniform acetylation within individual fibers, which apparently is due to intrinsic fiber irregularities. The reaction was studied by examination under the microscope of fibers from dyeings of samples taken during the acetylation of loose raw cotton by the first method. In examples to be described as typical, the direct violet (see Methods section, below) was used in place of the usual blue.

Under the microscope all of the fibers in dyed original cotton were of a pronounced violet when viewed longitudinally, and cross sections were violet throughout, all of the cotton being apparently very uniformly colored. There were changes, however, in the dyeing behavior of fibers after even a minute or two of reaction.

In a sample dyed after 7 min. of acetylation, when the over-all color was still violet, light violet areas showed on many fibers, sometimes alternating with darker areas, while other portions approached white, with a slight yellowing in a few spots. In a cross section there were still many violet fibers, some nearly white fibers, but no pronounced yellow ones. The acetyl content was 4.1%, but this is merely an average for fibers that were very irregularly reacted.

In a 15-min. sample which appeared brown when well blended, many fibers still had violet spots or areas, portions which were practically white, and others which were definitely yellow. No fiber was found which was entirely of one color. A cross section showed a similar variety of colors. Most of the fibers were white or light yellow, but some were still violet, and others were a pronounced yellow. The sample contained 6.9% acetyl, but this is obviously an average of widely different acetyl contents in many minute areas scattered apparently at random along the fibers.

The final sample, with 26.5% acetyl after 1¼ hrs. of acetylation, had all of its fibers dyed with the acetate yellow except for occasional spots or short lengths of violet and possibly a very little white. In cross sections, a few fibers had been cut where they were violet or nearly white, and the rest all appeared yellow. The violet spots clearly represented points of little or no acetylation, but were too few in number to constitute an appreciable element of weakness upon exposure to microbiological attack.

In another acetylation, fibers which had had an alkali boil went through just the same changes, but the dyeings showed that the reaction was somewhat more rapid and more thorough. A sample with 20.5% acetyl did not show any violet spots or cross sections.

In both of these acetylations the reaction was proceeding through segments of 2 to 25 times the width of a fiber, apparently distributed at random along the fibers and alternating with unacetylated portions of a similar variety of lengths. The reaction appeared also to be taking place throughout the whole cross section at once rather than taking place at fiber surfaces and then gradually proceeding inward. This is indicated by the loss of direct dyeing capacity throughout cross sections, by the intermediate nearly white appearance throughout sections, and by the increase in the depth of color of the acetate yellow dye throughout cross sections.

Acetylated layers on the outsides of fibers, of such composition and thickness as to be shown by dyeing and the microscope, have occasionally been seen in cross sections of fibers of a fairly high degree of acetylation, but have not been found on enough fibers for them to constitute a major factor in the long-time protection of the cotton by acetylation.

The conception of a definite layer as a means of protection [17, 18] seems to be excluded also by Abrams' experiments [1] on partially acetylated cotton which had been finely divided by grinding in a Wiley mill, or in a ball mill, and then submitted to tests for mildewing. The ground acetylated cotton showed no growth, although mildew flourished on untreated cotton controls. If the acetylated cotton fibers had been protected mainly by superficial acetylated layers, the fibers would certainly have been opened to attack by microorganisms by either type of grinding. Since the material used by Ab-

rams was prepared by one of the present authors at the Southern Regional Research Laboratory (by the first method), cross sections of fibers dyed while in the form of yarns ravelled from the cloth have since been examined. They were dyed throughout with the acetate yellow, which showed the acetylation to be microscopically uniform, with no tendency toward outer layers.

The ground partially acetylated cotton probably consisted mainly of: cellulose crystallites still surrounded by acetate; possibly crystalline portions with exposed cellulose; and amorphous triacetate. Crystallites in either state are not swollen by water, nor, probably, is the amorphous triacetate to any extent. If, after grinding, all the surfaces exposed were covered with acetyl groups, protection could be attributed to blocking of hydroxyls, or to blocking accompanied by lack of swelling; but if there were free crystalline cellulose areas exposed, their protection would necessarily seem due mainly to lack of swelling in water, with consequent exclusion of the enzymes.

While substituted celluloses may be highly resistant to attack by microorganisms under most severe conditions of exposure, probably none are completely resistant. For example, a fabric with 29% acetyl retained about 90% of its breaking strength in soil for 1 year, but cloth from the same acetylation, made into a sand bag and left on the ground in New Orleans for 2 years, retained only 35%–40% of its strength. The bag remained intact and both results were outstanding, but the protection was not permanent. The ultimate weakening of the acetylated cotton must have resulted from attack on some constituent, probably the unacetylated regions, by some organism. Cellulose-destroying organisms in the neighborhood must have subsisted meanwhile on other materials, although being present in close proximity to a relatively large amount of unacetylated cellulose—namely, unreacted crystalline portions, which constituted about half of the cellulose of this partially acetylated cotton. Some of the enzymes must finally have reached assimilable cellulose and set up a slow deterioration—slow, perhaps, because the crystalline regions, which are not swellable by water, are not readily attacked even though unacetylated.

An alternative possibility, that microorganisms exist which can actually attack the acetylated portions of cotton, will merely be mentioned since no evidence concerning them is available; if they had been present in the tests under consideration, they must have been few in number.

The experiments with partially acetylated cottons have indicated that reduction of swelling capacity by chemical substitution is an important factor in their rot-resistance. The importance of suppression of swelling is emphasized even more by the imparting of rot-resistance by the reaction of cotton to relatively low degrees of substitution with formaldehyde or with certain resins.

Formaldehyde and Resin Treatments

Experience with cotton reacted with formaldehyde [9] and with resins which contain formaldehyde as a constituent is similar in several respects to that with partially acetylated cotton. There is a gain in rot-resistance, accompanied by a decrease in swelling and by a loss of direct dyeing capacity. Examples are given below of cottons reacted with formaldehyde in the presence of an acid catalyst in acetone solution to produce partial methylene ethers.

Cotton with 1.3% to 1.4% combined formaldehyde retained 80% of its strength after 3 weeks of soil burial, and 50% after 5 weeks, while the strength of the untreated cotton was completely lost in 1 week.

The swelling in water of a cotton which had been similarly treated, containing about 1.5% combined formalydehyde, was reduced from 43.8% for the untreated to 23.4%, reported as water retained after centrifuging.

Cotton has been made completely resistant to ordinary dyeing with a direct fast blue 4GL dye by as little as 0.2% to 0.3% combined formaldehyde.

There are possibilities of imparting much greater resistance to rotting by formaldehyde treatment, but for practical application the loss of breaking strength encountered during some of the formaldehyde treatments would need to be considerably reduced. In a specific case, cotton had lost approximately half of its breaking strength by the time it reached a content of 2.64% combined formaldehyde. Then, however, it not only resisted direct dyeing completely and had greatly reduced swelling capacity, but after 11 weeks of soil burial it retained almost 80% of the half-strength of the treated material.

As in acetylation, the manner of combination of the formaldehyde in partially methylenated cottons may sometimes be more important for their resistance to mildew and rotting than the amount that is combined. In a type of experiment described earlier [9], cotton yarn was preswollen in water,

then the water was exchanged for acetone (so that the cotton remained in a state corresponding to approximately fully swollen), and the cotton was finally methylenated along with air-dry cotton. After the reaction, the first cotton was colored to a medium shade in a direct blue dyeing, and had the same amount of residual water in the centrifuge test as the original cotton. Although this product had 1.5% combined formaldehyde, it was no more rot-resistant than the other, which did not have much more than half as much combined formaldehyde (0.87%), but which failed to color in the direct dye test and had the low swelling capacity of little more than half that of the original cotton. The two partially methylenated cottons retained about equal strengths in soil-burial tests—85% to 90% of the original strengths after 5 weeks, and 60% to 70% after 10 weeks.

The dye-resistance of partially methylenated cottons may be partly explained by the blocking of some of the hydroxyl groups, but comparison with the very slight resisting effects of low degrees of substitution by acetylation—for example, the 4.15% above—indicates that far too few hydroxyl groups are blocked by formaldehyde reaction to have much effect alone upon dyeing [9]. Hence, the resisting is attributed mainly to the reduction of the swelling in the dye bath, which is normally depended upon to open the pore structure of the cotton for the admission of direct dye molecules.

The great reduction of swelling in water, brought about, for example, by a substitution of as few as one-twentieth of the hydroxyl groups in the cellulose (at 1.35% combined formaldehyde), is most reasonably explained as being due mainly to cross-linking. It seems equally probable that the cotton is rendered less open to attack by microorganisms by the same reduction of swelling due to cross-linking.

The cotton which had more combined formaldehyde but was not more protected from rotting may also have had formaldehyde present as cross-links but, evidently owing to a more open structure at the time of reaction, cross-links, if present, were unable to impart sufficient reduction of swelling capacity to cause dye-resisting, or to bring about rot-resistance in proportion to the larger amount of formaldehyde present. The need for more combined formaldehyde to protect the preswollen cotton is somewhat similar to that of cotton swollen before acetylation, which required more acetyl groups to impart high rot-resistance than were needed for cotton which entered the acetylation mixture in the relatively unswollen air-dry state.

Effects similar to some of those obtained with formaldehyde have been reported for cottons treated with resins which contain formaldehyde as a constituent. White and Siu [23] reported that 5% or 6% of a urea formaldehyde resin or a melamine formaldehyde resin protected cotton cloth completely for 2 weeks in a pure-culture mildew test and, in another instance, for 2 weeks of soil burial. The effect was thought to be due possibly to protective surface layers of resin around the fibers. On the other hand, Dean [7] described experiments in which 5%–6% of a resin or other material that might conceivably form surface layers around the fibers was applied to cotton cloth, and its effect tested by soil burial. All test pieces except those containing two of the resins lost the same amounts of strength as the untreated cotton cloth—nearly 90% in 1 week. Protective layers had obviously not been formed. The fabrics treated with the exceptional materials, which were urea and melamine formaldehyde resins applied as water-soluble monomers and cured in the conventional manner, were somewhat protected as they lost only 40% of their breaking strength.

Well-known properties of resin-treated cottons—reduced direct dyeing capacity and reduced water retention in the centrifuge—indicate a similarity to partially methylenated cottons and a similarity in the causes of the resistance of the two types of material to microorganisms. Cameron and Morton [4] are believed to express present-day views when they point out that both urea formaldehyde and melamine formaldehyde resins act by cross-linking to reduce swelling, and that the cross-links are of two kinds: very stable methylene ether bridges like those from simple formaldehyde treatment, due to reaction of formaldehyde freed during the resin-treating process; and more complex, less stable "resin" bridges. Hence, the rather moderate amount of protection from microbiological attack afforded by relatively small amounts of resins seems most plausibly explained as being due partly to substitution of hydroxyl groups, but mainly to the suppression of swelling and consequent reduced accessibility of amorphous cellulose.

The rot-resistance of the partially methylenated cottons prepared so far has been on a generally lower level than that obtainable with partial acetates, and the protection by resins seems to be even lower.

Data are not yet adequate for a "final" explanation of the results obtained in either case, or for an opinion as to the ultimate possibilities for rot-resistance.

Methods Employed

The usual methods of acetylation have been described above in general terms. Special acetylations of loose fiber were made by the first method given, essentially as employed for yarn and cloth [6, 10]. These experiments were performed especially to obtain samples to show the course of the reaction by dyeing, loose cotton being employed to ensure that all fibers would be freely accessible to the solutions —that is, not subject to any mechanical constriction that might cause them to be either acetylated or dyed below the normal degree. Raw cotton was presoaked in glacial acetic acid overnight, and was then transferred for acetylation to a mixture of 2 parts acetic anhydride and 8 parts glacial acetic acid containing 0.1% to 0.15% perchloric acid as catalyst, the smaller amount of catalyst being used to obtain a slightly slower reaction. With 0.1% catalyst, 18.3% acetyl was reached in 45 min., and 26.5% acetyl in 1¼ hrs. at room temperature. One lot of cotton which was boiled in a 2% solution of sodium hydroxide at atmospheric pressure for 4 hrs. before presoaking and acetylating reacted somewhat more rapidly (with only 0.05% catalyst), and reached 20.5% acetyl in ¾ hr.

Samples of the cotton were withdrawn from each acetylation at intervals, washed well, dried, and dyed together so that all would be comparative for examination under the microscope.

Acetyl contents were determined by the common method of saponification with alkali and titration of the excess.

Dyeings for checking the uniformity and general nature of acetylated cotton [6] were made with the direct-dyeing Pontamine Fast Blue RRL Conc. (Du Pont), which will dye cotton without staining acetate, and Celliton Fast Yellow RRA (General Dyestuff Corp.), which will dye well-acetylated cotton but will not stain cotton that is unacetylated.

For following acetylations more closely by observing dyed fibers under the microscope, a particular violet (Pontamine Fast Heliotrope B (Du Pont)) has been found to be better than the blue [6]. It has the advantage of dyeing all unacetylated fibers throughout their cross sections, which the blue frequently fails to do, so that its use removes one source of doubt as to the reason for the appearance of many fibers (fiber segments) which are described in the text as white or nearly white.

The dyeings are only qualitative tests, but in some of their applications they clearly point out different degrees of acetylation; they are especially useful and dependable when samples to be dyed are strictly comparative. From descriptions presented above, it can easily be seen that chemical analysis alone could hardly be employed to show in any detail how fibers respond to such a reaction as acetylation. Some other type of test is necessary, and the dyeing methods given have proved to be very satisfactory.

The centrifuge technique is essentially that described by Welo *et al.* [22]. It consists of wetting the samples in boiling water and allowing them to stand and swell overnight at room temperature, or soaking them for 2 hrs. in water containing 0.25% Deceresol OT; centrifuging in tubes with screen bottoms at a radius and speed corresponding to 5,000–6,000 g.; then determining moisture, and calculating its percentage on the dry basis. The percentages of retention given in the text are comparative for each pair or group of samples, but not necessarily from one group to another.

The only test employed for the action of fungi and bacteria was that of soil burial [2], which, in spite of its defects, is recognized as being one of the most useful tests. Even though the soil-burial test is made under conditions not commonly encountered by cotton in service, there seems to be no question that if cotton will withstand long soil burial, frequently considered the most potent microbiological test, it is well protected from attack by either type of organism. All recent tests have been made by complete burial in beds containing 30% moisture at 90°F. The activity of the beds, checked at frequent intervals, has always been sufficient for ordinary cotton to lose practically all of its strength within 1 week of burial.

The cotton yarns used were not usually purified, nor were the fabrics, except for the removal of warp size followed by an open caustic boil. Such considerations as the effects of primary wall, cuticle, and presence of small amounts of noncellulose constituents seem to have little importance in connection with long-time protection by chemical substitution.

Methods employed in preparing and testing the formaldehyde-treated cottons, and references, are given in the paper on that material [9].

Conclusions

Tentative conclusions drawn from the experimental evidence are supported by views that are widely accepted in the recent literature. These conclusions are believed to be important for consideration in the preservation of cellulosic fibers from microbiological deterioration by means of chemical substitution.

High resistance to mildew and rotting—ability to withstand 6 months or more of burial in active soil without notable loss of strength, as imparted to cotton by the substitution of one-third or more or its hydroxyl groups by fibrous acetylation—depends upon the reaction taking place in the amorphous cellulose of the cotton, where the microorganisms normally begin their attack. The mere substitution of hydroxyls probably imparts some resistance; the filling of spaces between cellulose chains by acetyl groups may help reduce the accessibility of some of the amorphous cellulose; but the reduction of accessibility through suppression of swelling seems especially important. Protection is most effective when most of the amorphous cellulose is reacted.

Since crystalline cellulose in the fiber does not swell in water, and is deteriorated little, if any, even after grinding, when the amorphous cellulose is protected by acetylation, it appears that crystalline cellulose by itself would not be subject to rapid microbiological deterioration.

Another method of protection is cross-linking by suitable substitution, which acts partly by the blocking of hydroxyls, but mainly by the reduction of accessibility of amorphous cellulose by suppression of its swelling, found effective so far only to a lower level of protection than attainable by acetylation.

Swelling in cotton at the time of a substitution reaction is unfavorable to high rot-resistance unless it is compensated for by a higher degree of substitution than required for cotton that has not been preswollen because cotton reacted in a swollen state is generally more accessible to microorganisms. Hence, chemically substituted cottons proposed for rot-resistance or processes for making them should be considered with reference to the state of swelling of the cotton at the time of reaction.

Cellulose derivatives in solution may be regarded as being in a still higher state of swelling, and may require some specific type of substitution for their protection, as suggested by Siu and his associates [16]; but conclusions regarding the type of substitution, drawn from tests on such products, cannot be applied to fibrous cellulose.

The great decrease in the resistance of a partially acetylated cotton by partial saponification may result from the freeing of blocked hydroxyls, but seems to be due mainly to restoration of freely swelling, readily attacked, amorphous cellulose.

Appreciable protection by partial methylenation of cotton is possible if more practical methods for such treatment can be developed. Cross-linking resins also deserve more attention.

Suitable dyeing tests can often be readily devised for showing the progress of chemical substitution in cotton fibers, and for helping to determine the properties of substituted products (other than mere dyeing capacity) which sometimes are not readily determined in other ways.

Acknowledgment

The authors wish to express their appreciation to members of the Cotton Fiber Research Division of this Laboratory for assistance in the initial studies with microscope and centrifuge; to Mrs. Jarrell H. Carra for special dyeings and for analyses for acetyl contents; to Mrs. Barbara A. Wright and Mrs. Lucille K. Davis for acetylations and experiments on partial methylenation; and to Miss Vera C. Hasling for the preparation and painstaking microscopic study of many slides of partially acetylated cotton fibers.

Note: The mention of trade products does not imply that they are endorsed by the Department of Agriculture over similar products not mentioned.

Literature Cited

1. Abrams, E., TEXTILE RESEARCH JOURNAL **20**, 71–86 (1950).
2. American Society for Testing Materials, "A.S.T.M. Standards," Part 5, Philadelphia, 1949, pp. 143–5 (D684–45T).
3. Barker, S. G., *Chemistry & Industry* **57**, 1222–9 (1938).
4. Cameron, W. G., and Morton, T. H., *J. Soc. Dyers Colourists* **64**, 329–36 (1948).
5. Castle, V., in Gt. Brit. Board of Trad. Selected Government Research Reports: No. 4: Textiles and Their Testing, London, H. M. Stationery Office, 1949, p. 71–6.
6. Cooper, A. S., Voorhies, S. T., Jr., Buras, E. M., Jr., and Goldthwait, C. F., *Textile Industries* (in press).
7. Dean, J. D., private communication.
8. Dorée, C., *Biochem. J.* **14**, 709–14 (1920).
9. Goldthwait, C. F., TEXTILE RESEARCH JOURNAL **21**, 55–62 (1951).

10. Goldthwait, C. F., McLaren, J., and Voorhies, S. T., Jr., *Textile World* **96**, 115–7, 212, 216 (1946).
11. Greathouse, G. A., TEXTILE RESEARCH JOURNAL **20**, 227–38 (1950).
12. Happey, F., *J. Soc. Dyers Colourists* **66**, 14–6 (1950).
13. Happey, F., *J. Textile Inst.* **41**, T381–403 (1950).
14. Heuser, E., "The Chemistry of Cellulose," New York, John Wiley & Sons, 1944, 660 pp.
15. Heuser, E., Shockley, W., Adams, A., and Grunwald, E. A., *Ind. Eng. Chem.* **40**, 1500–6 (1948).
16. Reese, E. T., Siu, R. G. H., and Levinson, H. S., *J. Bact.* **59**, 485–97 (1950).
17. Siu, R. G. H., TEXTILE RESEARCH JOURNAL **20**, 281–8 (1950).
18. Siu, R. G. H., Darby, R. T., Burkholder, P. R., and Barghorn, E. S., TEXTILE RESEARCH JOURNAL **19**, 484–8 (1949).
19. Thaysen, A. C., Bunker, H. J., Butlin, K. R., and Williams, L. H., *Ann. Applied Biol.* **26**, 750–81 (1939).
20. Timell, T., "Studies on Cellulose Reactions," Stockholm, Esselte Aktiebolag, 1950, 275 pp.
21. Vermaas, D., and Hermans, P. H., *J. Polymer Sci.* **2**, 397–405 (1947).
22. Welo, L. A., Ziifle, H. M., and McDonald, A. W. (in manuscript).
23. White, W. L., and Siu, R. G. H., *Ind. Eng. Chem.* **39**, 1628–30 (1947).

(Manuscript received August 15, 1951.)

Thermal Degradation in Tire Cords

Part II: Effects on Modulus, Toughness, and Degree of Resilience*

Verne W. Tripp, Trinidad Mares, and Carl M. Conrad

Southern Regional Research Laboratory,† New Orleans, Louisiana

Introduction

In Part I of this study [1] it was shown that the chemical degradation of the cellulose of cotton and rayon tire cords achieved by heating at temperatures in the range 230°–302°F for various periods of time is reflected in the fundamental physical properties of the cords, such as breaking strength and elongation. It is to be expected that when such properties are affected, any mechanical properties that derive from them will also exhibit a change. The stress-strain—*i.e.*, load-elongation—relations of tire cords in tension are among the more important characteristics to be considered in determining the over-all utility of the cords, and investigation of the extent to which these relationships are changed as a result of thermal degradation is pertinent to the study of tire cord deterioration in use.

It has been emphasized by a number of workers [3, 4, 6, 11] that the manner in which a textile structure such as tire cord will behave under stresses in use cannot be judged adequately by measurements of only the breaking strength and elongation, although observations of these properties give a basis for the screening and rejection of unsuitable cords.

Along with strength and elongation, Smith [9] has listed modulus, toughness, and degree of resilience as significant properties of textiles. The latter three properties describe, to a great extent, the stress-strain relations which a textile material exhibits in tension. Measurement of these quantities made on cotton and rayon tire cords before and after heating are reported here. Brief definitions of the

* Presented in part at a meeting of The Fiber Society, April 14, 1949, Clemson, South Carolina.

Part I appeared in the October, 1951, issue of TEXTILE RESEARCH JOURNAL.

† One of the laboratories of the Bureau of Agricultural and Industrial Chemistry, Agricultural Research Administration, U. S. Department of Agriculture.

properties discussed in this report, which are essentially those of Smith, are as follows:

Modulus is the ratio of a load (stress) to the elongation (strain) that it produces.* Averaged over the entire range of stress of a tire cord, it is the ratio of the breaking load of the cord to the elongation at break.

Toughness is defined as the ability to absorb work without rupture. It has the dimensions of energy, and is proportional to the load imposed and the deformation produced by that load. Mathematically, the toughness, T, of a tire cord is given by the relation

$$T = \int_0^E L\,de, \qquad (1)$$

where L is the load causing elongation, e, to the extent E. The breaking toughness may be represented by the area bounded by the loading curve, the elongation ordinate, and the line perpendicular to this ordinate at the breaking elongation.

Degree of resilience is the ratio of the work recovered by a material when the deforming force is removed to the work done on the material in deforming it. As shown in Figure 1, the load-elongation curve for a tire cord (even after secondary creep [5, 7] has been removed by mechanical conditioning) is not coincident for both loading and unloading processes. This means that the work absorbed by the cord in the loading process is not returned completely to the cord system on removal of the load, but is partly lost to its environment. The energy returned to the cord system is the *resilience* energy, while that lost is *hysteresis*. The degree of resilience of the cord, then, is the ratio of the area $DAFE$, bounded by the unloading curve AFE (resilience), to the area $DAGE$, bounded by the loading curve AGE (resilience plus hysteresis). The area $OAGE$ represents the nonrecoverable work capacity removed from the cord by the cyclic-loading process.

Materials and Methods

The tire cords used in this study have been described previously [1]. They included cotton and rayon cords in commercial production, sampled at four stages of tire manufacture: before any processing; after dipping; after calendering into rubber; and after vulcanizing into the tire. Except for the control, all cords had been heated in a special oven at controlled temperatures of 230°, 248°, 266°, 284°, and 302°F. The relative humidity of the oven atmosphere was estimated to be 40% in each case. The tests also included cords from tires that had been run to failure on a National Bureau of Standards "wheel" at Washington, D. C.

The estimation of modulus was made from the breaking strength-elongation measurements on a Suter cord tester. It was calculated simply as the ratio of the breaking load to the elongation at break, and expressed as pounds per percent elongation. The modulus values reported here each represent the mean of 20 observations.

The breaking toughness of the cords was also measured from the load-elongation charts obtained in the breaking-strength test. A polar planimeter was used to integrate the area under the load-elongation curve, and the area was converted to foot-pounds of work by the appropriate factor. Each of the toughness values is the mean of 10 observations on each cord sample.

The choice of load to be used in measuring resilience is governed by the end-use of the material and the limitations of the method of measurment. In order to obtain areas of a suitable size for measurement, and to stay within the range of loading that it can be assumed a cord in a tire will be subjected to, 50% of the breaking load was chosen as the point at which the resilience would be measured. The Suter cord tester, implemented with a separate driving mechanism, was also used in the resilience measurements. The driving mechanism consisted of a weighted-pulley arrangement, actuated by a reversible motor, attached to the lower end of the loading bar of the instrument. The rate of travel of the

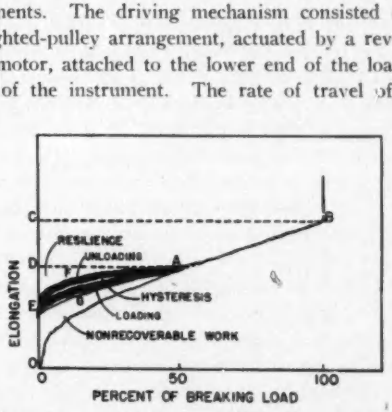

FIG. 1. *Cyclic-loading curve of a tire cord, defining resilience, hysteresis, and nonrecoverable work.*

* The term "stiffness" is used by Smith in this connection, but its connotation of resistance to bending has not made for general acceptance of the term.

loading bar could be controlled by means of a movable cone on the shaft of the motor driving the pulley system, and this was set at 12 in. per min.—the same speed as used in the breaking-strength measurements. The rate of jaw travel was checked from time to time, but required no adjustment. After clamping the cord in the jaws of the tester, as in the breaking-strength measurements, the drive was started and the cord loaded to 50% of its breaking strength, as previously determined in the breaking strength-elongation measurements on cords from the same sample. The motor was then reversed and the cord unloaded to approximately zero load. The loading-unloading cycle was repeated 10 times; on the eleventh loading the stress was increased until the cord broke (see Figure 1). The course of the cycling was followed on the autographic chart, and allowance was made for the inertia of the driving system when approaching reversal points. Loading to the 50% point could be reproduced with a precision of about 1 lb., or 5%–10% of the breaking load. It was found that the heated cords which had a breaking strength of less than 10 lbs. could not be cyclically loaded in this manner for 10 cycles because they invariably broke, often on the second or third cycle. Accordingly, no resilience measurements were made on these weak cords. In view of the time-consuming nature of these measurements, only 5 cords of each sample were tested. The degree of resilience was expressed as a percentage.

Results

Unheated and Wheel-Tested Cords

The results of the measurements of modulus, toughness, and resilience of the unheated and wheel-tested cords are given in Table I. It is apparent that the manufacturing process brought about increases in the modulus of both cotton and rayon cords—the increase was about 33% for the cotton cords and 22% for the rayon. These increases reflect the over-all effect of removal of extensibility and the small increases in strength that accompanied the manufacture of the tires [1].

As a result of running on the wheel, both cotton and rayon cords showed further increase of modulus. The cotton cord, taken from the tire which had run 2,360 miles, gained about 10% over that of the unrun tire. The modulus of the rayon cord from the tire that had run 6,375 miles was 23% greater than that of the cord from the vulcanized, but unoperated, tire.

TABLE I. MODULUS, TOUGHNESS, AND RESILIENCE OF UNHEATED AND WHEEL-TESTED COTTON AND RAYON TIRE CORDS

Cord	Modulus (lbs./%)	Toughness (ft.-lbs.)	Resilience (ft.-lbs.)	Degree of resilience (%)
Cotton				
Untreated	1.74	0.742	0.062	54
Dipped	1.84	0.780	0.059	51
Calendered	1.48	0.855	0.064	51
Vulcanized in tire	2.31	0.732	0.058	50
Wheel-tested	2.55	0.673	0.061	55
Rayon				
Untreated	0.89	1.036	0.049	50
Dipped	1.06	0.939	0.050	51
Calendered	1.06	0.942	0.051	53
Vulcanized in tire	1.09	0.979	0.054	52
Wheel-tested	1.34	0.342	0.025	58

The breaking toughness of the unheated cords showed relatively little change during manufacture. However, the wheel-tested cords lost toughness as a result of decreased extensibility as secondary creep was removed and, in the case of the rayon cord, as a result of severe strength loss [1].

The third column of Table I lists the magnitude of the resilience of the cords at 50% of their breaking loads. It is seen that the manufacturing process had little effect on this property, the cotton cords showing a small over-all decrease, and the rayon cords a small increase. The wheel-tested cotton cord gained about 5% in resilience over the vulcanized, but unrun, cord. The measured resilience of the wheel-tested rayon cord was much smaller, of course, due to the smaller applied load.

The variation in the degree of resilience of the unheated cords is less than 5% (absolute). The cords that had been run on the wheel apparently became slightly more efficient than the others in regaining work capacity.

Thermally Degraded Cords

Modulus.—The four panels of Figure 2, representing the four stages of manufacture, show the effect on the modulus of the cords of periods of heating at the temperatures employed. The modulus is expressed as a percentage of the modulus of the corresponding unheated cord. It is seen that thermal degradation produced a lowering of the modulus except in a few cases of the shortest and longest periods of heating at the lower temperatures. Extension of the heating period resulted in further decrease of modulus, and the rate of loss was greater at the

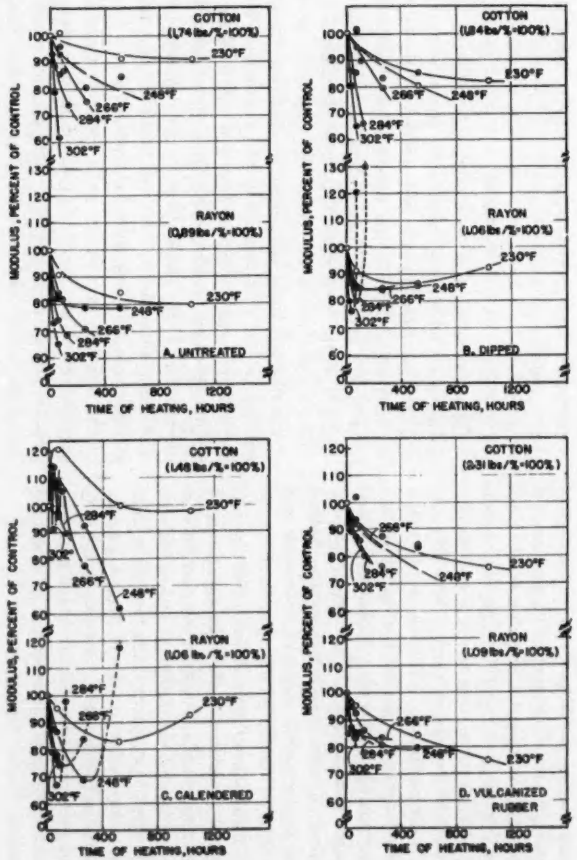

FIG. 2. *Change of modulus with time of heating at different temperatures for cotton and rayon tire cords at progressive stages of processing.*

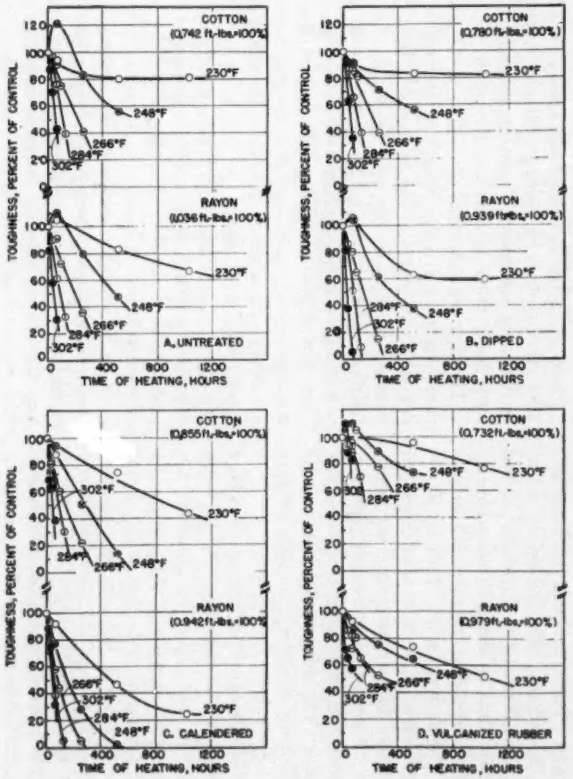

FIG. 3. *Change of toughness with time of heating at different temperatures for cotton and rayon tire cords at progressive stages of processing.*

higher temperatures. The behavior of the cotton and the rayon cords is similar. The data on the calendered cords is notably erratic. The cause of this probably lies in the effect on strength measurements of the somewhat incompletely removed rubber calender coating. The dashed curves of Figure 2(C), which go to high modulus values even after prolonged heating at the higher temperatures, are not necessarily significant because the breaking-strength and elongation measurements on these cords were too low to permit accuracy. The same explanation may be made in the case of the dipped rayon cords (Figure 2(B)).

The behavior of the cords vulcanized in rubber differed from that of the untreated and partially processed cords. At the higher temperatures the loss in modulus was not as great as that suffered by the incompletely processed cords, but at the lower temperatures the decrease in modulus was equal to that suffered in the dipped and calendered cords and exceeded that of the untreated cords.

Toughness.—The breaking toughness of the heated tire cords, expressed as a percentage of the toughness of the unheated cords, is plotted against time of heating at the various temperatures in the four panels of Figure 3, representing the four processing stages. The damaging effect of heat at these temperatures is apparent. As was the case with cord modulus, prolonging the heating period produced further losses in toughness in nearly all of the cords, and the loss was accelerated by raising the temperature.

The calendered cords (Figure 3(C)), both cotton and rayon, underwent the most severe loss of toughness; the untreated and dipped cords (A and B) also suffered to a serious extent. The vulcanized cords retained their toughness to a significantly greater degree than the other heated cords. Vulcanized cotton cords did not lose more than 35% of their original toughness after the most severe treatments, whereas cotton cords of the earlier stages of processing lost more than 60%. Similarly, the vulcanized rayon cords lost a maximum of only 50% of their toughness, compared to losses of 90% in the cords of earlier processing stages. However, whereas the loss of toughness in the untreated, dipped, and calendered cords was, in general, more severe at the higher than at the lower temperatures (for the longest periods of heating), no such difference was noted in the vulcanized cords, where heating at the lower temperatures eventually produced the same loss of toughness as heating at the higher temperatures.

Some of the cords showed increases in toughness after short periods of heating. This is a reflection of the slight increases in breaking strength in these same cords, noted in Part I of this study [1].

The data indicate that the cotton cords retained their toughness to a significantly greater extent than did the rayon cords. The advantage thus demonstrated for cotton is tempered by the fact that the toughness of the rayon cords, on an absolute basis, is initially about 40% greater than that of the cotton cords (*cf.* Table I). Thus, after appreciable heat degradation—*e.g.*, 20% loss of toughness in the cotton cords—the absolute toughness of both cords is approximately the same.

Degree of Resilience.—In Figure 4 are shown the degree-of-resilience data for the oven-heated cords plotted against duration of heating within the range of temperatures employed. It is evident that this property is virtually unaffected by heating in the temperature range of these experiments. The processing stage of the cords likewise did not seem to have any bearing upon the retention of this property. The degree of resilience of the cotton cords ranged from 43% to 55%, with a mean of 49%. For rayon, the range was from 45% to 60%, with a mean of 51%. These mean values are indicated by the lines drawn through the data points. Reference to Table I shows that the degree of resilience of the wheel-tested cords was greater than the mean values of their respective groups.

Discussion

On the premise that the mechanical properties of the tire cord, which is the supporting structure of the tire carcass, determine the performance of the tire, the behavior of a tire in use should be predictable in so far as the properties studied come into play. The modulus of the cord must determine the extent to which the tire will be deformed under stress: a cord of low modulus must yield more, and thereby transmit less, of the displacement to the supported load due to an external force than a cord of high modulus, which will transmit the displacement to the body of the vehicle. If the modulus is too low, however, it may allow extension of the tire fabric beyond the yielding point of contiguous parts of the tire.

The decrease in modulus as a result of thermal degradation under the conditions of these experiments in no case exceeded 40% of the original modulus of the cords, and in most cases was less than

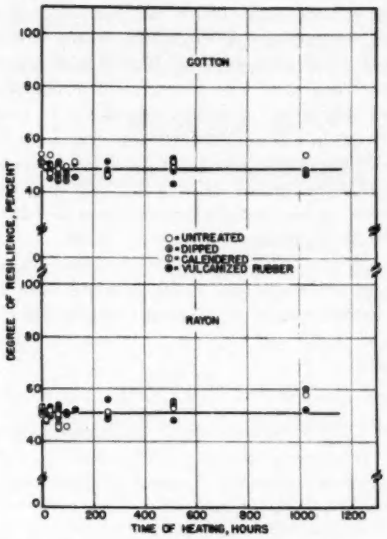

FIG. 4. *Relation of degree of resilience of cotton and rayon tire cords to time of heating.*

25%. The loss of strength in the cords [1] which showed the greatest decrease of modulus approached 70%–80%, a condition which would render them useless in tire operation. Thus, for practical considerations, the changes in modulus are overshadowed by changes in breaking strength.

Since the primary function of a tire cord is to elongate under a load—*i.e.*, to absorb energy, without rupture—its toughness may be considered one of the most, if not the most, important single property of the cord. Since heat degradation of the cords severely decreases both the breaking strength and the elongation at break [1], it is only to be expected that the toughness will be more severely affected than either of the properties from which it derives. In Figure 5, the toughness of all of the cotton and rayon cords studied is plotted against the breaking strength of the cords, both quantities being expressed as a percentage of the corresponding properties of the unheated controls. In the region from 100% to 50% strength retained, the relationship is nearly linear, and changes may be represented approximately by the expression

$$\Delta\,(\text{Toughness, }\%) = 0.7\Delta\,(\text{Breaking Strength, }\%). \quad (2)$$

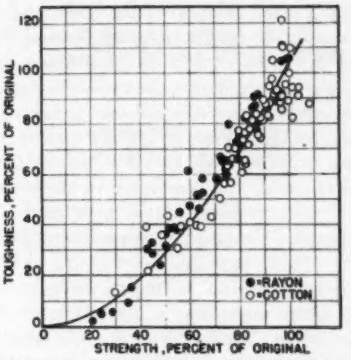

FIG. 5. *Relation of toughness and breaking strength of heat-degraded cotton and rayon tire cords.*

The regression line fitted to all of the data may be represented by the exponential relation

$$(\text{Toughness, }\%) = 0.0217\,(\text{Breaking Strength, }\%)^{1.84}. \quad (3)$$

While cords which have less than 20% of their original breaking strength possessed practically no toughness, the curve passes through the origin—theoretically, at least. It is evident that the ability of the cords to absorb energy is reduced far more rapidly with heat degradation than the loss of strength would indicate.

It was estimated from the construction and operating conditions of the tires [1, 2, 8] that the cotton cords studied would, in service, bear a normal load of approximately 3 lbs. per cord (15% of the breaking strength); the rayon cords would bear a corresponding load of approximately 2 lbs. (also 15% of the breaking load). The application of short-term stresses exceeding these by a factor of 3 or 4 (45%–60% of the breaking strength) during tire operation, due to obstacles in the road, is not unlikely. Thus, reduction of the breaking strength of the cords by heat degradation to 50% of the original value would bring the cord into a region where such operational stresses alone would result in rupture. But at this point of degradation the toughness of the cord has reached a value (30%) which is even a smaller fraction of the original value. If toughness is the determining factor in tire cord performance, rupture will occur more readily at this condition of degradation than strength would lead one to predict.

A consideration of the cyclic-loading curves of the tire cords studied, of which Figure 1 is typical, shows

that only a small fraction of the total toughness of the mechanically conditioned cord is involved when the cord is loaded to 50% of its breaking strength. Hence, the rupture during the cyclic-loading process of those cords whose strength due to heat degradation was less than 10 lbs. (50%–70% of the original breaking strength) indicates that the toughness, in itself, and under the conditions of these measurements, was not necessarily the governing factor in cord rupture. Changes in fatigue characteristics as a result of heat degradation must also be involved.

The magnitude of the hysteresis energy at the 50% loading point, amounting to approximately 50% of the total energy applied in these experiments, indicates that it may be an appreciable source of the heat built up in running tires [10]. Either relative or absolute increase of the resilience energy of the tire cords is obviously desirable. The observation of the relative constancy of the degree of resilience in these experiments, in which the heat-degraded cords suffered serious losses of breaking strength and marked decrease in the cellulose chain length, is difficult to account for in terms of the other properties measured. Apparently, neither the breaking strength nor the degree of polymerization of the cellulose is associated with the resilience behavior of the cords over the range studied. It is possible that the conditions of the test—*i.e.*, loading to the 50% level—give an indication of the behavior of the cord in a region in which the damage due to heat does not affect the mechanical properties of the cord. Loading to higher percentages of the breaking strength, or to a constant absolute load, may reveal resilience characteristics that are different from those observed.

Summary

The thermal degradation of cotton and rayon tire cords exposed to temperatures in the range 230°–302°F for periods from 16 to over 1,000 hrs. resulted in significant decreases in the average modulus and breaking toughness of the cords. The decrease of both of these properties was progressive with time of heating and occurred more rapidly at the higher temperatures. The degree of resilience of the mechanically conditioned cords at 50% of the breaking loads was not significantly changed by the heating.

The tire cords which had been vulcanized in rubber were not as severely affected by the heat treatments as were those which had been unprocessed, dipped, or calendered. Modulus of the cord was reduced to the same extent in both cotton and rayon cords. Toughness was decreased to a significantly greater degree in rayon than in cotton. In general, the change in modulus by heat degradation was considered to be less significant than the changes in strength or toughness. Cords that had been run to failure in a wheel test showed increased modulus and decreased toughness.

A good correlation exists between breaking strength and toughness of the heat-degraded cords over a wide range of breaking-strength loss. The relation could be expressed by the exponential equation

$$T = 0.0217\ S^{1.84}, \qquad (4)$$

where T is the toughness and S the breaking strength, both expressed in percent of the original. Toughness decreased more rapidly, on a proportional basis, than did breaking strength.

Acknowledgment

The authors wish to extend appreciation to Hilda M. Ziifle for preparation of the figures and assistance in the computations, and to Rollin S. Orr for his helpful interest and advice in certain details of the measurements.

Literature Cited

1. Conrad, C. M., Tripp, V. W., and Mares, T., TEXTILE RESEARCH JOURNAL **21**, 726 (1951).
2. DuPre, A. M., Jr., private communication.
3. Gurney, H. P., and Davis, E. H., *Textile World* **68**, 219 (1925).
4. Gurney, H. P., and Davis, E. H., *J. Textile Inst.* **21**, T463 (1930).
5. Hamburger, W., TEXTILE RESEARCH JOURNAL **18**, 102 (1948).
6. King, F. C. W., and Truesdale, R., *Textile Recorder* **41**, 41, 88 (Apr.); 86, 99 (June); 103 (July 1923).
7. Leaderman, H., "Elastic and Creep Properties of Filamentous Materials and Other High Polymers," Washington, D. C., The Textile Foundation, 1943.
8. Schippel, H. F., *Ind. Eng. Chem.* **15**, 1121 (1923).
9. Smith, H. deW., *Proc. A.S.T.M.* **44**, 543–92 (1944).
10. Wakeham, H., and Honold, E., *J. Applied Phys.* **17**, 698 (1946).
11. Wakeham, H., Honold, E., and Skau, E. L., *J. Applied Phys.* **16**, 388 (1945).

(*Manuscript received April 9, 1951.*)

Have YOU seen these new REINHOLD books?

Handbook of DANGEROUS MATERIALS

by N. Irving Sax, *Toxicologist,*
General Electric Co., Schenectady, N. Y.

Here is one of the most important technical books ever published by Reinhold. It covers over 5000 hazardous industrial materials and offers information of utmost value to those concerned with safely handling, storing and shipping such dangerous materials as solvents, dyes, and fibers. The complete text of the Interstate Commerce Commission Shipping Regulations is included for detailed instructions on labeling, packaging, storage, shipping, and all relevant subjects.

In addition to the hazards of general chemicals, this useful book also covers the important fields of explosives and radiation hazards. Of special interest to textile chemists is the section on fungi, many of which attack textiles destructively.

1951 850 double-column pages 7 × 10″ $15.00

MICROBIAL DECOMPOSITION of CELLULOSE

by Ralph G. H. Siu, *Research Director,*
Pioneering Research Laboratories, U. S. Army Quartermaster Corps, Philadelphia. Research Associate, Harvard University.

This book contains the only comprehensive collection of facts and data dealing with the whole story of fungus and bacterial attack on cotton fabrics. You get a clear, unified picture of the structure of cellulose; the biochemical mechanism of its decomposition; the physiology and manner of attack of the microorganisms concerned; and methods of preventing attack and protecting materials against deterioration.

Though the emphasis is on cotton textiles, the information in the book underlies problems confronting scientists in many fields. Its value is enhanced by the inclusion of a great deal of heretofore unpublished data from military and governmental laboratories and inaccessible reports of field operations, compiled during and since World War II in the United States, England, Canada, Australia and India.

1951 583 pages, illustrated $10.00

Send for copies on examination

REINHOLD PUBLISHING CORPORATION
Dept. M-326, 330 West 42nd Street, New York 18, N. Y.

FOR DE-SIZING

RAPIDASE®

For de-sizing cottons, rayons and mixed goods . . . at high or low temperatures.

RAPIDASE-M
Intermediate strength

RAPIDASE-CONCENTRATED
Highest strength

ZYMEX®

A powdered de-sizing agent . . . with all the advantages and economy of Rapidase.

SERIZYME®

Removes gelatin and protein sizes. For de-sizing acetates and acetate-rayon mixtures.

In conjunction with any enzyme preparation . . . USE **SACON** . . . a non-ionic wetting agent and detergent.

Technicians Available. Write for Booklet.

WALLERSTEIN COMPANY, INC.
180 MADISON AVE., NEW YORK 16

E. F. DREW & CO., INC.

Producers of Basic Raw Materials and Finished Products For Specific End Uses in the Textile Industry

Nature has proved that *fatty materials* are the best lubricant for fibrous materials. The wool on sheep is protected by a fatty coating . . . as are all fur bearing animals. Cotton and bast fibres are protected by natural waxes.

For over 40 years, Drew has specialized in the production of fatty products from nature's abundant store of vegetable, marine and animal oils. Applying modern chemistry to years of processing experience, Drew has produced a wide variety of superior textile finishing oils, finishing materials, detergents, wetting agents and other surface active chemicals. These products are truly "kind to all fibres."

For Information, Write

TEXTILE CHEMICALS DEPARTMENT

E. F. DREW & CO., Inc.

15 EAST 26th STREET, NEW YORK 10, N.Y.

DREW PRODUCTS